CHARLES UNIVERSITY

FACULTY OF MEDICINE IN PILSEN

DISSERTATION

CLINICOPATHOLOGICAL, MORPHOLOGICAL, IMMUNOHISTOCHEMICAL, AND MOLECULAR BIOLOGICAL CHARACTERISTICS OF RARE SALIVARY GLAND TUMORS

OLENA KOSHYK, MD

SUPERVISOR: Prof. ALENA SKALOVA, MD. PhD.

FIELD: PATHOLOGY

PILSEN 2023

DECLARATION

I declare hereby that I made this dissertation thesis by myself and that I mentioned and cited properly all sources and literature. I declare that this thesis was not used to obtain another or the same title.

I agree with permanent deposition of the digital version of this work in the database of Charles University in Prague, Medical Faculty in Pilsen.

Pilsen, 01th August 2023

SUMMARY

The actual dissertation is the result of Olena Koshyk's doctoral study at Charles University in Prague, Faculty of Medicine in Pilsen, from 2019 to 2023. The author focused the main part of her research on rare salivary gland tumors but also participated in studies related to sinonasal soft tissue tumors. The studies used a wide range of investigation methods including morphology, immunohistochemistry, and molecular genetic methods in order to provide new insights for accurate tumor diagnosis and to propose novel approaches and refinements in the classification of selected head and neck tumors.

The dissertation is divided into two parts. The first part represents four articles that present the latest data on rare salivary gland tumors.

The first paper concentrated on the new rare oncocytic variant of mucoepidermoid carcinoma with comprehensive morphological and immunohistochemical descriptions, and molecular alterations. Special attention was paid to the differential diagnosis with oncocytic tumors for accurate diagnosis.

The second study covered a clear cell subtype of myoepithelial carcinoma which showed *EWSR* gene rearrangements. Different fusions in the *PLAG1* gene were found in such tumors but fusion transcripts for the *EWSR* gene were not detected. The study also focusses on a comparison of the biology of myoepithelial tumors of the salivary gland and soft tissues and skin.

In the third article, rare *NR4A2* rearrangements in acinic cell carcinoma are discussed. We also investigated NR4A3 and NR4A2 immunostains as a cost-effective method for the accurate diagnosis of acinic cell carcinoma and surrogate markers of the gene rearrangements.

The next study is devoted to the newly reclassified neoplasm, sclerosing polycystic adenoma of the salivary gland. For the first time, diagnostic criteria for low-grade and high-grade dysplasia in the solid and cribriform epithelial proliferations in sclerosing polycystic adenoma were presented. We reported the molecular profile of these benign tumors with *PIK3CA*, *HRAS*, and *AKT1* mutations. In our work, we presented a unique case of a salivary gland apocrine intraductal carcinoma with transformation to salivary duct carcinoma, arising from sclerosing polycystic adenoma harboring a mutation in the *PI3K/Akt* pathway in all tumor components.

The second part represents two rare mesenchymal sinonasal malignant entities. First is the rare phenomenon of biphenotypic sinonasal sarcoma with *PAX3::MAML3* fusion with

transformation into high-grade rhabdomyosarcoma. The differential diagnosis and the mandatory use of molecular testing were discussed.

The last study covered a completely new aggressive polyphenotypic sarcoma with *EWSR::POU2AF3* fusion with sinonasal predilection. This type of sarcoma has only been described in two studies, where overall 11 cases of small round cell/spindle cell sarcoma with a novel *POU2AF3* rearrangement were presented. We analyzed 8 of our own cases and 11 cases from both previous studies. The subgroups with low and high-grade morphologies, were described for the first time, with comprehensive immunohistochemical and molecular characteristics, inlcuding the *EWSR1::POU2AF3* and *FUS::POU2AF3* fusion transcript, providing the evidence of a single entity with a wide morphological spectrum.

ABSTRACT

Vlastní disertační práce je výsledkem doktorandského studia Oleny Koshyk na Univerzitě Karlově v Praze, Lékařské fakultě v Plzni, v letech 2019 až 2023. Autorka zaměřila hlavní část svého výzkumu na vzácné nádory slinných žláz, ale podílela se i na studiích souvisejících se sinonazálními nádory měkkých tkání. Práce využívaly širokou škálu vyšetřovacích metod včetně morfologie, imunohistochemie a molekulárně genetických metod za účelem získání nových poznatků pro přesnou diagnostiku nádorů a navrhly nové přístupy a vylepšení v klasifikaci specifických nádorů.

Dizertační práce je rozdělena do dvou částí. První část představuje čtyři články, které prezentují nejnovější údaje o vzácných nádorech slinných žláz.

První práce se soustředila na novou vzácnou onkocytární variantu mukoepidermoidního karcinomu s komplexním morfologickým a imunohistochemickým popisem a molekulárními změnami. Zvláštní pozornost byla věnována diferenciální diagnostice s onkocytárními nádory.

Druhá studie se věnovala světlobuněčnému myoepiteliálnímu karcinomu, který vykazoval rearanži genu *EWSR*. V takových nádorech byly nalezeny různé fúze v genu *PLAG1*, ale fúzní transkripty pro gen *EWSR* nebyly nalezeny. Studie také pojednává o srovnání biologie myoepiteliálních nádorů slinné žlázy s myoepiteliálními nádorry měkkých tkání a kůže.

Ve třetím článku jsou diskutovány vzácné přestavby genu *NR4A2* u karcinomu z acinických buněk. Zkoumali jsme také imunohistochemické barvení NR4A3 a NR4A2 jakožto ekonomicky dostupné a diagnosticky užitečné alternativy k molekulárně genetickému testování..

Další studie je věnována nově reklasifikovanému novotvaru nazývajícímu se sklerotizující polycystický adenom slinné žlázy. Byla navržena diagnostická kritéria pro rozlišení dysplazie nízkého a vysokého stupně v solidních a kribriformních epiteliálních proliferacích u sklerotizujícího polycystického adenomu. Uvedli jsme molekulární profil těchto benigních nádorů s mutacemi *PIK3CA, HRAS* a *AKT1*. V naší práci jsme prezentovali unikátní případ apokrinního intraduktálního karcinomu slinných žláz s transformací v salivární duktální karcinom. Tato léze vznikla v terénusklerotizujícího polycystického adenomu s mutací v signální dráze PI3K/Akt ve všech složkách nádoru.

Druhá část představuje dvě vzácné mezenchymální sinonazální maligní entity. Prvním je vzácný fenomén bifenotypického sinonazálního sarkomu s fúzí genů *PAX3::MAML3* s transformací na rhabdomyosarkom vysokého stupně malignity. Diskutována byla diferenciální diagnostika a povinné použití molekulárního testování.

Poslední studie se týkala zcela nového agresivního polyfenotypického sarkomu s fúzí genů *EWSR::POU2AF3* a s predilekcí pro sinonazální lokalizaci. Tento typ sarkomu byl popsán pouze ve dvou studiích, kde bylo prezentováno celkem 11 případů malobuněčného/vřetenobuněčného sarkomu s nově popsanou rearanží genu *POU2AF3*. Analyzovali jsme 8 našich vlastních případů a 11 případů z obou předchozích studií. Poprvé byly popsány podskupiny s „low-grade“ a „high-grade“ morfologií s komplexními imunohistochemickými charakteristikami a fúzemi genů *EWSR1::POU2AF3* a *FUS::POU2AF3*. Morfologické znaky a výsledky molekulárně genetického testování poskytly důkaz o tom, že prezentované tumory představují morfologické spektrum jedné nádorové jednotky.

CONTENTS

Declaration 2

Summary 3

Abstract 5

Contents 7

List of abbreviations 8

Introduction 10

Goals and hypothesis 16

Materials and methods 17

Commented publications 22

1. Part – Salivary gland tumors 23

1.1 Molecular profiling of salivary oncocytic mucoepidermoid carcinomas helps to resolve differential diagnostic dilemma with low-grade oncocytic lesions 23

1.2 Molecular profiling of clear cell myoepithelial carcinoma of salivary glands with the *EWSR1* rearrangement identifies frequent *PLAG1* gene fusions but no *EWSR1* fusion transcripts. 36

1.3 A minority of cases of acinic cell carcinoma of the salivary glands driven by an *NR4A2* rearrangement: the diagnostic utility of the assessment of *NR4A2* and *NR4A3* alterations in salivary gland tumors. 51

1.4. Sclerosing polycystic adenoma of the salivary gland. A novel neoplasm characterized by *PI3K-AKT* pathway alterations – new insights into a challenging entity. 61

2. Part – Mesenchymal sinonasal tumors 76

2.1 Biphenotypic sinonasal sarcoma with *PAX3::MAML3* fusion transforming into high-grade rhabdomyosarcoma: report of an emerging rare phenomenon 76

2.2 *EWSR1::POU2AF3(COLCA2)* Sarcoma: an aggressive, polyphenotypic sarcoma with a head and neck predilection 84

References 124

List of own publications 131

Conclusions 133

Acknowledgments 134

LIST OF ABBREVIATIONS

ACC - and adenoid cystic carcinoma

AciCC - acinic cell carcinoma

BSNS - biphenotypic sinonasal sarcoma

CCC - clear cell carcinoma

CCMC - clear cell variant of myoepithelial carcinoma

CHCHD7 - coiled-coil helix-coiled-coil helix domain containing 7

CXPA - carcinoma ex pleomorphic adenoma

EBV – Epstein-Barr virus

EMCMT - ectomesenchymal chondromyxoid tumor

FISH - fluorescence in situ hybridization

HGT - high-grade transformation

HPV - Human Papillomavirus

IDC – intraductal carcinoma

IHC – immunohistochemistry

LIFR - leukemia inhibitory factor receptor

MC - myoepithelial carcinoma

MEC - mucoepidermoid carcinoma

MMR – mismatch repair

NGS - next-generation sequencing

NTRK - neurotrophic receptor tyrosine kinase

OMEC – oncocytic variant of mucoepidermoid carcinoma

PA - pleomorphic adenoma

PCR - polymerase chain reaction

PLGA - polymorphous low-grade adenocarcinoma

RMS - rhabdomyosarcoma

RT-PCR - reverse transcription polymerase chain reaction

SDC - salivary duct carcinoma

SPA - sclerosing polycystic adenoma

WHO - World Health Organization

WT - Warthin’s tumor

INTRODUCTION

Salivary gland tumors comprise approximately 3–6% of all head and neck neoplasms. Their incidence is 0.4 to 13.5 cases per 100,000 population, and most salivary gland tumors are benign neoplasms [1]. The most affected site is the parotid gland, followed by the submandibular and minor salivary glands. The current 2022 World Health Organization (WHO) salivary gland tumor classification comprises mostly benign and malignant epithelial entities which are summarized in Table 1 [2]. Tumors of the hematolymphoid and soft tissue of the salivary gland have a very low incidence.

Table 1 WHO classification of the salivary gland tumors 2022

Benign epithelial tumors	Malignant epithelial tumors
Pleomorphic adenoma	Mucoepidermoid carcinoma
Basal cell adenoma	Adenoid cystic carcinoma
Warthin tumour	Acinic cell carcinoma
Oncocytoma	Secretory carcinoma
Salivary gland myoepithelioma	Microsecretory adenocarcinoma
Canalicular adenoma	Polymorphous adenocarcinoma
Cystadenoma of the salivary glands	Hyalinizing clear cell carcinoma
Ductal papillomas	Basal cell adenocarcinoma
Sialadenoma papillaferum	Intraductal carcinoma
Lymphadenoma	Salivary duct carcinoma
Sebaceous adenoma	Myoepithelial carcinoma
Intercalated duct adenoma and hyperplasia	Epithelial-myoepithelial carcinoma
Striated duct adenoma	Mucinous adenocarcinoma
Sclerosing polycystic adenoma	Sclerosing microcystic adenocarcinoma
Keratocystoma	Carcinoma ex pleomorphic adenoma
	Carcinosarcoma of the salivary glands
	Sebaceous adenocarcinoma
	Lymphoepithelial carcinoma
	Squamous cell carcinoma
	Sialoblastoma
	Salivary carcinoma NOS and emerging entities

The most common entities are pleomorphic adenoma (PA), Warthin's tumor (WT), mucoepidermoid carcinoma (MEC), and adenoid cystic carcinoma (ACC) [3,4]. An overwhelming majority of salivary gland malignancies (85-95%) form MEC, ACC, acinic cell carcinoma (AciCC), polymorphous low-grade adenocarcinoma (PLGA), carcinoma ex pleomorphic adenoma (CXPA) and salivary duct carcinoma (SDC) [5,6].

Some neoplasms are commonly seen in routine practice and most of them are recognized based on the histological features alone, whereas the diagnosis of complex and rare tumors requires histological changes together with immunohistochemical and molecular-genetic studies.

Histologically, salivary gland consists of a variety of serous and mucous acinar cells, myoepithelial, and ductal cells (intercalated, striated, and interlobular ducts). So, the tumors can originate from one to several cell types leading to overlapping different entities.

Besides, immunohistochemical and molecular heterogeneity of salivary gland tumors makes this group of neoplasms challenging and may cause diagnostic problems.

Immunohistochemistry (IHC) is an important diagnostic method for difficult salivary gland lesions. Numerous immunohistochemical markers are used routinely in salivary gland pathology for diagnostic purposes (collections of different types of cytokeratins, myoepithelial markers, DOG1, mammaglobin, GATA3, SOX10, CD117, MIA, hormone receptors, Ki67, etc). In some neoplasms, however, the role of IHC is limited. For such cases, further genetic testing may be helpful for diagnosis and biology understanding. In some cases, IHC is used as a surrogate method for the identification of genetic rearrangements (e.g., antibodies NR4A3 and NR4A2 as markers of *NR4A3* and *NR4A2* rearrangements respectively in acinic cell carcinoma, etc).

Recently, various molecular techniques have also been integrated into routine diagnostic practice. The molecular genetic methods include fluorescence in situ hybridization (FISH), reverse transcription polymerase chain reaction (RT-PCR), and next-generation sequencing (NGS). In salivary gland pathology, molecular alterations were included in the WHO 2022 definition of mucoepidermoid carcinoma, adenoid cystic carcinoma, secretory carcinoma, polymorphous adenocarcinoma, hyalinizing clear cell carcinoma, mucinous adenocarcinoma, and microsecretory adenocarcinoma [2]. Genetic findings also help to understand the biology of lesions, and correctly classify them. For example, sclerosing

polycystic adenosis is now classified as sclerosing polycystic adenoma because of *PI3K* pathway alterations findings [7]. In recent years, newly described genetic alterations in salivary gland pathology emerged. The list of selected salivary gland tumors and their most common corresponding alterations is provided in Table 2.

Table 2. Newly described genetic alterations in salivary gland pathology

Secretory carcinoma	*ETV6-NTRK3* gene rearrangement; novel *ETV6::RET, ETV6::MET, ETV6::MAML3, MYB::SMR3B, VIM::RET* gene fusion
Acinic cell carcinoma	(t(4;9)(q13;q31) translocation with upregulation of the transcription factor *NR4A3*
Hyalinizing clear cell carcinoma	*EWSR1::ATF1*
Adenoid cystic carcinoma	*MYB::NFIB, MYBL1::NFIB,* activating *NOTCH 1,2,3* mutations in a subset of patients with poor prognosis and higher rates of distant metastasis
Intraductal carcinoma	*NCOA4::RET, TRIM27::RET*, novel *TUT1::ETV5, KIAA1217::RET* and *STRN::ALK* in invasive tumors
Polymorphous and cribriform adenocarcinoma	PRKD point mutation, *ARID1A::PRKD1 DDX3::PRKD1, PRKD2* and *PRKD3* rearrangements
Carcinoma-ex-pleomorphic adenoma	*PLAG1* and *HMGA2* gene fusions or amplification

Due to the complexity of the structure, many tumors of the salivary glands have different morphological subtypes. Sometimes this may be due to a specific genetic alteration that is realized in a specific morphological phenotype. Finding such relationships can help in the subsequent correct interpretation of morphological changes, which leads to an accurate diagnosis.

Some recurrent genetic alterations can serve not only as a diagnostic tool but also gained importance as therapeutic targets. For instance, the finding of *NTRK1/2/3* gene fusion that encodes tropomyosin-related kinase transmembrane proteins TRKA, TRKB, and TRKC in secretory carcinoma and leads to the activation of cell growth, makes it possible to treat patients with such tumors using the NTRK inhibitors [8].

Other rare tumors with a variety of genetic rearrangements are sinonasal neoplasm. Sinonasal malignancies make up <5% of all head and neck neoplasms, with an incidence of 0.556 per 100,000 individuals per year [61]. The current WHO classification of sinonasal tumors is listed in Table 3 [2]. It includes a few entities, the diagnosis of which is based on genetic events (e.g., SWI/SNF complex-deficient sinonasal carcinomas, NUT and *DEK*::*AFF2* carcinoma, *IDH*-mutant sinonasal malignancies). Some genetic alterations have correlated with specific morphological features, e.g., SWI/SNF complex-deficient sinonasal carcinomas with monomorphic structure and sometimes with rhabdoid phenotype, NUT carcinoma with monotonous undifferentiated cells and abrupt keratinization focuses.

Table 3 WHO classification of the sinonasal tumors 2022

Benign epithelial lesions and tumors	**Malignant epithelial tumors**
Respiratory epithelial adenomatoid hamartoma Seromucinous hamartoma Nasal chondromesenchymal hamartoma Sinonasal papilloma, inverted type Sinonasal papilloma, oncocytic type Sinonasal papilloma, exophytic type	Keratinizing squamous cell carcinoma Non-keratinizing squamous cell carcinoma NUT carcinoma SWI/SNF complex-deficient sinonasal carcinoma Sinonasal lymphoepithelial carcinoma Sinonasal undifferentiated carcinoma Teratocarcinosarcoma HPV-associated multiphenotypic sinonasal carcinoma Intestinal-type sinonasal adenocarcinoma Non-intestinal-type sinonasal adenocarcinoma
Mesenchymal tumours of the sinonasal tract Sinonasal tract angiofibroma Sinonasal glomangiopericytoma Biphenotypic sinonasal sarcoma Chordoma	Other sinonasal tumours Sinonasal ameloblastoma Adamantinomatous craniopharyngioma Meningioma of the sinonasal tract, ear, and temporal bone Olfactory neuroblastoma

Immunohistochemistry (IHC) has an important role in the differential diagnosis of sinonasal neoplastic lesions, especially in poorly differentiated cases. Sometimes, IHC is also

used as a surrogate cost-effective method for the identification of genetic rearrangements (e.g., NUT protein as a marker of *NUTM1* gene rearrangement in NUT carcinoma, SMARCB1 or SMARCA4 proteins as markers of inactivating SMARCB1 or SMARCA4 mutations in SWI/SNF-deficient sinonasal carcinomas, etc).

In recent years, some entirely new entities were added to the WHO classification of sinonasal tumors. Their immunohistochemical features and genetic findings specific to these neoplasms are summarized in Table 4.

Table 4 Immunohistochemical and genetic findings in novel sinonasal entities

Tumor type	IHC	Molecular profile
DEK::AFF2 carcinoma	panCK, CK5/6, p63, p40, EMA	*DEK::AFF2*
ETV6::TNFRSFs carcinoma	panCK, CK5/6, p63, p40, EMA	*ETV6::TNFRSF8*
NUT carcinoma	panCK, CK5/6, p63, p40	*NUT::BRD4* t(15,19), rarely *NUT::BRD3* and *NUT::NSD3*
IDH2 mutated carcinoma	CK7, IDH1/2	*IDH 2 R172S, R172T, and R172M*
Non-ITAC	panCK, CK7, CDX2, MUC2	*ETV6::NTRK3, ETV6::RET, OTX1*
ACC	CD117 (inner epithelial cells) and p63, SMA (peripheral myoepithelial cells). MMP-7, 25 (better prognosis) and MMP-9, 15 (poor prognosis)	*MYB::NFIB* t(6,9), *KIT, EGFR, FGFR1, VEGF, NOTCH1/2/3, EN1, DLX6, OTX1*
INI1/SMARCB1- deficient carcinoma	panCK, CK5, p63, CK7, neuroendocrine markers. INI1 loss	*SMARCB1* deletion
BRG/SMARCA4-deficient carcinoma	panCK, neuroendocrine markers. BRG/SMARCA4 loss DEK::AFF2	Loss-of-function/ truncating mutations in *SMARCA4*
HPV-related multiphenotypical carcinoma	panCK, S100, actin, calponin, p63 (myoepithelial cells) and CD117, CK7 (ductal cells). SOX10, LEF-1	Negativity for *MYB, MYBL1, or NFIB* fusion genes
Biphenotypic Sinonasal Sarcoma	S100, SMA, calponin, b-catenin	*PAX3::MAML3* t(2;4)

	Variable desmin, myogenin, factor XIIIa	
Adamantinoma-like Ewing sarcoma	CD99, NKX2.2, NSE, S100, Fli-1, synaptophysin, chromogranin	*FET::ETS,* typicaly *EWSR1::FLI1* t(22;11)
TFCP2-Rhabdomyosarcoma	desmin, myogenin, myosin, myoglobin	*TFCP2::EWSR1/FUS*

In the dissertation thesis, the new subtypes of rare salivary gland tumors were delineated based on the application of IHC and the broad spectrum of molecular tests. We also described new gene fusions for some tumors and gave the possible genotype-phenotype correlations for tumor subtypes.

Due to the wide variety of salivary gland tumors, in the dissertation, the author focuses on the clinicopathological, morphological, immunohistochemical, and molecular biologic characteristics of selected benign and malignant rare salivary gland and sinonasal tumors. The results of the studies have been published in 6 articles in high-ranking American and European journals with impact factors in which the author is listed as the first author and as a co-author. The dissertation consists of comments on the publications. All publications are accompanied by a copy of the reprints (5 articles) or by the submitted and accepted manuscripts with proof of acceptance (1 article).

The first part of the doctoral thesis is concentrated on epithelial salivary gland tumors, including a rare oncocytic variant of mucoepidermoid carcinoma and a clear cell variant of myoepithelial carcinoma, acinic cell carcinoma and a rare benign tumor named sclerosing polycystic adenoma.

The second part focused on selected rare mesenchymal sinonasal tumors, such as *EWSR1::POU2AF3* (*COLCA2*) sarcomas and biphenotypic sinonasal sarcomas due to the presence of similar genetic alterations with salivary gland tumors.

GOALS AND HYPOTHESIS

The goals of the dissertation "Clinicopathological, morphological, immunohistochemical, and molecular biological characteristics of rare salivary gland tumors" include:

1. Revise rare variants of salivary gland tumors for identifying diagnostic criteria and distinguishing tumors with different biological behavior.
2. Identify specific immunohistochemical markers that can aid in the differential diagnosis of rare salivary gland and sinonasal tumors.
3. Investigate the molecular biological characteristics of rare salivary gland and sinonasal tumors, including genetic alterations, mutations, and molecular pathways involved in tumor development and progression, identifying potential therapeutic targets and predictive markers.
4. Establish correlations between the clinical presentation, histopathology, and molecular profile to aid in their accurate diagnosis and clinical management.
5. Add new data to the tumor registry for rare salivary gland tumors to facilitate research, sharing of data, and collaborative efforts in understanding these diseases.

By pursuing these goals, we can improve the understanding diagnosis, and management of rare tumors in the salivary gland and sinonasal pathology, ultimately leading to better patient outcomes for those affected by these uncommon neoplasms.

MATERIALS AND METHODS

Clinical and follow-up information was obtained from the medical databases or referring pathologists.

Immunohistochemistry

Immunohistochemistry (IHC) for some projects was performed at several different laboratories based on the original differential diagnostic considerations (staining protocols and antibody sources are available upon request). For such studies, some markers were added in selected cases for the purposes of every study. In other research for IHC analysis, 4-µm-thick sections were cut from paraffin blocks and mounted on positively charged slides (TOMO; Matsunami Glass IND, Japan). Sections were processed on a BenchMark ULTRA (Ventana Medical System, Tucson, AZ), deparaffinized, and then subjected to heat-induced epitope retrieval by immersion in a CC1 solution at 95°C and pH 8.6, CC2, citrate buffer, pH 6.0, 92°C; EnVision High pH, pH 9,0, 97°C or EnVision low pH, pH 6.0, 97°C. All primary antibodies used are summarized in Table 5. The bound antibodies were visualized using the ultraView Universal DAB Detection Kit (Roche, Basel, Switzerland) and the ultraView Universal Alkaline Phosphatase Red Detection Kit (Roche, Basel, Switzerland). The slides were counterstained with Mayer hematoxylin. Appropriate positive and negative controls were employed.

Table 5 Antibodies Used for IHC Studies

Antibody	Clone	Dilution	Antigen Retrieval/ Time	Source
***EWSR1::POU2AF3 (COLCA2)* sarcomas study**				
GFAP	Polyclonal	RTU	CC1/36 min	Dako
SATB2	EP281	1:100	CC1/36 min	Cell Marque
Synaptophysin	SP11	RTU	CC1/44 min	Ventana
Chromogranin	LK2H10	RTU	CC1/36 min	Ventana
CD56	123C3	RTU	CC1/36 min	Ventana
INSM1	BSB-123	RTU	CC1/36 min	BioSB

Salivary oncocytic mucoepidermoid carcinomas study				
MIA	113-1	1:100	CC1/36 min	BioGenex
S100 protein	Polyclonal	RTU	CC1/20 min	Ventana
CK7	OV-TL 12/30	1:200	CC1/36 min	Dako
CK 14	SP53	RTU	CC1/64 min	Ventana
CK 5/6	D5/16B4	1:50	CC1/36 min	Dako
p63	4A4	RTU	CC1/64 min	Ventana
p40	Polyclonal	RTU	CC1/52 min	Biocare Medical
SOX10	Polyclonal	1:100	CC1/64 min	Cell Marque
MIB1	30-9	RTU	CC1/64 min	Ventana
Clear Cell Myoepithelial Carcinoma of Salivary Glands Study				
S100 protein	Polyclonal	RTU	CC1/20 min	Ventana
CK7	OV-TL 12/30	1:200	CC1/36 min	Dako
CK 14	SP53	RTU	CC1/64 min	Ventana
p63	4A4	RTU	CC1/64 min	Ventana
p40	Polyclonal	RTU	CC1/52 min	Biocare Medical
SOX10	Polyclonal	1:100	CC1/64 min	Cell Marque
MIB1	30-9	RTU	CC1/64 min	Ventana
SMA	1A4	RTU	CC1/36 min	Cell Marque
Calponin	EP798y	RTU	CC1/36 min	Ventana
SMARCB1	INI1	RTU	CC1/52 min	Cell Marque
SMARCA4	BRG-1	1:10000	CC1/52 min	AbCam
Sclerosing Polycystic Adenoma of Salivary Glands Study				
S100 protein	Polyclonal	RTU	EnVision high pH/30 min	Dako
CK7	OV-TL 12/30	RTU	EnVision high pH/30 min	Dako

AE1-AE3	AE1-AE3	RTU	CC1/64 min	Dako
p63	DAK-p63	RTU	EnVision low pH/30 min	Dako
p40	Polyclonal	RTU	CC1/52 min	Biocare Medical
SOX10	SP267	RTU	CC1/64 min	Cell Marque
MIB1	30-9	RTU	CC1/64 min	Ventana
Calponin	EP798Y	RTU	CC1/36 min	Dako
Mammaglobin	304-1A5	RTU	EnVision high pH/30 min	Dako
DOG1	SP31	RTU	CC1/36 min	Cell Marque
NOR-1	H-7	1:50	CC2/68 min	Ventana
PLAG1	3B7	1:100	CC1/64 min	Sigma Aldrich
AR	SP107	RTU	CC1/64 min	Cell Marque
Ki-67	MIB1	RTU	EnVision high pH/30 min	Dako
GATA3	L50-823	1:200	CC1/52 min	BioCareMedical
Acinic cell carcinoma of the salivary glands with *NR4A2* rearrangement study				
DOG1	SP31	RTU	CC1/36 min	Ventana
NR4A2	N1404	1:100	CC1/64 min	Abcam
NR4A3	H-7	1:50	CC1/64 min	Santa Cruz
SOX10	SP267	RTU	CC1/64 min	Ventana

CC1 indicates EDTA buffer, pH 8.6, 95°C; CC2, citrate buffer, pH 6.0, 92°C; EnVision High pH, pH 9,0, 97°C; EnVision low pH, pH 6.0, 97°C; RTU, ready to use.

Molecular-genetic study

NGS Sequencing and PCR

For NGS and RT-PCR analysis, 2 to 3 FFPE sections (10 μm thick) were macrodissected to isolate tumor-rich regions. Samples were extracted for total nucleic acid using Agencourt FormaPure Kit (Beckman Coulter, Brea, CA). To assess RNA quality, the PreSeq RNA QC assay using iTaq Universal SYBR Green Supermix (Biorad, Hercules, CA) was performed on all samples during library preparation to generate a measure of the integrity of RNA (in the form of a cycle threshold [Ct] value). Library preparation and RNA QC were

performed following the Archer FusionPlex Protocol for Illumina (ArcherDX Inc., Boulder, CO). RNA sequencing was performed using various customized versions of FusionPlex assay (Archer, Inc) or TruSight RNA Fusion panel (Illumina Inc.), while DNA and RNA sequencing was performed using TruSight Oncology 500 kit (Illumina Inc.) or QIAGEN's (Germantown, MD) QIAseq chemistry.

Final libraries were diluted to 1:100,000 and quantified in a 10 µL reaction following the Library Quantification for Illumina Libraries protocol and assuming a 200 bp fragment length (KAPA, Wilmington, MA). The concentration of final libraries was around 200 nM. The threshold representing the minimum molar concentration for which sequencing can be robustly performed was set at 50 nM.

Libraries were diluted to 4 nM and sequenced on a NextSeq sequencer (Illumina, San Diego, CA). The optimal number of raw reads per sample was set to 3 million. Library pools were diluted to 1.6 pM library stock with 20% 1.8 pM PhiX and loaded in the NextSeq cartridge.

The fusion and other rearrangement detection algorithm in Archer Analysis relies on the specificity of the gene-specific primers used in the amplification steps in the AMP process. The resulting FASTQ files were analyzed using the Archer Analysis software (version 5.1.7; or 6.2 ArcherDX Inc.).

The RNA from FFPE tissue samples was isolated using Transcriptor First Strand cDNA Synthesis Kit (Roche). For the fusion detection, 2 µl of cDNA was added to a reaction consisting of 12.5 µl of HotStar Taq PCR Master Mix (QIAGEN), 10 pM of each primer (Table 6), and distilled water up to 25 µl. The amplification program comprised initial denaturation at 95°C for 14 minutes, then 40 cycles of denaturation at 95° C for 1 minute, annealing at 55°C for 1 minute, and extension at 72°C for 1.5 minutes. The program was finished by incubation at 72°C for 7 minutes.

Successfully amplified polymerase chain reaction products of fusion transcript were purified using Agencourt AMPure (Agencourt Bioscience Corporation, A Beckman Coulter Company, Beverly, MA). Then, the polymerase chain reaction products were sequenced both sides using a Big Dye Terminator Sequencing kit (Applied Biosystems, California), purified using the Agencourt CleanSEQ kit (Agencourt Bioscience Corporation), and run on an automated genetic analyzer ABI Prism 3130xl (Applied Biosystems) at a constant voltage of

13.2 kV for 20 minutes and compared with the GenBank sequence database. All primers used are summarized in Table 6.

Table 6. Names of primers used for the detection of fusions by PCR

Name of Primer	Sequence 5′-3′
CRTC1A (outer)	TCGCGCTGCACAATCAGAAG
CRTC1B (inner)	GAGGTCATGAAGGACCTGAG
MAML2A (outer)	GGTCGCTTGCTGTTGGCAGG
MAML2B (inner)	TTGCTGTTGGCAGGAGATAG
CHCHD27-PLAG1-F2	TTGACGTGTTTGGAGCTGGA
CHCHD27-PLAG1-R2	TCTTAGCCAGTCCCATTGACTC

FISH Analysis

4 μm thick FFPE sections were placed onto positively charged slides. Hematoxylin and eosin–stained slides were examined for the determination of areas for cell counting.

The unstained slides were deparaffinized and incubated in the 1× Target Retrieval Solution Citrate pH 6 (Dako, Glostrup, Denmark) at 95°C for 40 minutes and subsequently cooled for 20 minutes at room temperature in the same solution. Slides were washed in deionized water for 5 minutes and digested in protease solution with pepsin (0.5 mg/mL) (Sigma Aldrich, St. Louis, MO) in 0.01 M HCl at 37°C for 35 to 60 minutes according to the sample conditions. Slides were then placed into deionized water for 5 minutes, dehydrated in a series of ethanol solutions (70%, 85%, 96% for 2 min each), and air-dried.

For the detection of rearrangements, the commercial probes used are summarized in Table 7.

An appropriate amount of mixed and premixed probes was applied on specimens, covered with a glass coverslip, and sealed with rubber cement. Slides were incubated in the ThermoBrite instrument (StatSpin/Iris Sample Processing, Westwood, MA) with denaturation at 85°C/8 minutes and hybridization at 37°C/16 hours. The rubber-cemented coverslip was then removed and the slide was placed in a posthybridization wash solution (2×SSC/0.3% NP-

40) at 72°C/2 minutes. The slide was air-dried in the dark, counterstained with 4′,6′-diamidino-2-phenylindole DAPI (Vysis/Abbott Molecular), coverslipped, and immediately examined.

Table 7. Names of probes used for the FISH analysis.

Names of probe	Source	Cut-off
ZytoLight SPEC *MAML2* Dual Color Break-Apart Probe	ZytoVision GmbH, Bremerhaven, Germany	10%
Vysis *EWSR1* Break-Apart (BA) FISH Probe Kit	Abbott Molecular, IL	10%
oligo probe SureFISH 12/q13.12 *ATF1* BA	SureFISH/ Agilent Technologies, Santa Clara, CA, USA	10%
SureFISH 8q12.1 *PLAG1* BA	SureFISH/ Agilent Technologies, Santa Clara, CA, USA	10%
SureFISH *NR4A2* break-apart probe	SureFISH/ Agilent Technologies, Santa Clara, CA, USA	10%
ZytoLight SPEC *NR4A3* Dual Color Break Apart Probe	ZytoVision Gmbh, Bremerhaven, Germany	10%
SureFISH *MAML3* break-apart probe	SureFISH/ Agilent Technologies, Santa Clara, CA, USA	10%
SureFISH *PAX3* (2q36.1) break-apart probe	SureFISH/ Agilent Technologies, Santa Clara, CA, USA	10%

The sections were examined with an Olympus BX51 fluorescence microscope (Olympus Corporation, Tokyo, Japan) using a ×100 objective and filter sets triple bandpass (DAPI/SpectrumGreen/SpectrumOrange), dual bandpass (SpectrumGreen/SpectrumOrange) and Single Bandpass (SpectrumGreen or SpectrumOrange).

For each probe, we selected 100 randomly nonoverlapping tumor cell nuclei and examined them for the presence of fluorescent signals. The yellow signals were regarded as negative; separate orange and green signals were considered positive. The distance between separate signals should be > 2 diameters of signal apart. Cutoff values for break-apart probes were set to > 10% of nuclei with chromosomal breakpoint (mean+3 SD in normal non-neoplastic control tissues).

COMMENTED PUBLICATIONS

1. PART – SALIVARY GLAND TUMORS

1.1 MOLECULAR PROFILING OF SALIVARY ONCOCYTIC MUCOEPIDERMOID CARCINOMAS HELPS TO RESOLVE DIFFERENTIAL DIAGNOSTIC DILEMMA WITH LOW-GRADE ONCOCYTIC LESIONS

The oncocytic variant of mucoepidermoid carcinoma (OMEC) is a rare variant of mucoepidermoid carcinoma (MEC), but it poses diagnostic challenges due to its overlapping morphological features with benign and low-grade malignant salivary gland tumors with oncocytic morphology [9-11]. Typically, the diagnosis of mucoepidermoid carcinoma is foregone by the identification of mucin-containing cells. The presence of mucin-containing cells, mucinous cysts formations, and foci of extravasated mucin are considered characteristic features of MEC. However, in OMECs, true mucocytes may be few and difficult to identify or completely absent, making the diagnosis potentially inaccurate.

Although most OMECs are low-grade tumors with a favorable prognosis, they can exhibit locally aggressive behavior, emphasizing the importance of an accurate diagnosis.

In our study, we reviewed 125 archived cases of tumors classified as "low-grade/uncertain oncocytic tumor," "oncocytoma," and "oncocytic carcinoma" from 1996 to 2019. As a result of our work, 22 cases were reclassified as OMEC.

In our study, we described the morphological features of OMEC. The tumors showed nested and multinodular growth patterns composed of oncocytic cells, most tumors have invasive growth into the surrounding tissues. Encapsulated tumors are also present in minority cases. The oncocytic changes of neoplastic cells covered up to 100% of all tumor cells. In some cases represented by solid nests and sheets of large oncocytic cells, true mucocytes were completely absent. Focally, there were tubular structures with dense intraluminal secretions lined by oncocytes. The conventional non-OMEC structure was not seen.

We also identified the immunohistochemical characteristics that could be useful in routine histological examinations, such as strong diffuse nuclear staining for p63 and p40 proteins. The staining was distributed throughout the solid oncocytic nests and was abluminal in glandular/tubular structures. Antimitochondrial antigen (MIA) was also diffuse positive. In some cases, OMEC displayed double-layered tubular structures with concentrations of p40 and p63 staining on the periphery of the nests, similar to the staining pattern seen in oncocytoma. We believe that strong diffuse staining of tumor cells for p63, along with corresponding morphological changes, is in favor of OMEC and, in the absence of other specific features, requires further molecular-genetic testing.

Importantly, conventional MECs are negative for SOX10, unlike OMECs, which can show both positive and negative reactions. This difference makes SOX10 less useful in the differential diagnosis of OMEC with other salivary gland tumors.

MECs are harboring *CRTC1::MAML2* or *CRTC3::MAML2* gene fusions in up to 80% of cases [12,13,14,15,16,17]. In our study, we found *CRTC1::MAML2* gene fusion in 59% of OMEC cases. *CRTC3::MAML2* gene fusion was detected in only 1 case (4.5%). Interestingly, the tumor harboring a *CRTC3::MAML2* fusion has S100 protein and SOX10 positivity. 23% of OMEC cases were negative on NGS but *MAML2* rearrangement was confirmed by FISH.

In conclusion, we recommend *MAML2* rearrangement testing for all patients with salivary gland tumors exhibiting oncocytic morphology to identify this rare variant of MEC achieving an accurate morphological diagnosis.

Molecular Profiling of Salivary Oncocytic Mucoepidermoid Carcinomas Helps to Resolve Differential Diagnostic Dilemma With Low-grade Oncocytic Lesions

Alena Skálová, MD, PhD,† Abbas Agaimy, MD,‡ Olga Stanowska, MD,§ Martina Baneckova, MD,*† Nikola Ptáková, MSc,‖ Laura Ardighieri, MD,¶ Piero Nicolai, MD, PhD,# Davide Lombardi, MD,** Monika Durzynska, MD,§ Luigi Corcione, MD,†† Jan Laco, MD, PhD,‡‡ Olena Koshyk, MD,§§ Radim Žalud, MD,‖‖ Michal Michal, MD,* Tomáš Vanecek, PhD,‖ and Ilmo Leivo, MD, PhD¶¶##*

Abstract: Oncocytic mucoepidermoid carcinoma (OMEC) is a rare but diagnostically challenging variant of mucoepidermoid carcinoma (MEC). OMEC is notable for differential diagnostic considerations that are raised as a result of overlap with other benign and low-grade oncocytic salivary gland tumors. Diffuse and strong immunoreactivity of p63 protein may be useful in distinguishing OMEC from its mimics. However, focal p63 staining can be present in benign oncytomas. Presence of mucin-containing cells, mucinous cystic formation, and foci of extravasated mucin are considered a hallmark of MEC. True mucocytes may be, however, very few and hardly discernable in OMECs. Recent evidence has shown that most MECs harbor gene fusions involving *MAML2*. A retrospective review of archived pathology files and the authors' own files was conducted to search for "low-grade/uncertain oncocytic tumor," "oncocytoma," and "oncocytic carcinoma" in the period from 1996 to 2019. The tumors with IHC positivity for p63 and/or p40, and S100 negativity, irrespective of mucicarmine staining, were tested by next-generation sequencing using fusion-detecting panels to detect *MAML2* gene rearrangements. Two index cases from consultation practice (A.S. and A.A.) of purely oncocytic low-grade neoplasms without discernible mucinous cells showed a *CRTC1-MAML2* fusion using next-generation sequencing, and were reclassified as OMEC. In total, 22 cases of oncocytic tumors, retrieved from the authors' files, and from the Salivary Gland Tumor Registry, harbored the *MAML2* gene rearrangements. Presence of mucocytes, the patterns of p63 and SOX10 immunopositivity, and mucicarmine staining were inconsistent findings. Distinguishing OMEC devoid of true mucinous cells from oncocytoma can be very challenging, but it is critical for proper clinical management. Diffuse and strong positivity for p63 and visualization of hidden mucocytes by mucicarmine staining may be misleading and does not always suffice for correct diagnosis. Our experience suggests that ancillary studies for the detection of *MAML2* rearrangement may provide useful evidence in difficult cases.

Key Words: salivary gland neoplasms, mucoepidermoid carcinoma, oncocytic, *MAML2*, oncocytoma, gene fusion, *CRTC1-MAML2*

(*Am J Surg Pathol* 2020;44:1612–1622)

From the *Department of Pathology, Faculty of Medicine in Pilsen, Charles University; †Biopticka Laboratory Ltd; ‖Molecular and Genetic Laboratory, Biopticka Laboratory Ltd, Pilsen; ‡‡The Fingerland Department of Pathology, Charles University, Faculty of Medicine and University Hospital Hradec Kralove, Hradec Kralove; ‖‖Department of Pathology, Regional Hospital Kolín, Kolín, Czech Republic; ‡Department of Pathology, Friedrich-Alexander University Erlangen-Nürnberg (FAU), University Hospital of Erlangen, Erlangen, Germany; §Department of Pathology and Laboratory Diagnostics, Maria Sklodowska-Curie National Research Institute of Oncology, Warsaw, Poland; ¶Department of Pathology, Hospital Spedali Civili; **Department of Otorhinolaryngology—Head and Neck Surgery, University of Brescia, Brescia; #Department of Otorhinolaryngology—Head Neck Surgery, University of Padua, Padua; ††Department of Pathology, University of Parma, Parma, Italy; §§Medical Laboratory CSD, Kyiev, Ukraine; ¶¶Institute of Biomedicine, University of Turku; and ##Department of Pathology, Turku University Hospital, Turku, Finland.

Preliminary results of the study were presented as a poster presentation at the 109th Annual Meeting of the USCAP, Los Angeles, CA, February 29 to March 5, 2020.

Conflicts of Interest and Source of Funding: Supported in part by study grant SVV 260 539 from the Ministry of Education, Czech Republic and the Finnish Cancer Society, Helsinki, Finland. The authors have disclosed that they have no significant relationships with, or financial interest in, any commercial companies pertaining to this article.

Correspondence: Alena Skálová, MD, PhD, Sikl's Department of Pathology, Faculty of Medicine in Pilsen, Charles University, E. Benese 13, Pilsen 305 99, Czech Republic (e-mail: skalova@fnplzen.cz).

Salivary gland carcinomas represent <10% of head and neck malignancies, the most common type being mucoepidermoid carcinoma (MEC).[1,2] MEC is a distinctive salivary gland malignancy composed of mucinous, intermediate, clear, and squamoid neoplastic cells arranged in cystic and solid growth patterns in variable proportions.[1] Morphologic features compatible with low-grade MECs include the presence of cells with true intracytoplasmic mucin, intermediate and squamoid cells, and usually combined solid and cystic growth patterns. In intermediate-grade and high-grade MECs intermediate cells may not always be readily identifiable and in high-grade MECs cells with intracytoplasmic mucin may be scarce

and difficult to identify. The diagnosis of MEC is, however, generally straightforward on histologic grounds alone. In less typical cases, the application of mucicarmine or Alcian blue (AB)/periodic acid-Schiff (PAS) or PAS-diastase stain could facilitate the identification of true intracytoplasmic mucin. There is, however, a spectrum of rare monomorphic variant tumors, such as sclerosing, oncocytic, and clear-cell MECs that differ from the conventional appearance, and in these cases a correct diagnosis can be very difficult.

Oncocytic mucoepidermoid carcinoma (OMEC) is a rare and diagnostically challenging variant of MEC.[3] Before the Weinreb et al's[3] paper, in which the authors report 12 cases, only case reports of this lesion have been published.[4–10] Most of such neoplasms were described as low grade, and having a good prognosis, but the method of their grading was not always well defined. OMEC is notable for differential diagnostic considerations that are raised as a result of overlap with other benign and low-grade oncocytic salivary gland tumors.[3,11] Diffuse and strong immunoreactivity for p63 protein may be useful in distinguishing OMEC from its mimics. Salivary oncocytomas and oncocytic carcinomas are, however, also invariably positive for p63, even if the immunopositivity seems to be largely restricted to the most peripheral or basal layers of the individual tumor nests.[12,13] Presence of mucin-containing cells, mucinous cystic formation, and foci of extravasated mucin are considered a hallmark of MEC.[1] True mucocytes, however, may be very few and hardly discernible in OMECs.

Recent evidence has shown that up to 80% of MECs harbor gene fusions involving *MAML2*, with the highest occurrence in low-to-intermediate–grade tumors.[14–19] Even though the *MAML2* alteration is specific for MEC, *MAML2* testing is generally regarded as unnecessary. The role of *MAML2* testing as a diagnostic adjunct is reserved for those tumors that differ from the conventional appearance of MEC and more closely resemble some other tumor types. In those MECs where the histologic picture is dominated by oncocytic cells (ie, oncocytic variant of MEC), the finding of a *MAML2* rearrangement is extremely useful in distinguishing the OMECs from other oncocyte-rich neoplasms including oncocytoma and oncocytic carcinoma.[11,20]

Recently, 2 index cases of low-grade oncocytic neoplasms without any mucous cells, received as consultation cases with primary diagnosis of oncocytoma/oncocytic tumor of uncertain malignancy (A.A. and A.S.), were reclassified as OMEC, based on molecular profiling. To examine the usefulness of *MAML2* testing, we collected a cohort of oncocytic neoplasms from the consultation files of the authors, and identified 22 cases, which were reclassified as OMECs. In this study, we highlight the usefulness of *MAML2* testing in the identification of challenging variants of MEC.

MATERIALS AND METHODS

The study was approved by the institutional review board. A retrospective review of Salivary Gland Tumor Registry (A.S.) was conducted to search for "low-grade/uncertain oncocytic tumor," "oncocytoma," and "oncocytic carcinoma" in the period from 1996 to 2019. The search yielded 125 salivary gland neoplasms. Clinical features and outcomes, for example age, sex, site of the primary tumor, follow-up period, recurrence, and distant metastasis, were recorded. All slides were reviewed by 3 pathologists (A.S., M.B., and O.S.) to collect the following pathologic parameters: predominant oncocytic features (>75% tumor cells), solid and cystic growth pattern (>50% solid), at least focal invasive growth, and features suspicious of malignancy, such as cellular atypia, necrosis, and/or enhanced mitotic and proliferative activity. Any unusual histologic features were documented.

All cases retrieved from archived salivary gland pathology files in Pilsen were stained with mucicarmine, PAS, and/or AB/PAS and investigated immunohistochemically (IHC) for S100 protein, SOX10, and p63/p40 proteins. This search yielded 19 oncocytic tumors with IHC positivity for p63 and/or p40, and S100 negativity (19/125). In addition, available cases of oncocytic neoplasms considered as OMECs were retrieved from the archived pathology files and personal consultation files of the coauthors. Irrespective of mucicarmine staining and SOX10/p63 immunostaining results, 30 selected neoplasms were tested by next-generation sequencing (NGS) using fusion-detection panels to detect *MAML2* gene rearrangements. The NGS results were confirmed by reverse-transcription polymerase chain reaction (RT-PCR) and/or fluorescence in situ hybridization (FISH).

For conventional microscopy, the excised tissues were fixed in formalin, processed routinely, embedded in paraffin (FFPE), cut, and stained with hematoxylin andeosin.

For IHC analysis, 4-μm-thick sections were cut from paraffin blocks and mounted on positively charged slides (TOMO; Matsunami Glass IND, Japan). Sections were processed on a BenchMark ULTRA (Ventana Medical System, Tucson, AZ), deparaffinized and then subjected to heat-induced epitope retrieval by immersion in a CC1 solution at pH 8.6 at 95°C. All primary antibodies used are summarized in Table 1. The bound antibodies were visualized using the ultraView Universal DAB Detection

TABLE 1. Antibodies Used for IHC Study

Antibody Specificity	Clone	Dilution	Antigen Retrieval/ Time	Source
MIA	113-1	1:100	CC1/36 min	BioGenex
S100 protein	Polyclonal	RTU	CC1/20 min	Ventana
CK7	OV-TL 12/30	1:200	CC1/36 min	DakoCytomation
CK 14	SP53	RTU	CC1/64 min	Ventana
CK 5/6	D5/16B4	1:50	CC1/36 min	Dako
p63	4A4	RTU	CC1/64 min	Ventana
p40	Polyclonal	RTU	CC1/52 min	Biocare Medical
SOX10	Polyclonal	1:100	CC1/64 min	Cell Marque
MIB1	30-9	RTU	CC1/64 min	Ventana

CC1 indicates EDTA buffer, pH 8.6; RTU, ready to use.

Kit (Roche, Basel, Switzerland) and ultraView Universal Alkaline Phosphatase Red Detection Kit (Roche). The slides were counterstained with Mayer hematoxylin. Appropriate positive and negative controls were used.

Where available, clinical follow-up information was obtained from hospitals records, the patients, their physicians, or from referring pathologists.

MOLECULAR GENETIC STUDY

Sample Preparation for NGS and RT-PCR

For NGS and RT-PCR analysis, 2 to 3 FFPE sections (10 μm thick) were macrodissected to isolate tumor-rich regions. Samples were extracted for total nucleic acid using Agencourt FormaPure Kit (Beckman Coulter, Brea, CA). The RNA integrity was evaluated using PreSeq RNA QC Assay as was previously described.[21]

RNA Integrity Assessment and Library Preparation for NGS

Unless otherwise indicated, 250 ng of FFPE RNA was used as input for NGS library construction. To assess RNA quality, the PreSeq RNA QC assay using iTaq Universal SYBR Green Supermix (Biorad, Hercules, CA) was performed on all samples during library preparation to generate a measure of the integrity of RNA (in the form of a cycle threshold [C_t] value). Library preparation and RNA QC were performed following the Archer FusionPlex Protocol for Illumina (ArcherDX Inc., Boulder, CO). The Archer FusionPlex Solid Tumor Kit or *ETV6-EWSR1-MAML2* custom Archer Fusion Plexkit were used. Final libraries were diluted to 1:100,000 and quantified in a 10 μL reaction following the Library Quantification for Illumina Libraries protocol and assuming a 200 bp fragment length (KAPA, Wilmington, MA). The concentration of final libraries was around 200 nM. Threshold representing the minimum molar concentration for which sequencing can be robustly performed was set at 50 nM.

NGS Sequencing and Analysis

Libraries were diluted to 4 nM and sequenced on a NextSeq sequencer (Illumina, San Diego, CA). The optimal number of raw reads per sample was set to 3 million. Library pools were diluted to 1.6 pM library stock with 20% 1.8 pM PhiX and loaded in the NextSeq cartridge.

The fusion and other rearrangement detection algorithm in Archer Analysis relies on the specificity of the gene-specific primers used in the amplification steps in the AMP process. The resulting FASTQ files were analyzed using the Archer Analysis software (version 5.1.7; ArcherDX Inc.)

RNA Preparation for CRTC1-MAML2 Fusion Polymerase Chain Reaction

The RNA from FFPE tissue samples was reverse transcribed using Transcriptor First Strand cDNA Synthesis Kit (Roche) according to manufacturer´s instructions. RNA integrity was determined by control polymerase chain reaction (PCR) comprising 2 μL of cDNA, 12.5 μL of HotStarTaq PCR Master Mix (QIAGEN, Hilden, Germany), 10 pM of each primer, and distilled water up to 25 μL. The amplification program comprised 95°C for 14 minutes, then 40 cycles of denaturation at 95°C for 1 minute, annealing at 60°C for 0.5 minute, extension at 72°C for 1 minute, and final extension at 72°C for 7 minutes. Samples with RNA integrity below 133 bp (showing <2 desired bands on agarose gel) were excluded from further analysis.

TABLE 2. Names of Primers Used for the Detection of *CRTC1-MAML2* Fusion by PCR

Name of Primer	Sequence 5′-3′
CRTC1A (outer)	TCGCGCTGCACAATCAGAAG
CRTC1B (inner)	GAGGTCATGAAGGACCTGAG
MAML2A (outer)	GGTCGCTTGCTGTTGGCAGG
MAML2B (inner)	TTGCTGTTGGCAGGAGATAG

Detection of CRTC1-MAML2 Fusion by PCR

Two microliters of cDNA was added to the PCR reaction consisting of 12.5 μL of HotStarTaq PCR Master Mix (QIAGEN), 10 pmol of each outer primer complementary to *CRTC1-MAML2* fusion transcripts (Table 2), and distilled water up to 25 μL. The amplification conditions comprised denaturation at 95°C for 14 minutes and then 35 cycles of denaturation at 95°C for 30 seconds, annealing at 55°C for 30 seconds, and extension at 72°C for 30 seconds.

The PCR product from the first run was diluted with distilled water at a ratio of 1:50. One microliter of the diluted product was added to a second run of the same PCR with the same reagents as in the first run except for the inner primers (Table 2).

Successfully amplified PCR products of the *CRTC1-MAML2* fusion gene were purified using Agencourt AMPure (Agencourt Bioscience Corporation, A Beckman Coulter Company). Then, the PCR products were both sides sequenced using the BigDye Terminator Sequencing kit (Applied Biosystems, CA), purified using Agencourt Clean SEQ kit (Agencourt Bioscience Corporation) and run on an automated genetic analyzer ABI Prism 3130xl (Applied Biosystems) at a constant voltage of 13.2 kV for 20 minutes and compared with the GenBank sequence database.

FISH Analysis of MAML2 Rearrangement

Four-micrometer-thick FFPE sections were placed onto positively charged slides. Hematoxylin and eosin–stained slides were examined for the determination of areas for cell counting.

The unstained slides were deparaffinized and incubated in the 1× Target Retrieval Solution Citrate pH 6 (Dako, Glostrup, Denmark) at 95°C for 40 minutes and subsequently cooled for 20 minutes at room temperature in the same solution. Slides were washed in deionized water for 5 minutes and digested in protease solution with pepsin (0.5 mg/mL) (Sigma Aldrich, St. Louis, MO) in 0.01 M HCl at 37°C for 35 to 60 minutes according to the

sample conditions. Slides were then placed into deionized water for 5 minutes, dehydrated in a series of ethanol solution (70%, 85%, 96% for 2 min each), and air-dried.

For the detection of *MAML2* rearrangement, the commercial probe ZytoLight SPEC MAML2 Dual Color Break-Apart Probe (ZytoVision GmbH, Bremerhaven, Germany) was used.

An appropriate amount of mixed and premixed probes was applied on specimens, covered with a glass coverslip and sealed with rubber cement. Slides were incubated in the ThermoBrite instrument (StatSpin/Iris Sample Processing, Westwood, MA) with codenaturation at 85°C/8 minutes and hybridization at 37°C/16 hours. Rubber-cemented coverslip was then removed and the slide was placed in a posthybridization wash solution (2×SSC/0.3% NP-40) at 72°C/2 minutes. The slide was air-dried in the dark, counterstained with 4′,6′-diamidino-2-phenylindole DAPI (Vysis/Abbott Molecular), cover slipped, and immediately examined.

FISH Interpretation

The sections were examined with an Olympus BX51 fluorescence microscope (Olympus Corporation, Tokyo, Japan) using a ×100 objective and filter sets triple bandpass (DAPI/SpectrumGreen/SpectrumOrange), dual bandpass (SpectrumGreen/SpectrumOrange) and Single Bandpass (SpectrumGreen or SpectrumOrange).

For *MAML2* break-apart probe, 100 randomly selected nonoverlapping tumor cell nuclei were examined for the presence of yellow or green and orange fluorescent signals. The yellow signals were considered negative; separate orange and green signals were considered as positive. Cutoff values for break-apart probes were set to >10% of nuclei with chromosomal breakpoint (mean+3 SD in normal non-neoplastic control tissues).

RESULTS

Molecular Genetic Findings

Thirty selected cases of low-grade oncocytic neoplasms were analyzed by NGS using the Anchored Multiplex PCR (AMP) technique (ArcherDX), and 22 of them were reclassified as OMEC. The remaining 8 cases were excluded from the study, and interpreted in 4 cases as oncocytic metaplastic pleomorphic adenoma (PLAG1 gene break detected by FISH), in 3 cases as benign oncocytoma with extensive mucinous metaplasia, and in 1 case as oncocytic benign myoepithelioma.

Thirteen OMEC cases (59%) presented the classic *CRTC1-MAML2* fusion (Fig. 1), and in 1 case alternative *CRTC3-MAML2* fusion was detected (4.5%). Five OMEC cases were negative on NGS (23%) but *MAML2* rearrangement was confirmed by FISH in all cases (Fig. 2). Two tumors were not analyzable (9%) and in 1 case the tissue was not available for NGS testing (4.5%). Molecular genetic findings of all 22 OMEC cases are summarized in Table 3.

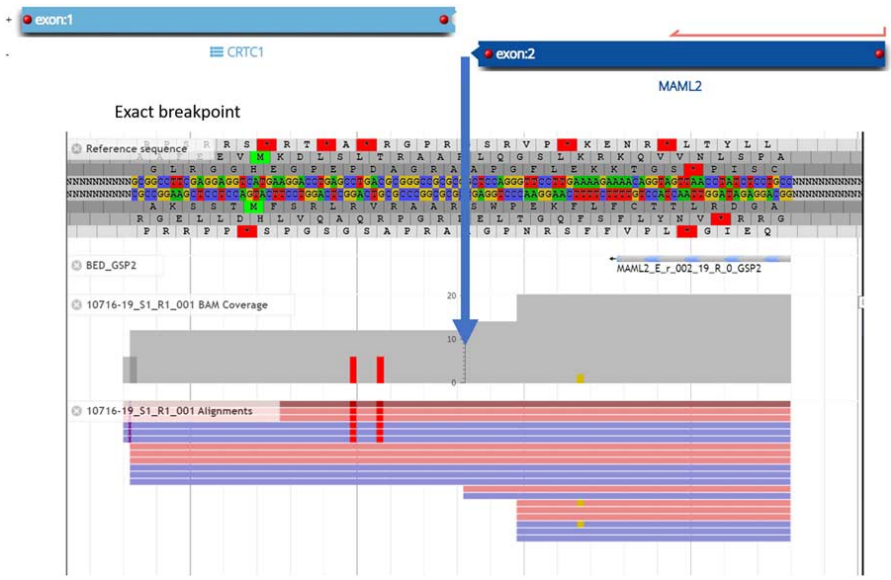

FIGURE 1. Detection of specific fusion transcript *CRTC1-MAML2* identified by ArcherDX assay. Schematic representation of the *CRTC1-MAML2* fusion transcript as revealed by NGS. The upper section: the scheme of joining of exon 1 of *CRTC1* gene and exon 2 of *MAML2* gene. The lower section: the sequencing coverage of point of fusion is indicated in gray. Several unique reads in red and blue, respectively. Blue arrow shows the exact breakpoint.

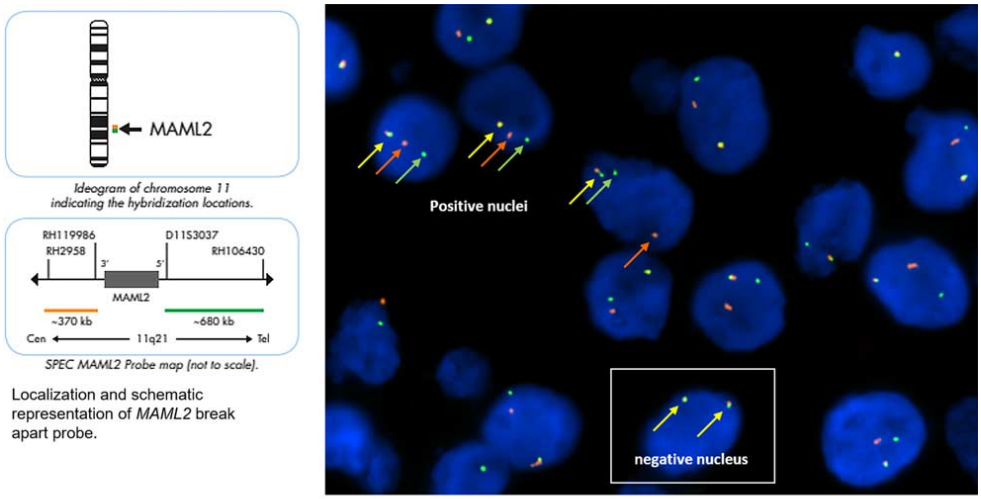

FIGURE 2. Detection of breakpoint of *MAML2* gene by FISH. FISH analysis using MAML2 break-apart probe with "classic" break-apart design. The figure shows several nuclei while yellow arrows indicate signals of an intact *MAML2* gene region.

Clinical Findings

The clinicopathologic data for the 22 identified OMEC cases are summarized in Table 4. There were 12 females and 10 males aged between 13 and 83 years, with a mean of 57 years. Fifteen tumors occurred in the parotid gland (68%), 2 cases each in the sublingual gland (9%), in the minor salivary gland of the palate (9%), and in the mucosa of the tongue (9%), and 1 in the submandibular gland (5%). The size of the tumors ranged from 0.9 to 3.5 cm (average of 2.6 cm).

The tumors were low grade (16 cases), and intermediate grade (6 cases) using the Armed Forces Institute of Pathology (AFIP) system[22]; while they were low grade (5 cases), intermediate grade (12 cases), and high grade (5 cases) using the modified Brandwein system.[23] Most of the tumors were upgraded 1 category using the Brandwein system as compared with the AFIP system. However, 2 tumors were upgraded even 2 categories being grade 1 using the AFIP system and grade 3 using the Brandwein system.

Follow-up was available for 18 patients ranging from 2 to 184 months with an average of 38.3 months. Seventeen patients showed no evidence of disease at latest control (94%). Only 1 patient developed regional lymph node metastasis, and died of disease at 20 months. The remaining 4 patients were lost to follow-up.

Index Case

A 48-year-old woman presented with a tumor mass of 7 months duration in the right parotid gland. Magnetic

TABLE 3. Molecular Genetic Findings of 22 Cases of OMEC

Case No.	FISH *MAML2*	RT-PCR *CRTC1-MAML2*	NGS FusionPlex Solid Tumor Kit Archer
1	+	ND	*CRTC1-MAML2*
2	+	ND	*CRTC1-MAML2*
3	+	ND	*CRTC1-MAML2*
4	+	Neg	*CRTC1-MAML2*†
5	+	*CRTC1-MAML2*	*CRTC1-MAML2*
6	+	ND*	ND*
7	+	Neg	NA
8	+	Neg	Neg
9	+	ND	*CRTC1-MAML2*
10	+	ND	Neg
11	+	Neg	*CRTC1-MAML2*†
12	+	Neg	Neg
13	+	*CRTC1-MAML2*	*CRTC1-MAML2*
14	+	ND	*CRTC1-MAML2*
15	+	ND	*CRTC1-MAML2*
16	+	*CRTC1-MAML2*	NA
17	+	ND	*CRTC3-MAML2*
18	+	ND	*CRTC1-MAML2*
19	+	ND	Neg
20	+	ND	*CRTC1-MAML2*
21	+	ND	Neg
22	+	ND	*CRTC1-MAML2*

*Tissue not available.
†Custom panel *ETV6-EWSR1-MAML2* using ArcherDx kit.
+ indicates FISH detected break in *MAML2* gene; NA, not analyzable; ND, not done; neg, no fusions found.

TABLE 4. Clinicopathologic Features of 22 Cases of OMEC

Case No.	Age (y)/Sex	Original Diagnosis	Site	AFIP Grade	Brandwein Grade	Outcome (mo)
1	48/female	Oncocytic neoplasm of uncertain malignant potential	Parotid	G1	G2	7 NED
2	53/male	Oncocytic neoplasm	Parotid	G2	G2	*
3	45/female	Recurrent oncocytoma	Sublingual	G1	G3	18 NED
4	74/male	Oncocytic neoplasm, possibly OMEC	Parotid	G2	G3	*
5	83/female	PA with oncocytic metaplasia	Parotid	G1	G2	*
6	41/female	Oncocytic neoplasm of uncertain malignant potential	Parotid	G1	G3	8 NED
7	46/male	Benign mucinous oncocytoma	Parotid	G1	G2	34 NED
8	71/female	Multifocal oncocytoma	Parotid	G1	G1	31 NED
9	13/female	OMEC	Palate	G1	G2	184 NED
10	59/female	Adenocarcinoma oncocytic NOS	Parotid	G2	G3	96 NED
11	13/male	Cystic sialometaplasia	Parotid	G1	G2	48 NED
12	74/female	Adenocarcinoma oncocytic, low grade	Parotid	G1	G1	60 NED
13	51/female	Oncocytic neoplasm	Palate	G2	G2	48 NED
14	72/male	Myoepithelial carcinoma	Tongue	G2	G3	20 DOD, lymph node metastasis
15	67/female	OMEC, low grade oncocytic tumor	Sublingual	G1	G2	24 NED
16	74/male	OMEC	Submandibular	G1	G1	*
17	57/male	Clear cell oncocytoma/PA/MEC	Parotid	G1	G1	2 NED
18	63/female	OMEC without mucinous cells	Parotid	G1	G2	2 NED
19	71/male	OMEC	Parotid	G1	G2	5 NED
20	70/female	Cystic intranodal oncocytic inclusion/cystic sialometaplasia	Parotid	G1	G1	72 NED
21	54/male	OMEC	Parotid	G2	G2	24 NED
22	56/male	Oncocytoma benign	Base of tongue	G1	G2	6 NED

Case 16 has been published earlier.[5]
*Not known.
NED indicates no evidence of disease; NOS, not otherwise specified; PA, pleomorphic adenoma.

resonance imaging showed a solid lesion of 30×22×26 mm involving the superficial and deep portions of the gland giving clear and polycystic profiles. The lesion extended around the branch of the mandible and into the proximity of the masseter muscle, from which it was separated by a rim of normal parotid parenchyma. Furthermore, there was dislocation of the external carotid artery and the retromandibular vein, but they appeared free of tumor.

On clinical examination preoperative facial motility was normal. On palpation the lesion appeared firm and it was not tender. The overlying skin was not infiltrated. Intraoperatively, the lesion could be separated from the surrounding normal parotid tissue but not from the nerve branches. The lesion and the nerves were fused in a whitish fibrous tissue.

Radical parotidectomy and a super selective neck dissection of levels IIA, IIB, and III were performed and were followed by radiotherapy. The tumor was staged as pT4aN0. The patient is alive with no signs of recurrence or metastatic spread after 7 months of follow-up. The original histopathologic diagnosis was an oncocytic neoplasm of uncertain malignant potential.

Histopathologic and IHC Findings

Histologically, at low power magnification the tumors showed nested and multinodular growth patterns composed of oncocytic cells (Fig. 3A) with focal and occasionally prominent stromal sclerosis (Fig. 3B). Hyalinized and focally interrupted tumor capsule was present in 7 cases, while 15 neoplasms showed invasive growth into the surrounding tissues. Perineural and lymphovascular invasion were detected in 6 and in 2 cases, respectively. In most cases, the oncocytic change of neoplastic cells was extensive, ranging between 75% and 100% of all tumor cells. Foci of conventional non-OMEC were not seen in any case. In 1 case, multiple large communicating cystic spaces were seen and the tumor showed extracellular keratinization (Fig. 3C). Another macrocystic tumor was lined by a complete layer of mucinous cells, and it contained intracapsular solid nests of oncocytes devoid of intracellular mucin (Fig. 3D).

Five cases were essentially solid, composed of nests and sheets of large oncocytic cells, and were completely devoid of true mucocytes (Fig. 4A). Focal tubular structures containing dense intraluminal secretions lined by fully developed oncocytes without any intracellular mucin were observed in these 5 cases (Fig. 4B). In 15 cases, mucin-containing cells were identified, but they were very scarce and hardly discernible on hematoxylin and eosin staining (Fig. 4C). In these cases, mucin-containing cells were identifed on mucicarmine or AB/PAS staining. Mucinous cyst formation was seen in 4 cases with 2 containing <5% cystic component (Fig. 4D). In only 1 case, the area of mucinous cysts amounted to about 20% of tumor tissue. Small foci of extravasated mucin were identified in another case. Hyalinized and focally interrupted tumor capsule was present in 6 cases, while 14 neoplasms showed invasive growth into the surrounding

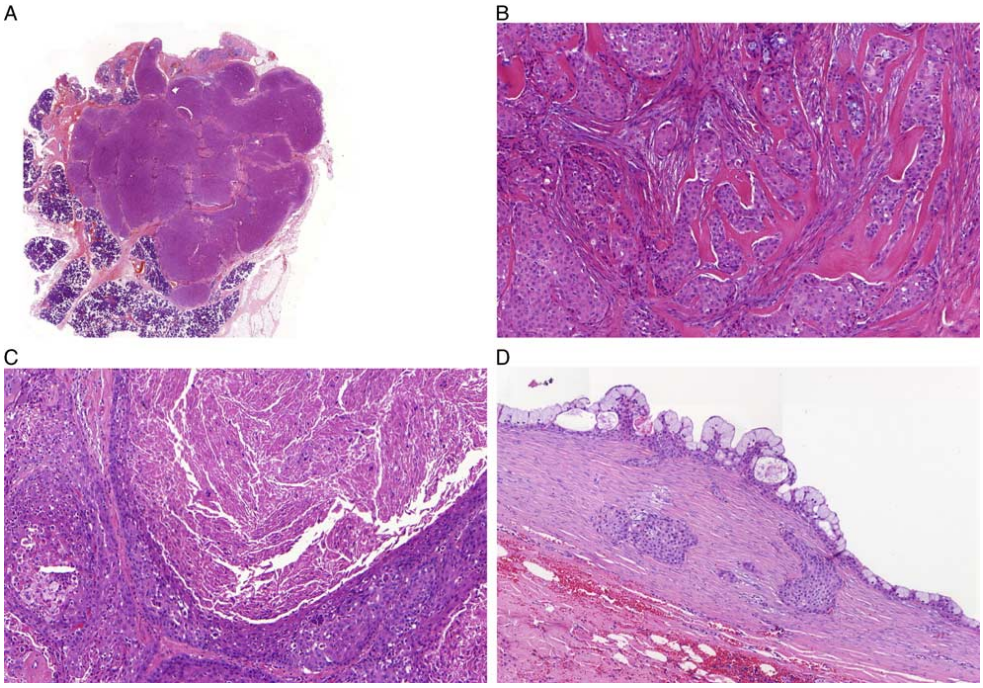

FIGURE 3. OMEC. At low power, the tumor shows nested and multinodular growth pattern (A) composed exclusively of oncocytic cells with focal prominent stromal sclerosis (B). Multiple large communicating cystic spaces with evidence of keratinization were found (C) and still another macrocystic tumor was lined by a complete layer of mucinous cells, and contained intracapsular solid nests composed of oncocytes devoid of intracellular mucin (D).

salivary gland parenchyma. Three cases contained foci of squamoid cell differentiation. In one of them multiple small squamous eddies, and in the other 2 squamous metaplasias due to previous fine needle aspiration injury were seen.

Cytologically, the individual oncocytes showed a low nuclear-cytoplasmic ratio, centrally placed nuclei, and abundant granular eosinophilic cytoplasm filled by the mitochondria (Fig. 5A). The tumor cells were bland looking in most cases, but a moderate degree of nuclear atypia with enlarged and irregular nuclei was seen in 2 cases (Fig. 5B). Five cases showed a clear cell phenotype with tumor cells having watery clear cytoplasm and distinct small nuclei (Fig. 5C). In places, oncocytic tumor cells with clear cell and eosinophilic phenotypes were interspersed (Fig. 5D).

Immunohistochemically, tumor cells in all studied cases were positive for CK7 (17/17), CK 14 (6/6), CK 5/6 (7/7), and antimitochondrial antigen MIA (16/16). In most cases, there was a strong nuclear staining for p63 (18/21) and p40 proteins (9/12). Nuclear staining for p63 was distributed throughout the solid oncocytic nests in an abluminal position of glandular/tubular structures (Fig. 6A). This staining pattern for p63 was seen in most cases. In other cases, OMEC displayed double-layered tubular structures where p40 and p63 stainings were concentrated in the peripheral cells of the nests, in a pattern similar to that reported previously for oncocytomas[12] (Fig. 6B). In 6 tumors, there was remarkable SOX10 immunopositivity. In 2 of these cases, the staining was strong, and distributed within the whole tumor in diffuse pattern (Fig. 6C), while in another 4 cases it was focal. S100 protein was negative in all but 1 case (Fig. 6D). Interestingly, this S100 protein and SOX10-positive case harbored a *CRTC3-MAML2* fusion. Proliferative activity in our tumors was predominantly low with MIB1 index ranging from 1 to 10% (average: 5.4%). Only 1 case showed a high hotspot type proliferative activity with a focal MIB1 index of 30%.

DISCUSSION

OMEC is a rare variant of MEC, composed predominantly of oncocytic cells, although the percentage of oncocytic cells justifying this diagnosis has not been defined.[1,3] To define OMEC in this study, we used an arbitrary cutoff of >75% of oncocytic cells. The real importance of recognizing OMEC is in distinguishing it from

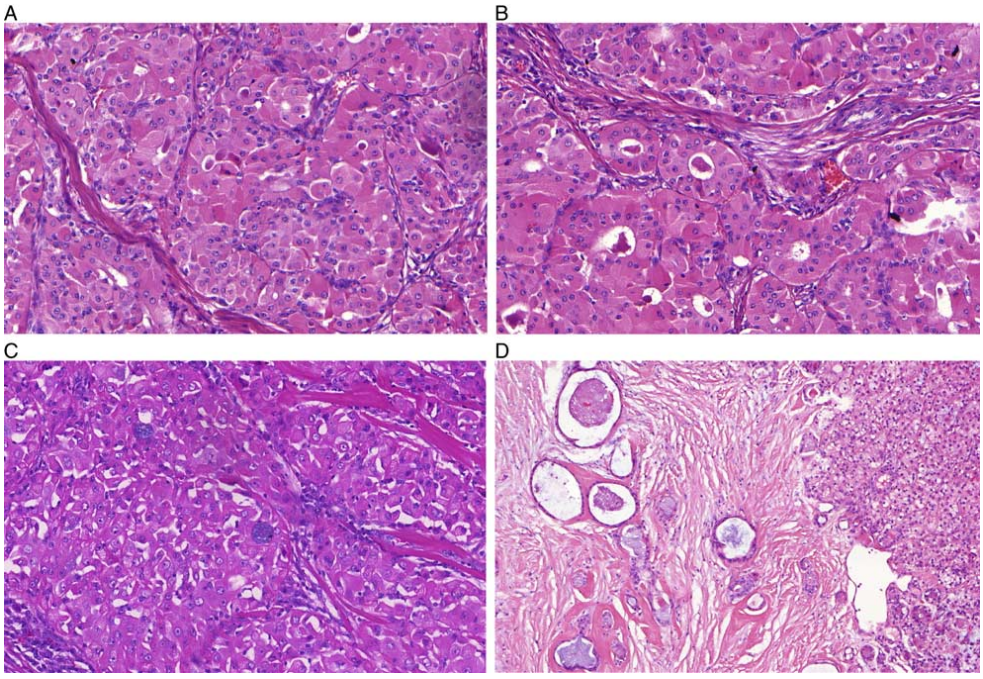

FIGURE 4. OMEC. A, OMEC is composed solid sheets of large oncocytic cells and completely devoid of true mucocytes. B, Focal tubular structures containing dense intraluminal secretions lined by fully developed oncocytes without any intracellular mucin are observed. C, Mucin-containing cells are rare and hardly discernible. D, Mucinous cyst formation.

its mimickers. The distinction of OMEC from other oncocytic and oncocytoid tumors is particularly challenging in cases composed entirely of oncocytes[24] or in cases of MEC with a significant proportion of oncocytic cells devoid of mucous cells. In our experience, the most difficult differential diagnosis was the distinction of OMEC from a benign oncocytoma/low-grade oncocytic tumor of uncertain malignancy and from a cellular pleomorphic adenoma and/or myoepithelioma with extensive mucinous and oncocytic metaplasia.[25] Another differential diagnostic consideration was the oncocytic variant of a benign cystadenoma. Cystadenoma of salivary glands is a rare benign tumor characterized by predominantly multicystic growth in which the epithelium demonstrates adenomatous proliferation.[26] Extensive oncocytic change may be seen, and these lesions are classified as oncocytic cystadenomas.[27–29] A diagnostically challenging case of oncocytic papillary cystadenoma with prominent mucinous differentiation has been reported recently.[30]

According to the study of Weinreb et al,[3] diffuse p63 immunopositivity may be a reliable marker for the diagnosis of OMEC. Indeed, most OMEC cases of our study showed p63 immunostaining. However, a diffuse and strong p63 positivity was not seen in all cases. In 2 tumors the staining was focal, while another 2 showed abluminal positivity similar to that described in oncocytomas.[12,13] Finally, in 3 cases p63 protein was completely negative. Contrary to this, other salivary tumor types including pleomorphic adenomas, myoepitheliomas, and Warthin tumors show extensive p63 immunostaining. The identification of mucous cells in OMEC can be useful, but oncocytic cystadenomas, metaplastic Warthin tumors, and oncocytic metaplastic pleomorphic adenomas may also have mucous cells. Moreover, true mucocytes may be very few and hardly discernible in OMECs.

Another possible pitfall in the differential diagnosis of OMEC relates to the SOX10 immunopositivity, which we encountered in a subgroup of OMECs. In the normal salivary gland, expression of SOX10 is limited to acinar cells and the intercalated ducts (both luminal and abluminal cells).[31] Until recently, it was proposed that salivary gland tumors can be divided into a subgroup of SOX10-positive, including acinic cell carcinoma, secretory carcinoma (mammary analogue), adenoid cystic carcinoma, epithelial-myoepithelial carcinoma, myoepithelioma, myoepithelial carcinoma, and pleomorphic adenoma, while a subgroup of SOX10-negative tumors comprised salivary duct carcinoma, MEC, oncocytic carcinoma, oncocytoma, and Warthin

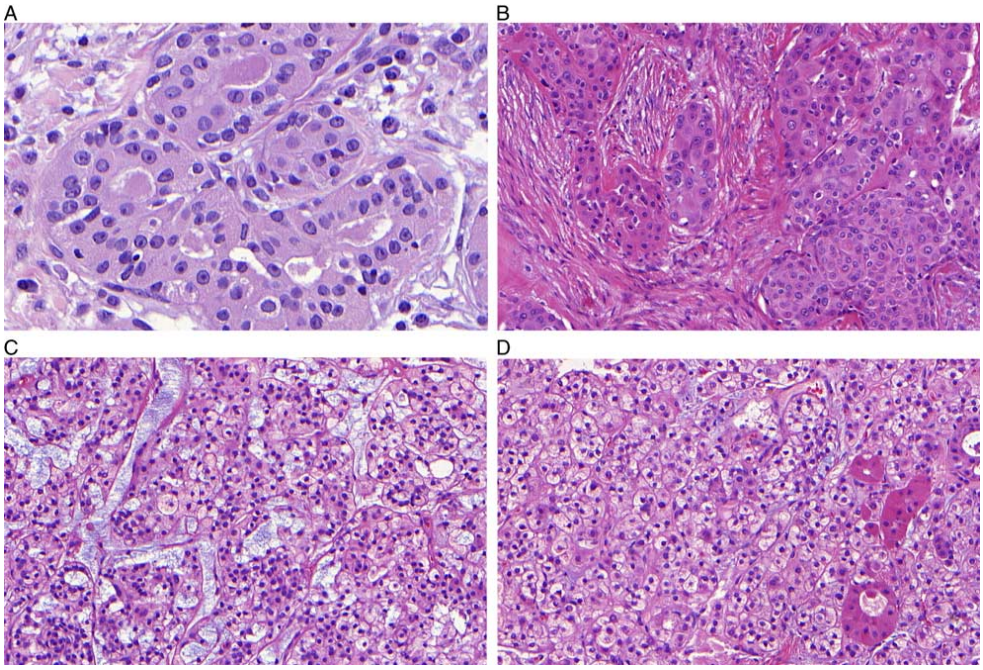

FIGURE 5. OMEC. Oncocytes show centrally placed nuclei with abundant granular eosinophilic cytoplasm, and a low nuclear-cytoplasmic ratio (A). The tumor cells show a moderate degree of nuclear atypia with enlarged and irregular nuclei (B). Oncocytes with a watery clear cytoplasm and distinct small nuclei are seen (C). In places, neoplastic oncocytic cells with clear and eosinophilic phenotype are intermingled (D).

tumor.[31] Agreeably SOX10 is very useful in distinguishing myoepithelial tumors, mammary analogue secretory carcinoma, and acinic cell carcinoma from ductal cell-derived salivary neoplasms, but it cannot be used for the diagnosis of MEC because of a subgroup of SOX10-positive MECs.[32] In our series, 6 of 20 OMECs were positive for SOX10.

Thus, due to these differential diagnostic difficulties, ancillary diagnostic testing to support a diagnosis of MEC is desirable. Here, we have evaluated the utility of testing for *MAML2* rearrangement using FISH and NGS to confirm the diagnosis of OMEC. MECs are known to harbor *CRTC1-MAML2* or *CRTC3-MAML2* as characteristic gene fusions in up to 80% of cases.[14–19] While the prognostic value of *MAML2* fusions has been questioned recently,[16,18,19,33] the finding of recurrent translocations seems to be a useful diagnostic "gold standard" for confirming the diagnosis of MEC in difficult cases.[11,20]

Last but not least, diversity in clinical presentation and variability of histologic appearances has made MEC challenging to grade, stage, and treat. Multiple histopathologic grading systems for MEC have been created to stratify patients better for prognostication and treatment, namely the AFIP system,[22] the Brandwein system,[23] and the system by Katabi et al.[34] All these grading systems have 3 grades: low, intermediate, and high. However, applying the different systems to the same tumor may result in different grades, so that the Brandwein system tends to assign higher grades and the AFIP system lower grades. This is particularly true for OMEC because of its typical solid and nested growth pattern. In our series of 20 OMECs, use of the Brandwein system resulted in upgrading of 11 tumors by 1 grade and 2 tumors by 2 grades as compared with the AFIP system. These OMECs had an uneventful clinical follow-up. The important consequence is that the patients may receive more aggressive management schemes in such cases. Low-grade MECs generally require complete surgical excision while high-grade MECs are also treated with adjuvant radiotherapy with or without chemotherapy.[35] Intermediate-grade carcinomas may behave similar to low-grade carcinomas, and treatment with surgical excision alone has been considered.[36,37] While the Brandwein high grade is likely the best predictor of aggressive behavior, upgrading of OMECs from low-to-intermediate grade because of the mere presence of isolated solid growth seems not warranted.[19]

In our series, follow-up was available for 16 patients ranging from 2 to 184 months, and all but 1 were alive at the latest follow-up. Only 1 patient (grade 2 by the AFIP

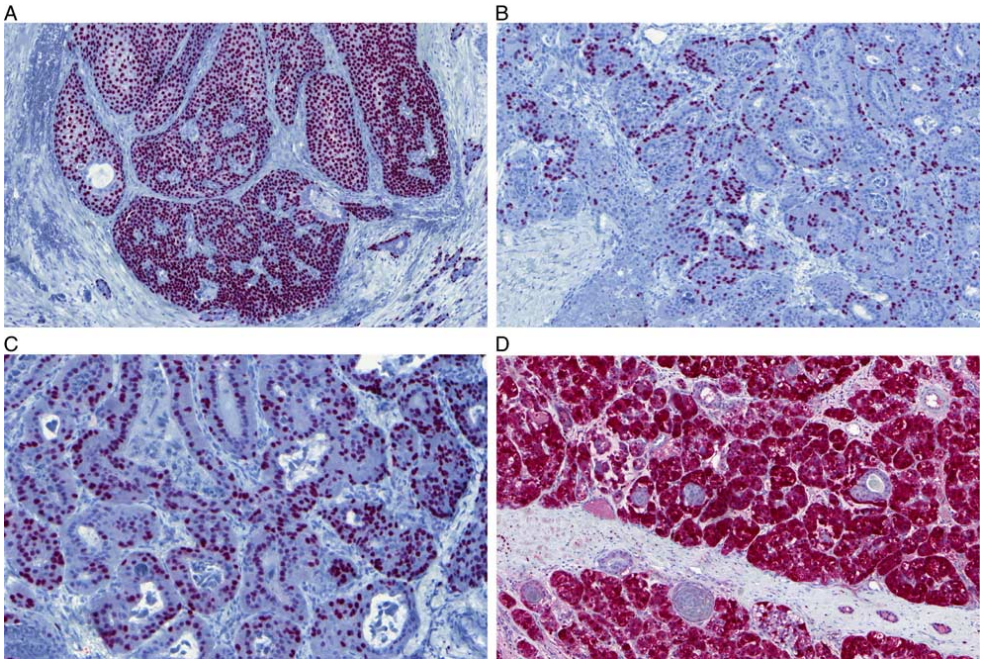

FIGURE 6. IHC stainings in OMEC. Nuclear staining for p63 was distributed throughout the solid oncocytic nests in abluminal position to glandular/tubular structures in most OMECs (A). Less common pattern of p63 nuclear staining concentrated in the peripheral cells of the nests (B). In 6 tumors, there was remarkable SOX10 immunopositivity (C). S100 protein was expressed only in 1 case (D). Interestingly, this tumor was also strongly positive for SOX10 and harbored *CRTC3-MAML2* fusion.

system and grade 3 by the Brandwein system) developed regional lymph node metastases and died of disease at 20 months. Until the present study, the largest series of OMEC with follow-up information was presented by Weinreb et al.[3] Compiling all published cases with follow-up information, including the review of literature in Weinreb et al's[3] report, only 2 recurrences have been documented. None of the cases has shown lymph node metastases or death due to disease. Generally, it seems that OMEC is biologically a low-grade malignancy with potential for locally aggressive disease. In our study, however, we document the first OMEC with metastatic behavior and death of the patient due to disease. This case presented with lymph node metastases at the time of diagnosis, and was distinguished by a focally abrupt (hotspot) Ki-67 index of 30% centered around vessels.

In conclusion, we have described a series of 22 OMECs which is the largest so far. The novel finding in our series is a description of 5 OMECs that were essentially solid, composed of nests and sheets of large oncocytic cells and completely devoid of true mucocytes. Our study highlighted the usefulness of *MAML2* testing in the identification of OMEC and its distinction from mimickers.

ACKNOWLEDGMENTS

The authors thank Hanna Majewska, MD, PhD, Gdańsk, Poland (case 4); Giovanni Falconieri, MD, Udine, Italy (case 5); V. Canconieri, MD, Aviano, Italy (case 11); Jacqueline Hwang MD, Singapore (case 12); and Michal Kheck, MD, Jihlava, Czech Republic (case 20) for submitting their cases, and thus contributing toward the study.

REFERENCES

1. Brandwein-Gensler M, Bell D, Inagaki H, et al. Mucoepidermoid carcinoma. In: El-Naggar A, Chan JKC, Grandis JR, Takata T, Slootweg PJ, eds. *World Health Organization (WHO) Classification of Head and Neck Tumours*, 4th ed. Lyon, France: IARC Press; 2017:163–164.
2. Boukheris H, Curtis RE, Land CE, et al. Incidence of carcinoma of the major salivary glands according to the WHO classification, 1992 to 2006: a population-based study in the United States. *Cancer Epidemiol Biomarkers Prev*. 2009;18:2899–2906.
3. Weinreb I, Seethala RR, Perez-Ordonez B, et al. Oncocytic mucoepidermoid carcinoma: clinicopathologic description in a series of 12 cases. *Am J Surg Pathol*. 2009;33:409–416.
4. Brannon RB, Willard CC. Oncocytic mucoepidermoid carcinoma of parotid gland origin. *Oral Surg Oral Med Oral Pathol Oral Radiol Endod*. 2003;96:727–733.
5. Corcione L, Giordano G, Gnetti L, et al. Oncocytic mucoepidermoid carcinoma of a submandibular gland: a case report and review of the literature. *Int J Oral Maxillofac Surg*. 2007;36:560–563.

6. Fujimaki M, Fukumura Y, Saito T, et al. Oncocytic mucoepidermoid carcinoma of the parotid gland with *CRTC1-MAML2* fusion transcript: report of a case with review of the literature. *Hum Pathol*. 2011;42:2052–2055.
7. Deveci MS, Deveci G, Gunhan O, et al. Oncocytic mucoepidermoid carcinoma of the parotid gland: report of a case with DNA ploidy analysis and review of the literature. *Pathol Int*. 2000;50:905–909.
8. Hamed G, Shmookler BM, Ellis GL, et al. Oncocytic mucoepidermoid carcinoma of the parotid gland. *Arch Pathol Lab Med*. 1994; 118:313–314.
9. Krishnanand G, Kaur M, Rao RV, et al. Oncocytic variant of mucoepidermoid carcinoma of submandibular gland: an unusual clinical and morphological entity. *Indian J Pathol Microbiol*. 2007;50:538–540.
10. López-Terrada D, Bloom MG, Cagle PT, et al. Oncocytic mucoepidermoid carcinoma of the trachea. *Arch Pathol Lab Med*. 1999;123:635–637.
11. García JJ, Hunt JL, Weinreb I, et al. Fluorescence in situ hybridization for detection of *MAML2* rearrangements in oncocytic mucoepidermoid carcinomas: utility as a diagnostic test. *Hum Pathol*. 2011;42:2001–2009.
12. McHugh JB, Hoschar AP, Dvorakova M, et al. P63 immunohistochemistry differentiates salivary gland oncocytoma and oncocytic carcinoma from metastatic renal cell carcinoma. *Head Neck Pathol*. 2007;1:31–34.
13. Weiler CH, Reu S, Zengel P, et al. Obligate basal cell component in salivary oncocytoma facilitates distinction from acinic cell carcinoma. *Pathol Res Pract*. 2009;205:838–842.
14. Behboudi A, Enlund F, Winnes M, et al. Molecular classification of mucoepidermoid carcinomas-prognostic significance of the *MECT1-MAML2* fusion oncogene. *Genes Chromosomes Cancer*. 2006;45: 470–481.
15. Chiosea SI, Dacic S, Nikiforova MN, et al. Prospective testing of mucoepidermoid carcinoma for the MAML2 translocation: clinical implications. *Laryngoscope*. 2012;122:1690–1694.
16. Seethala RR, Dacic S, Cieply K, et al. A reappraisal of the *MECT1/MAML2* translocation in salivary mucoepidermoid carcinomas. *Am J Surg Pathol*. 2010;34:1106–1121.
17. Okabe M, Miyabe S, Nagatsuka H, et al. *MECT1-MAML2* fusion transcript defines a favorable subset of mucoepidermoid carcinoma. *Clin Cancer Res*. 2006;12:3902–3907.
18. Jee KJ, Persson M, Heikinheimo K, et al. Genomic profiles and *CRTC1-MAML2* fusion distinguish different subtypes of mucoepidermoid carcinoma. *Mod Pathol*. 2013;26:213–222.
19. Cipriani NA, Lusardi JJ, McElherne J, et al. Mucoepidermoid carcinoma. A comparison of histologic grading systems and relationship to *MAML2* rearrangement and prognosis. *Am J Surg Pathol*. 2019;43:885–897.
20. Bishop JA, Cowan ML, Shum CH, et al. *MAML2* rearrangements in variant forms of mucoepidermoid carcinoma. Ancillary diagnostic testing for the ciliated and Warthin-like variants. *Am J Surg Pathol*. 2018;42:130–136.
21. Skálová A, Ptáková N, Santana T, et al. *NCOA4-RET* and *TRIM27-RET* are characteristic gene fusions in salivary intraductal carcinoma, including invasive and metastatic tumors. Is "Intraductal" correct? *Am J Surg Pathol*. 2019;43:1303–1313.
22. Goode RK, Auclair PL, Ellis AL. Mucoepidermoid carcinoma of the major salivary glands: clinical and histologic analysis of 234 cases with evaluation of grading criteria. *Cancer*. 1998;82:1217–1224.
23. Brandwein NS, Ivanov K, Wallace DI, et al. Mucoepidermoid carcinoma: a clinicopathologic study of 80 patients with special reference to histological grading. *Am J Surg Pathol*. 2001;25: 835–845.
24. Liao X, Haghighi P, Coffey CS, et al. A rare case of exclusively oncocytic mucoepidermoid carcinoma with MAML2 translocation. *Rare Tumors*. 2016;8:6166.
25. Skalova A, Michal M, Ryska A, et al. Oncocytic myoepithelioma and pleomorphic adenoma of the salivary glands. *Virchows Arch*. 1999;434:537–546.
26. Budnik S, Simpson RHW. Cystadenoma. In: El-Naggar AK, Chan JKC, Grandis J, Takata T, Slootweg PJ, eds. *World Health Oragnization Classification of Head and Neck Tumours*. Lyon, France: IARC Press; 2017:191.
27. Bezic J, Glavina-Durdov M. Salivary oncocytic cystadenoma with intraluminal crystalloids: a case report with review of the literature. *Head Neck Pathol*. 2011;5:419–422.
28. Michal M, Hrabal P, Skalova A. Oncocytic cystadenoma of the parotid gland with prominent signet-ring cell features. *Pathol Int*. 1998;48:629–633.
29. Skalova A, Leivo I, Wolf H, et al. Oncocytic cystadenoma of the parotid gland with tyrosine-rich crystals. *Path Res Pract*. 2000;196: 849–851.
30. Alexiev BA, Jennings LJ, Samant S, et al. Oncocytic papillary cystadenoma with prominent mucinous differentiation of parotid gland: a case report. *Path Res Pract*. 2017;213:1310–1314.
31. Ohtomo R, Mori T, Shibata S, et al. SOX10 is a novel marker of acinus and intercalated duct differentiation in salivary gland tumors: a clue to the histogenesis for tumor diagnosis. *Mod Pathol*. 2013;26:1041–1050.
32. Hsieh M-S, Lee Y-H, Chang Y-L. SOX10-positive salivary gland tumors: a growing list, including mammary analogue secretory caricnoma of the salivary glands, sialoblastoma, low-grade salivary duct carcinoma, basal cell adenoma/adenocarcinoma, and a subgroup of mucoepidermoid carcinoma. *Hum Pathol*. 2016;56:134–142.
33. Anzick SL, Chen W-D, Park Y, et al. Unfavorable prognosis of *CRTC1-MAML2* positive mucoepidermoid tumors with *CDKN2A* deletions. *Genes Chromosom Cancer*. 2010;49:59–69.
34. Katabi N, Ghossein R, Ali S, et al. Prognostic features in mucoepidermoid carcinoma of major salivary glands with emphasis on tumour histologic grading. *Histopathology*. 2014;65:793–804.
35. Luna MA. Salivary mucoepidermoid carcinoma: revisited. *Adv Anat Pathol*. 2006;13:293–307.
36. Nance MA, Seethala RR, Wang Y, et al. Treatment and survival outcomes based on histologic grading in patients with head and neck mucoepidermoid carcinoma. *Cancer*. 2008;113:2082–2089.
37. McHugh CH, Roberts DB, El-Naggar AK, et al. Prognostic factors in mucoepidermoid carcinoma of the salivary glands. *Cancer*. 2012;118:3928–3936.

1.2 MOLECULAR PROFILING OF CLEAR CELL MYOEPITHELIAL CARCINOMA OF SALIVARY GLANDS WITH THE *EWSR1* REARRANGEMENT IDENTIFIES FREQUENT *PLAG1* GENE FUSIONS BUT NO *EWSR1* FUSION TRANSCRIPTS.

Myoepithelial carcinoma (MC) of salivary glands is a challenging entity with diverse morphology. One of the subtypes of MC is the clear cell variant (CCMC), which typically presents as a multi-nodular structure. Rarely, the tumor may exhibit a solid or trabecular growth pattern. The nodes consist of a hypocellular myxoid central zone with occasional necrosis, hypercellular areas are present at the periphery. In most cases, clear cells dominate, although spindle and rhabdoid/plasmacytoid areas may also be observed.

In our study, the morphological features of the tumors were consistent with those described in previous works [18, 19]. Notably, a wide spectrum of nuclear atypia ranging from bland nuclei to pronounced pleomorphism, areas of necrosis, and a high mitotic index (mean of 42%) were observed.

Low mutational burden and a high prevalence of oncogenic gene fusions, mainly involving the *PLAG1* gene in MC were reported [66]. Additionally, Skalova A. et al. [18]. described an *EWSR1* gene rearrangement in a subset of MCs of salivary glands, predominantly composed of clear cells with myoepithelial differentiation. Another entity harboring *EWSR1* rearrangement is hyalinizing clear cell carcinoma (HCCC) with *EWSR1::ATF1* or *EWSR1::CREM* fusions [19]. *EWSR1* rearrangement with the other fusion partners *EWSR1::POU5F1* and *EWSR::PBX3* have been identified in myoepithelial tumors of soft tissues and skin but not in salivary glands [63,64,65]. Notably, a subset of skin and soft tissue myoepithelial tumors showing tubuloductal differentiation morphologically has *PLAG1* rearrangements [67].

To understand the biological nature of clear cell myoepithelial carcinoma, a molecular-genetic study was conducted. We found 94 cases met the selection criteria for CCMC in the Salivary Gland Tumor Registry in Pilsen, and tested them for *EWSR1* rearrangement using fluorescence in situ hybridization. Tumors positive for *EWSR1* gene rearrangement were further tested using next-generation sequencing with fusion-detecting panels. The NGS results were confirmed either by reverse-transcription polymerase chain reaction or FISH.

The study revealed that 27.6% of the tumors showed split signals for *EWSR1* by FISH, but none of these tumors exhibited an *EWSR1* fusion transcript. Fusion transcripts were found in 40% of cases, such as *LIFR::PLAG1, CTNNB1::PLAG1, CHCHD7::PLAG1*, and *EWSR1::ATF1*. The case with *EWSR1::ATF1* fusion was reviewed and reclassified as clear cell carcinoma (CCC). Overall, *PLAG1* gene rearrangements were detected in 26% of the tested cases.

In conclusion, the novel findings from our study suggest that CCMC is a gene fusion-driven disease with *PLAG1* rearrangement involving fusion partners *CTNNB1, LIFR,* and *CHCHD7,* as well as *EWSR1*-FISH positivity. The presence of *EWSR1*-FISH abnormality in CCMCs without identifiable gene fusion may represent a passenger mutation with no oncologic effect. The study also highlighted genetic differences between salivary gland myoepithelial carcinomas and myoepithelial carcinomas of soft tissues and skin, despite the morphological, immunohistochemical similarities and common *EWSR1* rearrangement. The authors believe that the existence of *PLAG1* rearrangements reflects pleomorphic adenoma-like features in MCs, while *EWSR1* fusions may be associated with the clear cell phenotype.

Molecular Profiling of Clear Cell Myoepithelial Carcinoma of Salivary Glands With *EWSR1* Rearrangement Identifies Frequent *PLAG1* Gene Fusions But No *EWSR1* Fusion Transcripts

Alena Skálová, MD, PhD,† Abbas Agaimy, MD,‡ Tomas Vanecek, PhD,§ Martina Baněčková, MD,*† Jan Laco, MD, PhD,‖ Nikola Ptáková, MSc,§ Petr Šteiner, MSc, PhD,§ Hanna Majewska, MD, PhD,¶ Wojciech Biernat, MD, PhD,# Luigi Corcione, MD,** Václav Eis, MD, PhD,†† Olena Koshyk, MD,‡‡ Jan Vondrák Jr, MSc,§§ Michal Michal, MD,* and Ilmo Leivo, MD, PhD‖‖¶¶*

Abstract: Myoepithelial carcinoma of salivary glands is an underrecognized and challenging entity with a broad morphologic spectrum, including an *EWSR1*-rearranged clear cell variant. Myoepithelial carcinoma is generally aggressive with largely unknown genetic features. A retrospective review of Salivary Gland Tumor Registry in Pilsen searching for the key words "clear cell myoepithelial carcinoma," "hyalinizing clear cell," and "clear cell malignant myoepithelioma" yielded 94 clear cell myoepithelial carcinomas (CCMCs) for molecular analysis of *EWSR1* rearrangement using fluorescence in situ hybridization (FISH). Tumors positive for *EWSR1* gene rearrangement were tested by next-generation sequencing (NGS) using fusion-detecting panels. NGS results were confirmed by reverse-transcription polymerase chain reaction or by FISH. Twenty-six tumors originally diagnosed as CCMC (26/94, 27.6%) revealed split signals for *EWSR1* by FISH. Six of these tumors (6/26, 23%) displayed amplification of the *EWSR1* locus. Fifteen cases were analyzable by NGS, whereas 9 were not, and tissue was not available in 2 cases. None of the CCMCs with *EWSR1* rearrangements detected by FISH had an *EWSR1* fusion transcript. Fusion transcripts were detected in 6 cases (6/15, 40%), including *LIFR-PLAG1* and *CTNNB1-PLAG1*, in 2 cases each, and *CHCHD7-PLAG1* and *EWSR1-ATF1* fusions were identified in 1 case each. Seven cases, including those with *PLAG1* fusion, were positive for *PLAG1* rearrangement by FISH, with notable exception of *CHCHD7-PLAG1*, which is an inversion not detectable by FISH. One single case with *EWSR1-ATF1* fusion in NGS showed *ATF1* gene rearrangement by FISH and was reclassified as clear cell carcinoma (CCC). In addition, another 4 cases revealed *ATF1* rearrangement by FISH and were reclassified as CCC as well. Moreover, 12/68 (17%) CCMCs with intact *EWSR1* gene were selected randomly and analyzed by NGS. *PLAG1* fusions were found in 5 cases (5/12, 41.6%) with *LIFR* (2 cases), *FGFR1* (2 cases), and *CTNNB1* (1 case) as partner genes. Overall, *PLAG1* gene rearrangements were detected in 10/38 (26%) tested cases. None of the tumors had SMARCB1 loss by immunohistochemistry as a possible explanation for the *EWSR1* abnormalities in FISH. Novel findings in our NGS study suggest that *EWSR1*-FISH positive CCMC is a gene fusion-driven disease with frequent oncogenic *PLAG1* fusions, including *LIFR-PLAG1* and *CTNNB1-PLAG1* in most cases. Productive *EWSR1* fusions are found only in a minority of *EWSR1-ATF1*-rearranged cases, which were in part reclassifiable as CCCs. Detectable *EWSR1*-FISH abnormality in CCMCs without gene fusion perhaps represents a passenger mutation with minor or no oncologic effect.

Key Words: salivary glands, clear cell myoepithelial carcinoma, *EWSR1* gene rearrangement, molecular, gene fusion, *PLAG1*

(*Am J Surg Pathol* 2021;45:1–13)

From the *Department of Pathology, Faculty of Medicine in Pilsen, Charles University; †Bioptic Laboratory Ltd; §Molecular and Genetic Laboratory, Bioptic Laboratory Ltd, Pilsen; ‖The Fingerland Department of Pathology, Charles University, Faculty of Medicine and University Hospital Hradec Kralove, Hradec Kralove; ††Department of Pathology, 3rd Faculty of Medicine, Charles University and Kralovske Vinohrady University Hospital, Prague; §§Molecular and Genetic Laboratory, South Bohemian University, Ceske Budejovice, Czech Republic; ‡Department of Pathology, Friedrich-Alexander University Erlangen-Nürnberg (FAU), University Hospital of Erlangen, Erlangen, Germany; ¶Department of Pathology, Warmia nad Mazury University, Olsztyn; #Department of Pathology, Medical University of Gdansk, Gdansk, Poland; **Department of Pathology, University of Parma, Parma, Italy; ‡‡Medical Laboratory CSD, Kyiv, Ukraine; ‖‖Institute of Biomedicine, University of Turku; and ¶¶Department of Pathology, Turku University Hospital, Turku, Finland.

Preliminary results of the study were presented as a platform presentation at the 109th Annual Meeting of the USCAP, Los Angeles, CA, February 29 to March 5, 2020.

Conflicts of Interest and Source of Funding: Supported in part by study grant SVV 260 539 from the Ministry of Education, Czech Republic and the Finnish Cancer Society, Helsinki, Finland. The authors have disclosed that they have no significant relationships with, or financial interest in, any commercial companies pertaining to this article.

Correspondence: Alena Skálová, MD, PhD, Sikl's Department of Pathology, Faculty of Medicine in Pilsen, Charles University, E. Benese 13, Pilsen 305 99, Czech Republic (e-mail: skalova@fnplzen.cz).

Myoepithelial carcinoma (MC) is an underrecognized and challenging entity with a broad morphologic

spectrum. Histologically, MC is defined as a tumor composed almost exclusively of myoepithelial cells and characterized by an invasive growth pattern. Salivary gland neoplasms are generally rare and histologically diverse, with 20 distinct types recognized by the World Health Organization (WHO) Classification of Tumors of the Head and Neck.[1] Among salivary gland malignancies, MC seems particularly challenging, as it is rare and understudied, and it features poorly defined diagnostic and prognostic criteria.

In earlier studies, MC was reported to account for < 2% of all salivary gland malignancies, but the incidence of MC is currently believed to be higher. This is mainly because MC is easily underrecognized given its broad histologic spectrum and overlapping morphologic features with other salivary gland tumors, benign or malignant.[2–4] MC may arise in the context of a preexisting pleomorphic adenoma (MC ex-PA) or de novo, and it may affect major or minor salivary glands.[1]

When the morphologic features of malignancy such as infiltrative destructive growth or overt cytologic atypia with high-grade features are obvious, the malignant nature of this tumor can be readily recognized. However, MC often appears histologically and cytologically exceptionally bland.[4] In such cases, the diagnosis may be easily overlooked and the tumor may be misclassified as a benign salivary gland neoplasm, such as cellular or myoepithelial-rich PA. This is challenging in cases of MC ex-PA, particularly if the tumor shows minimal or no capsular invasion.[3–5] Misinterpreting MC is not uncommon, and distinguishing it from its mimics, especially cellular myoepithelial-rich pleomorphic adenoma (PA), can be difficult.

Clinically, MC seems to be relatively aggressive even when it is intracapsular or minimally invasive MC ex-PA.[4,5] MC is reported to have a high frequency of recurrence, including 37% risk of local recurrence and 22% occurrence of distant metastasis.[5–10] It is important to distinguish MC from its benign mimics at an early stage of the disease to provide adequate management and follow-up.

MC of salivary glands displays a broad spectrum of morphologies, including a clear cell variant.[10,11] The genetic features of MC are largely unknown.[12,13] In a recent multidimensional genomic analysis of a series of 40 MCs of salivary glands, Dalin et al[14] identified a low mutational load and high prevalence (70%) of oncogenic gene fusions, mostly involving the *PLAG1* gene.[14] Recently, our group described an *EWSR1* gene rearrangement in a subset of MCs from major and minor salivary glands composed predominantly of clear cells with frequent necrosis.[10] Most patients with *EWSR1*-rearranged clear cell myoepithelial carcinomas (CCMC) revealed poor clinical outcomes. In contrast to our results,[10] *EWSR1* rearrangements were not described by Dalin et al.[14] *EWSR1* gene fusions with a high frequency of *EWSR1-POU5F1* and *EWSR1-PBX3* fusions have been, however, previously identified in a wide spectrum of myoepithelial tumors of soft tissues and skin but not in salivary glands.[15–17]

Despite histomorphologic similarities with soft tissue tumors, salivary MCs appear molecularly different from myoepithelial tumors of soft tissues. In particular, *PLAG1* gene fusions are a distinct feature of salivary MCs.[14] To identify possible oncogenic gene fusions, salivary CCMCs with *EWSR1* gene rearrangement detected by fluorescence in situ hybridization (FISH) in the previous study[10] were now tested by next-generation sequencing (NGS) using gene fusion-detecting panels and compared with a cohort of salivary CCMCs with an intact *EWSR1* gene.

MATERIALS AND METHODS

Case Selection and Clinicopathologic Review

The study was approved by the institutional review board. A retrospective review of Salivary Gland Tumor Registry of the authors' files (A.S. and M.M.) was conducted by searching for the key words "clear cell myoepithelial carcinoma," "hyalinizing clear cell," and "clear cell malignant myoepithelioma." A total of 94 cases of MC were retrieved from the consultation files of the Salivary Gland Tumor Registry, at the Department of Pathology, Faculty of Medicine in Pilsen, and Biopticka Laboratory Ltd, Pilsen, Czech Republic, and from the consultation files of the coauthors. Twenty-six cases originally diagnosed as CCMC (26/94) revealed split signals for *EWSR1* by FISH.[10] Tumors positive for *EWSR1* gene rearrangement were tested by NGS using fusion-detecting panels. NGS results were further confirmed by reverse-transcription polymerase chain reaction (RT-PCR) and/or FISH. As a reference group, 12 cases of CCMC with intact *EWSR1* by FISH were studied with NGS for comparison.

The histopathologic features and the immunohistochemical (IHC) stains of all 94 tumors were reviewed (A.S., M.B.), and the diagnosis of MC was confirmed in cases that displayed morphologic and IHC features consistent with the original description.[10] The latter is represented by the coexpression of cytokeratins (CKs) or epithelial membrane antigen with at least 2 myoepithelial markers, such as S100, p63, CK14, SOX10, smooth muscle actin, and calponin (Table 1). Salivary gland tumors with tubuloductal and/or

TABLE 1. Antibodies Used for IHC Study

Antibody Specificity	Clone	Dilution	Antigen Retrieval/ Time	Source
S100 protein	Polyclonal	RTU	CC1/20 min	Ventana
CK7	OV-TL 12/30	1:200	CC1/36 min	DakoCytomation
CK14	SP53	RTU	CC1/64 min	Ventana
p63	4A4	RTU	CC1/64 min	Ventana
p40	Polyclonal	RTU	CC1/52 min	Biocare Medical
SOX10	Polyclonal	1:100	CC1/64 min	Cell Marque
MIB1	30-9	RTU	CC1/64 min	Ventana
SMA	1A4	RTU	CC1/36 min	Cell Marque
Calponin	EP798y	RTU	CC1/36 min	Ventana
SMARCB1	INI1	RTU	CC1/52 min	Cell Marque
SMARCA4	BRG-1	1:1000	CC1/52 min	AbCam

CC1 indicates EDTA buffer, pH 8.6; RTU, ready to use; SMA, smooth muscle actin.

epithelial-myoepithelial biphasic differentiation were excluded from the study.

For conventional microscopy, the excised tissues were fixed in formalin, processed routinely, embedded in paraffin (FFPE), cut, and stained with hematoxylin and eosin.

For IHC analysis, 4-μm-thick sections were cut from paraffin blocks and mounted on positively charged slides (TOMO; Matsunami Glass IND, Japan). Sections were processed on a BenchMark ULTRA (Ventana Medical System, Tucson, AZ), deparaffinized, and then subjected to heat-induced epitope retrieval by immersion in a CC1 solution at 95°C and pH 8.6. All primary antibodies used are summarized in Table 1. The bound antibodies were visualized using the ultraView Universal DAB Detection Kit (Roche, Basel, Switzerland) and the ultraView Universal Alkaline Phosphatase Red Detection Kit (Roche). The slides were counterstained with Mayer hematoxylin. Appropriate positive and negative controls were employed.

Clinical follow-up information was obtained when available from hospitals records, the patients, their physicians, or from referring pathologists.

MOLECULAR GENETIC STUDY

Sample Preparation for NGS and RT-PCR

For NGS and RT-PCR analysis, 2 to 3 FFPE sections (10 μm thick) were macrodissected to isolate tumor-rich regions. Samples were extracted for total nucleic acid using Agencourt FormaPure Kit (Beckman Coulter, Brea, CA). The RNA integrity was evaluated using PreSeq RNA QC Assay as was previously described.[18]

RNA Integrity Assessment and Library Preparation for NGS

Input of 250 ng of FFPE RNA was used as an input for NGS library construction. To assess RNA quality, the PreSeq RNA QC Assay using iTaq Universal SYBR Green Supermix (Biorad, Hercules, CA) was performed on all samples during library preparation to generate a measure of the integrity of RNA (in the form of a cycle threshold [C_t] value). Library preparation and RNA QC were performed following the Archer FusionPlex Protocol for Illumina (ArcherDX Inc.). A customized panel including *EWSR1*, *PLAG1*, and 58 other genes was used. The method enables detection of unknown fusion partners of included genes. Final libraries were diluted 1:100,000 and quantified in a 10 μL reaction following the Library Quantification for Illumina Libraries protocol and assuming a 200 bp fragment length (KAPA, Wilmington, MA).

NGS Sequencing and Analysis

Libraries were diluted to 4 nM and sequenced on a NextSeq sequencer (Illumina, San Diego, CA). The optimal number of raw reads per sample was set at 6 million. Library pools were diluted to 1.6 pM library stock with 20% 1.8 pM PhiX and loaded in the NextSeq cartridge.

The resulting FASTQ files were analyzed using the Archer Analysis software (version 5.1.7; ArcherDX Inc.). The algorithm for the detection of fusions and other rearrangements in Archer Analysis relies on the specificity of the gene-specific primers used in the amplification steps of the AMP process.

TABLE 2. Primers Used for RT-PCR

Name of Primer	Sequence 5′-3′
CHCHD27-PLAG1-F2	TTGACGTGTTTGGAGCTGGA
CHCHD27-PLAG1-R2	TCTTAGCCAGTCCCATTGACTC

Detection of CHCHD27-PLAG1 Fusion by RT-PCR

The RNA from FFPE tissue samples was reverse-transcribed using Transcriptor First Strand cDNA Synthesis Kit (Roche) according to manufacturer's instructions. For the fusion detection, 2 μl of cDNA was added to a reaction consisting of 12.5 μl of HotStar Taq PCR Master Mix (QIAGEN), 10 pM of each primer (Table 2), and distilled water up to 25 μl. The amplification program comprised initial denaturation at 95°C for 14 minutes, then 40 cycles of denaturation at 95°C for 1 minute, annealing at 55°C for 1 minute, and extension at 72°C for 1.5 minutes. The program was finished by incubation at 72°C for 7 minutes.

Successfully amplified polymerase chain reaction products of the *CHCHD27-PLAG1* fusion transcript were purified using Agencourt AMPure (Agencourt Bioscience Corporation, A Beckman Coulter Company, Beverly, MA). Then, the polymerase chain reaction products were sequenced both sides using a Big Dye Terminator Sequencing kit (Applied Biosystems, California), purified using the Agencourt CleanSEQ kit (Agencourt Bioscience Corporation), and run on an automated genetic analyzer ABI Prism 3130xl (Applied Biosystems) at a constant voltage of 13.2 kV for 20 minutes and compared with the GenBank sequence database.

FISH Analysis of EWSR1, ATF1, and PLAG1 Rearrangement

Overall, 4-μm-thick FFPE sections were placed onto positively charged slides. Hematoxylin and eosin stained slides were examined for determination of areas for cell counting.

The unstained slides were deparaffinized and incubated in the 1× Target Retrieval Solution Citrate pH 6 (Dako, Glostrup, Denmark) at 95°C for 40 minutes and subsequently cooled for 20 minutes at room temperature in the same solution. Slides were washed in deionized water for 5 minutes and digested in protease solution with Pepsin (0.5 mg/mL) (Sigma Aldrich, St. Louis, MO) in 0.01 M HCl at 37°C for 35 to 60 minutes according to sample conditions. Slides were then placed into deionized water for 5 minutes, dehydrated in a series of ethanol solution (70%, 85%, and 96% for 2 min each), and air-dried.

For the detection of *EWSR1*, *ATF1*, and *PLAG1* gene rearrangement, the commercial probes Vysis *EWSR1* Break-Apart (BA) FISH Probe Kit (Abbott Molecular, IL), oligo probe SureFISH 12/q13.12 *ATF1* BA (SureFISH/Agilent), and SureFISH 8q12.1 *PLAG1* BA

(SureFISH/Agilent) were used, respectively. An appropriate amount of mixed and premixed probes was applied on specimens, covered with a glass coverslip, and sealed with rubber cement. Slides were incubated in the ThermoBrite instrument (StatSpin/Iris Sample Processing, Westwood, MA) with codenaturation at 85°C/8 minutes and hybridization at 37°C/16 hours. A rubber cemented coverslip was then removed, and the slide was placed in posthybridization wash solution (2×SSC/0.3% NP-40) at 72°C/2 minutes. The slide was air-dried in the dark, counterstained with 4′,6′-diamidino-2-phenylindole DAPI (Vysis/Abbott Molecular), cover slipped, and examined immediately.

FISH Interpretation

The sections were examined with an Olympus BX51 fluorescence microscope (Olympus Corporation, Tokyo, Japan) using a ×100 objective and filter sets Triple Band Pass (DAPI/SpectrumGreen/SpectrumOrange), Dual Band Pass (SpectrumGreen/SpectrumOrange), and Single Band Pass (SpectrumGreen or SpectrumOrange).

For each probe, 100 randomly selected nonoverlapping tumor cell nuclei were examined for the presence of yellow or green and orange fluorescent signals. The yellow signals were considered negative, whereas separate orange and green signals with a distance of > 2 diameters of signal apart) were considered as positive. Cutoff values for BA probes were set to > 10% of nuclei with chromosomal break (mean ± 3 SD in normal nonneoplastic control tissues).

RESULTS

Clinical Findings and Pathologic Features

The clinicopathologic data for the 26 salivary gland tumors with original diagnosis of *EWSR1*-rearranged salivary CCMC are summarized in Table 3. All but one of these salivary gland tumors were published earlier.[10]

There were 16 females and 10 males, aged between 33 and 87 years, with a mean of 58.9 years. Fifteen of these salivary gland tumors occurred in the parotid gland (57.7%), 3 in the submandibular gland (11.5%), 5 in the

TABLE 3. *EWSR1*-FISH–positive Salivary Gland Tumors Originally Diagnosed as CCMC

Case No.	Diagnosis	IHC (S100/SOX10/PLAG1)	Sex/Age	Site	Size (cm)	TNM Stage	Therapy
1	CCMC, HG	+/ND/ND	Female/51	Pa	5×4×4.5	T3N1M0	SP, NeD, RT
2	CCMC ex-Pa	+/ND/ND	Female/43	Palate	3.5×4.0×2.0	T3N0M0	Exc, RT, CHT
3	CCMC ex-Pa	+/+/ND	Male/60	Pa	7.5×6.5×6.0	T4N0M0	Exc, RT, CHT
4	CCMC ex-Pa	+/+/ND	Female/35	Pa	9×6×5	T4aN1M1	RP, CHT
5	CCMC, HG	+/+/ND	Female/74	Pa	4×3×2	T2N1M0	RP, NeD, RT
6	CCMC, HG	+/ND/ND	Male/70	Palate	5×4×4	T4bN0M0	PMax, CHT, RT
7	CCMC, LG	+/+/neg	Female/67	Pa	8×4×2.5	T4N0M0	SP, CHT
8	CCMC, LG	+/ND/ND	Female/46	Palate	1×1.3×1.2	T1N0M0	Exc
9	CCC, NOS	Neg/neg/neg	Male/53	Pa	1×1.5×1.2	T1N0M0	Exc, RT
10	CCMC, HG	+/ND/ND	Female/67	Pa	4×5×3	T3N1M0	SP, RT
11	CCMC, LG	+/ND/ND	Female/81	Pa	3	T2N0M0	SP
12	EMC	+/ND/ND	Female /54	Pa	6×6×1.5	T4N0M0	SP
13	EMC	+/ND/ND	Female/34	Pa	2.5	T2cN0M0	SP
14	CCMC ex-Pa	+/ND/ND	Female/84	Subm	9×8×7	T4N0M0	Exc
15	CCC, HG	Neg/neg/neg	Female/72	Floor mouth	2×0.8×0.5	T1N0M0	Exc, refused RT
16	CCMC ex-Pa	+/+/+	Male/56	Pa	1.5	T1N0M0	Exc
17	CCMC, LG	+/ND/ND	Male/73	Palate	10×5.5×5	T3NxMx	BPMa
18	CCMC, LG	+/ND/ND	Male/70	Palate	2	T1bNxMx	CL, RMa after 2. Rec, RT
19	CCMC, HG	+/ND/ND	Female/55	Maxill sinus	8	T4bNxMx	RMa
20	CCMC, HG	+/ND/ND	Male/66	Lung	8×5×5.5	T3N1M0	Lobectomy
21	CCMC, HG	+/ND/ND	Female/87	Pa	5.5×5×3.5	T3N0M0	RP, RT
22	CCMC ex-Pa	+/ND/ND	Female/54	Subm gland	2.2×1.7×1.5	T2N0M0	Exc
23	CCMC, LG	+/+/ND	Female/33	Pa	2.4×2×2	T2N1M0	Exc, RT
24	CCMC, EMC	+/+/neg	Male/69	Pa	2.0	T1N0M0	Exc
25	CCC, HG	Neg/neg/neg	Male/78	Pa	2.5	T3N1M0	RP, RT
26	CCC, NOS, HG	Neg/neg/neg	Male/63	Subm	5.6	T3N2cM0	Exc, RT

*Neg *CHCHD7-PLAG1* is an inversion, FISH cannot detect.
†Amplification of the *EWSR1* locus.
+ indicates FISH positive; BPMa, bilateral partial maxillectomy; CHT, chemotherapy; CL, Caldwell-Luc procedure; DOC, dead of other causes; DOD, dead of disease; exc, complete excision; HG, high grade; LG, low grade; LN, lymph node; NA, not available; ND, not done; NeD, neck dissection; NED, no evidence of disease; neg, FISH negative; NOS, not otherwise specified; Pa, parotid; PMa, partial maxillectomy; Rec, recurrence; RMa, radical maxillectomy; RP, radical parotidectomy; RT, radiotherapy; SP, subtotal parotidectomy (conservative, partial, superficial, lateral); subm, submandibular.

minor salivary glands of the palate (19%), and 1 each in the mucosa of the maxillary sinus (3%), the lung (3%), and the floor of the mouth (3%). Size of the tumors ranged from 1.3 to 10 cm (average of 4.7 cm).

The tumors were diagnosed as de novo CCMC, low grade (n = 4); and CCMC, high grade (n = 8), using the system proposed by Kong et al,[5] and CCMC ex-PA (n = 6) based on medical history and using criteria as suggested by Katabi et al.[9] The remaining 8 salivary gland tumors were reclassified as (hyalinizing) clear cell carcinoma (CCC) (n = 5), epithelial-myoepithelial carcinoma (EMC) (n = 2), and CCC, high grade, not otherwise specified (n = 1) (Table 3).

Follow-up was available for 22 patients ranging from 1 to 18 years, with an average of 6.7 years. Five patients showed no evidence of disease at their latest control (5/22; 23%). Recurrence of the tumor appeared in 12 patients (12/22; 55%), and 3 of them developed regional lymph node metastases, whereas 6 patients had distant metastases. Fourteen patients (14/22; 64%) died owing to the disease at 1 to 16 years (average: 5.8 y). Five patients were found alive without evidence of disease at 1 to 18 years of follow-up (average: 8.6 y), and 2 died of other causes with no evidence of disease at 3 and 10 years after diagnosis (average: 6.5 y). The remaining 4 patients were lost to follow-up.

Data on treatment are available for all 26 patients. All tumors of the submandibular gland were treated by resection of the gland (n = 3). All 15 salivary gland tumors of the parotid gland were removed surgically, by radical parotidectomy in 4 patients, by subtotal parotidectomy in 6 patients, and by nonradical excision of the tumor in the other 5 patients. Five patients with carcinoma of the palate were treated either by partial maxillectomy (n = 2), by radical excision with clear margins (n = 2), or by the Caldwell-Luc procedure (n = 1), followed by a radical maxillectomy after second recurrence of the tumor. One patient with CCC of the sublingual gland and floor of the mouth underwent a simple nonradical excision, and refused radiotherapy. The remaining 1 patient with CCMC arising in the minor salivary glands of the maxillary sinus underwent radical maxillectomy. Neck dissection was

TABLE 3. *(Continued)*

Outcome	Follow-up	NGS	EWSR1 (Positive/Total)	FISH (PLAG1 BA)	FISH (ATF1 BA)
Rec (2 y) LN metastases (2 y)	DOD 6 y	Neg	21/100	Neg	ND
(1) rec (2 y), (2) rec to orbit (3 y), tumor progression (4 y), (3) rec to orbit (4 y), soft tissue metastases (4 y)	DOD 7 y	*LIFR-PLAG1*	19/100 31/100	+	ND
Rec (4 mo), lung metastases (12 mo)	DOD 1 y	*CTNNB1-PLAG1*	15/100	+	ND
Rec (1 y), LN metastases (1 y), metastases liver (1 y)	DOD 3 y	*CTNNB1-PLAG1*	30/100	+	ND
NED	DOC 11 y	NA	52/100	NA	NA
(1) rec (11 mo), (2) rec (5 y) invasion of orbit, (3) multifocal rec (6 y) invasion of ethmoid sinus, nasal cavity	DOD 8 y	Neg	29/100	Neg	ND
NED	NED 18 y	*CHCHD7-PLAG1*	23/100	Neg*	ND
NED	NED 16 y	NA	28/100	+	ND
Rec (1 y)	DOD 3 y	NA	33/100	Neg	+
Rec (3 y)	DOD 4 y	NA	24/100	Neg	ND
NA	NA	ND*	27/100	ND*	ND*
NED	DOC 10 y	NA	15/100	NA	ND
NA	NA	ND*	14/100	ND*	ND*
NED	DOC 3 y	NA	75/100	+	ND
Rec (4 y), LN metastases (4 y)	DOD 13 y	*EWSR1-ATF1*	95/100	ND	+
Rec (10 y), metastasis mediastine, bone (13 y)	DOD 16 y	Neg	12/100	+	ND
NA	NA	NA	65/100	ND	+
(1) Rec (6 y), (2) rec (9 y), (3) rec (10 y)	DOD 10 y	Neg	12/100	ND	ND
Rec 2 y	DOD 2 y	Neg	21/100	ND	ND
NED	Alive NED 2 y lost follow-up	Neg	22/100	ND	ND
	DOD 1 y	Neg	26/100†	ND	ND
NED	Alive NED 6 y	*LIFR-PLAG1*	37/100†	+	ND
NED	Alive NED 1 y lost follow-up	Neg	11/100†	ND	ND
Rec (5 y)	DOD 6 y	NA	12/50†	Neg	+
LN metastases (5 mo), metastasis in floor of mouth and gingiva (50 mo)	DOD 1 y	NA	10/50†	Neg	+
NA	NA	Neg	11/50†	ND	ND

performed for 2 patients, whereas 10 patients received postoperative radiotherapy, and 5 patients were treated by adjuvant chemotherapy. Details of therapy and follow-up are provided in Table 3.

In addition, 12 cases of salivary CCMCs with intact *EWSR1* gene were selected randomly and analyzed by NGS. They comprised 6 females and 6 males aged between 35 and 79 years, with a mean of 62.3 years. Eight of these CCMCs arose in the parotid gland (67%), 2 in the submandibular gland (16.5%), and 1 case each were from the minor salivary glands of the palate and the maxilla (16.5%). The size of the tumors ranged from 2.2 to 6 cm (average of 3.6 cm). The tumors were diagnosed as de novo CCMC, low grade (n = 5); CCMC, high grade (n = 2); and CCMC ex-PA (n = 5).[5,9] In 1 case, there were areas of EMC in addition to CCMC, low grade. Information regarding the therapy and follow-up is provided in Table 4.

Molecular Findings and Clinicopathologic Correlates

A total of 94 salivary gland tumors with a prominent clear cell component and/or myoepithelial differentiation were analyzed for *EWSR1* gene rearrangement by FISH as published earlier.[10] Twenty-six cases (26/94, 27.6%) originally diagnosed as CCMCs revealed split signals for *EWSR1* by FISH (Fig. 1). In 6 of these tumors (6/26, 23%), amplification of *EWSR1* locus was detected (Table 3). Fifteen cases were analyzable by NGS, whereas 9 cases were not, and no tissue was available in 2 cases. Fusion transcripts were identified in 6 of the 15 (40%) salivary gland tumors, including *LIFR-PLAG1* and *CTNNB1-PLAG1* in 2 cases each. The fusion *CHCHD7-PLAG1* was identified in 1 case (Fig. 2). All *PLAG1* fusions were confirmed by FISH with a notable exception of *CHCHD7-PLAG1*, which is an inversion not detectable by FISH. In this case, RT-PCR was used for confirmation. A total of 7 cases, including those with *PLAG1* fusions, were positive for *PLAG1* gene rearrangement by FISH. In 1 case, *EWSR1-ATF1* fusion was detected by NGS, whereas 4 more cases were not analyzable by NGS and showed *ATF1* gene rearrangement by FISH. All 5 salivary gland tumors with an *ATF1* gene rearrangement were, therefore, reclassified as (hyalinizing) CCCs.[19] No other fusion partners were found for the *EWSR1* gene, except for *ATF1*. Molecular findings in the 26 salivary gland tumors analyzed by NGS are summarized in Table 3.

In the group of 12 salivary gland tumors with intact *EWSR1* gene by FISH, fusion transcripts were found in 5 cases (5/12; 42%), including *LIFR-PLAG1* and *FGFR1-PLAG1* in 2 cases each, and *CTNNB1-PLAG1* in 1 case. In 7 cases, gene fusions were not detected by NGS, but 3 of them revealed *PLAG1* gene rearrangement by FISH (Fig. 1). These results are summarized in Table 4.

Histologic and IHC Findings

The total cohort of salivary gland tumors included 26 cases originally diagnosed as CCMC with *EWSR1* rearrangement by FISH, and 12 cases of CCMC with an

TABLE 4. CCMC With Intact *EWSR1* Gene

Case No.	Diagnosis	IHC (S100/SOX10/PLAG1)	Sex/Age	Site	Size (cm)	TNM Stage	Therapy	Outcome	Follow-up	NGS (SAR5)	FISH (*PLAG1* BA)
1	CCMC ex-PA, HG	+/+/ND	Female/67	Pa	3.7	pT2N0M0	SP	NED	6 mo	*FGFR1-PLAG1*	+
2	CCMC ex-PA, Rec. HG	+/+/+	Female/79	Maxilla	2.2×1.8×1.3	pT2N0M0	Exc	Rec 10 mo, AWD	2 y	*LIFR-PLAG1*	+
3	CCMC, LG	+/+/ND	Female/79	Pa	5.5×5.0×4.5	pT3N0M0	SP	NED	2 y	Neg	Neg
4	CCMC ex-PA	+/+/+	Male/68	Pa	3×2.8×2.5	pT2N0M0	RP	NED	3 mo	*CTTNB-PLAG1*	+
5	CCMC, LG	Neg/+/ND	Male/35	Subm	4	pT3N1M0	Exc	AWD	2 y	Neg	ND
6	CCMC, HG	+/+/+	Male/60	Pa	3×2×2	pT2N0M0	SP	NED	3 y	Neg	Neg
7	CCMC, HG	+/ND/DN	Female/60	Pa	4	pT3N1M0	SP	Rec 6 mo, DOD 4 y	4 y	*FGFR1-PLAG1*	+
8	CCMC ex-PA	+/+/+	Male/69	Pa	3×2.8×1.9	cT4aN0M0	SP, RT	NED	4 y	Neg	+
9	CCMC, LG	Neg/+/+	Female/67	Pa	3.5	pT3N0M0	SP	NED	2 y	Neg	+
10	CCMC	+/+/+	Male/58	Palate	6×4.8×3.2	pT3N0M0	Exc	NA	NA	*LIFR-PLAG1*	+
11	CCMC ex-PA, LG	+/+/+	Male/36	Pa	3.5×3.0	pT3N0M0	SP	NED	1 y	Neg	+
12	CCMC, LG EMC	+/+/ND	Female/69	Subm	3×2×1.8	pT2pNx	Exc	NED	6 mo	Neg	Neg

+ indicates FISH positive; AWD, alive with disease; HG, high grade; DOC, dead of other causes; DOD, dead of disease; exc, excision; LG, low grade; NA, not available; ND, not done; NED, no evidence of disease; neg, FISH negative; NOS, not otherwise specified; Pa, parotid gland; RP, radical parotidectomy; RT, radiotherapy; SP, subtotal parotidectomy; subm, submandibular gland.

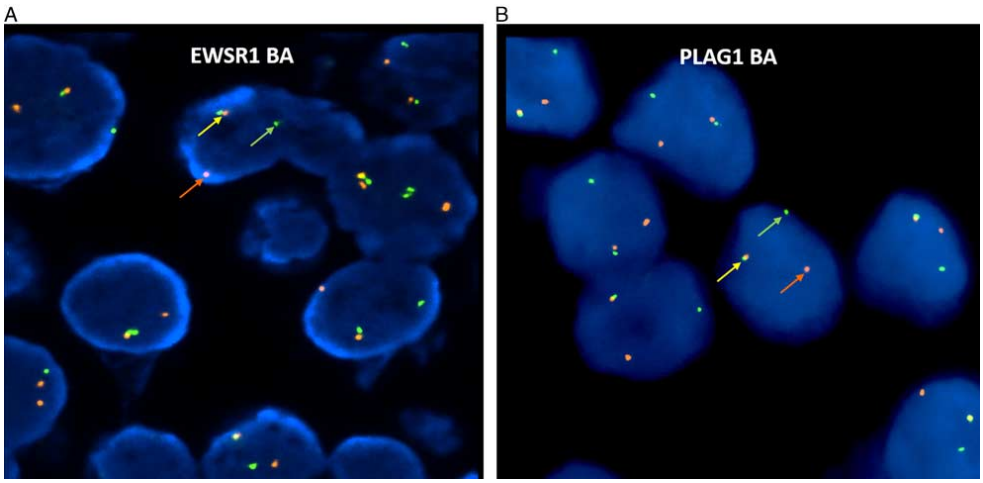

FIGURE 1. Examples of *EWSR1* and *PLAG1* BA probes. Positive BA result is represented by 1 orange-yellow-green (yellow arrows) complex signal from normal allele and one separated orange (orange arrows) and green (green arrows) signal from split allele. A, Vysis EWSR1 BA FISH Probe Kit (Abbott Laboratories, Lake Bluff, IL). B, SureFISH PLAG1 5′ BA 625 kbp and SureFISH PLAG1 3′ BA 295 kbp (SureFISH/Agilent Technologies, Santa Clara, CA).

intact *EWSR1* gene. After reevaluation of histologic, molecular, and IHC features of the 26 salivary gland tumors in the first group, 2 neoplasms were reclassified as EMC, 5 as (hyalinizing) CCC with *ATF1* gene rearrangement, and 1 as CCC with high-grade features, not otherwise specified, respectively (Tables 3, 4). After this, a final series of 30 salivary CCMCs derived from the groups with both rearranged and intact *EWSR1* included de novo CCMC, low grade (n = 9); CCMC, high grade (n = 10); and CCMC ex-PA (n = 11).

There were no major histomorphologic differences between the groups of *EWSR1*-rearranged versus *EWSR1*-intact CCMCs. All tumors showed invasive features at least focally. The tumors were partly encapsulated (n = 8) or frankly invasive (n = 8) (Figs. 3A, B). Twenty-two cases

FIGURE 2. Fusion transcripts involving PLAG1 gene in 5 cases of salivary CCMCs. Schematic visualization of detected fusion transcripts as revealed by NGS and detailed information about exon joining.

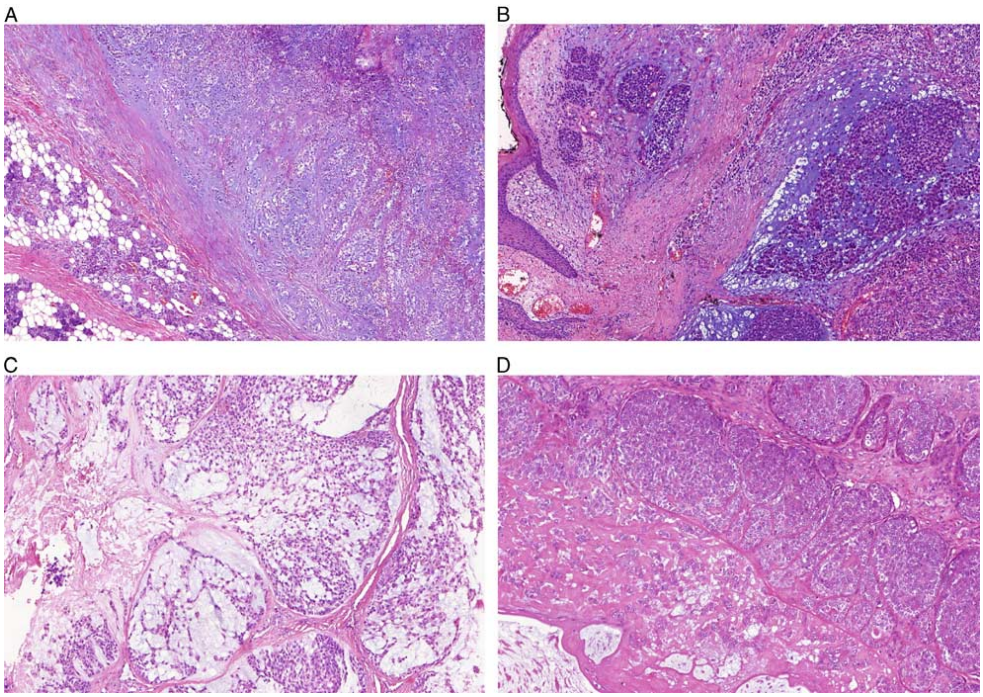

FIGURE 3. All CCMCs show at least focally invasive features. Tumor borders are multinodular, partly encapsulated (A), or infiltrative (B). The tumors had multinodular architecture divided by fibrous bands (C). In most cases, the tumor cells had a zonal arrangement with a hypercellular peripheral rim surrounding a hypocellular, usually myxoid and/or necrotic center (D).

(73%) showed well-delineated or broad pushing borders, whereas the remaining 8 cases (27%) showed more diffuse infiltrative growth into surrounding tissues. Majority (n = 24; 80%) of the tumors had multinodular architecture either as separate nodules divided by fibrous bands or as a single nodule with lobulated borders (Fig. 3C). A sheet-like arrangement was noted in 1 and a solid/trabecular growth pattern in 3 tumors, respectively, whereas 2 tumors displayed an encapsulated nodule with capsular invasion. In most cases, the tumor cells had a zonal arrangement with a hypercellular peripheral rim surrounding a hypocellular, usually myxoid and/or necrotic center (Fig. 3D).

Clear cells were a prominent component in 27 of the 30 cases examined (Fig. 4A). The remaining 3 cases showed spindle cell and rhabdoid/plasmacytoid cytology, respectively, with a minor clear cell component. Necrosis was a frequent feature, present in 25 of the 30 cases, and it varied widely from large necrotic areas (Fig. 4B) to small central foci in tumor islands resembling comedo necrosis, and to occasional minor necrotic foci that require careful search. Squamous pearls and/or areas of overt squamous differentiation were identified in 14 tumors (47%) (Fig. 4C), 1 of which had extensive squamous metaplasia (Fig. 4D). The amount of stroma varied widely among the cases. Myxoid stroma was noted in all cases at least focally. Various degrees of stromal hyalinization was observed in most cases (n = 24), varying from thickened basement membranes to hyaline stromal deposits accumulating between the cells (n = 13) (Fig. 5A), and to overt collagenous spherulosis-like formations (n = 7) and well-developed collagenous crystalloids (n = 4) (Fig. 5B).

Our CCMCs were classified as de novo in 19 cases (63%) and as CCMC ex-PA in 11 cases (37%). A benign PA component or a presence of a focal stromal hyalinized nodule was identified histologically in 4 cases (4/11, 36%). In the remaining 7 cases, the diagnosis of CCMC ex-PA was based on the patients' medical history with prior recurrent PAs.

Tumor cells showed a wide spectrum of nuclear atypia ranging from bland nuclei to pronounced pleomorphism (Fig. 5C). The latter was noted in 14 tumors (47%), and it was more prominent in the group of *EWSR1*-rearranged CCMC (12/18, 67%) than in the CCMC with intact *EWSR1* (4/12, 33%). Atypical mitoses were seen in 4 tumors, all of which had large areas of tumor necrosis and belonged to the group of *EWSR1*-rearranged CCMC. Proliferative activity, as measured by the MIB1 index (27/30), ranged from 10% to 100%, with a mean of 42%. The mean MIB1 index was

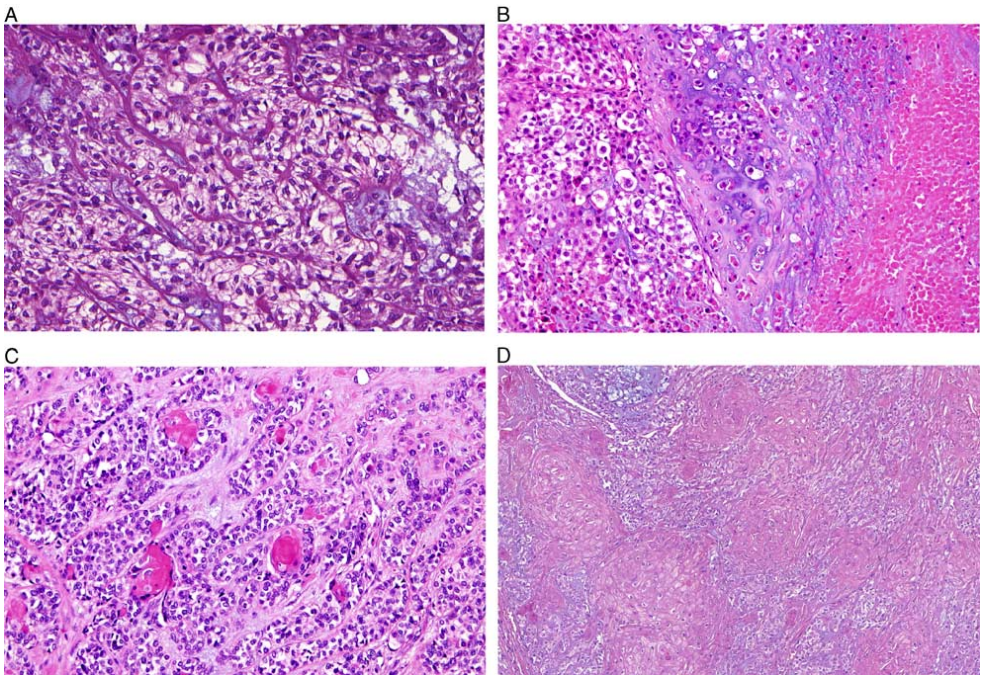

FIGURE 4. Clear cells represent a prominent component of CCMC (A). Necrosis is present in most cases (B). Squamous pearls or overt squamous differentiation are seen (C). A case with extensive squamous metaplasia (D).

slightly higher in the *EWSR1*-rearranged group (44.7%) compared with the group with intact *EWSR1* (37.3%) (Fig. 5D). All 5 salivary gland tumors with *ATF1* gene rearrangement, reclassified as (hyalinizing) CCCs, were multilobulated divided by fibrous septae and variable amounts of myxoid stroma (Fig. 6A). Four tumors (4/5, 80%) were composed exclusively of clear cells. Their growth patterns were suggestive of CCMC with invasive margins, comedo-necroses (Fig. 6B), multiple deposits of hyalinized extracellular matrix (Fig. 6C), and collagenous spherules in 1 case.

IHC Features

Immunohistochemical stains were performed on all 38 salivary gland tumors. All CCMCs were positive for CKAE1/AE3 (11/11), p63 protein (30/30), and SOX10 (15/15) (Fig. 7A). Positive staining for other myoepithelial markers included S100 protein (29/30) (Fig. 7B), calponin (9/15), p40 (8/10), CK14 (17/19), and SMA (11/18). Positive immunoexpression for CK7 (15/24) and PLAG1 (6/10) was detected as well (Fig. 7C). The 5 salivary gland tumors were reclassified as CCC were all positive for both p63 and p40, whereas staining for CK14, S100 protein, and SOX10 was seen in 4/5 (80%), 3/5 (60%), 1/5 (20%) of them, respectively (Fig. 6D). The 2 salivary gland tumors reclassified as EMC were biphasic by IHC with prominent staining of an abluminal myoepithelial layer for S100 protein and p63, and luminal staining for CK7. IHC staining for *SMARCB1 (INI1)* and *SMARCA4* was performed in 25 cases (in 1 case tissue material was not available). *SMARCB1* (Fig. 7D) and *SMARCA4* (Fig. 7E) showed positive protein staining in 23 and 16 cases, respectively. An invalid IHC result was obtained in 2 and 9 cases, respectively, owing to the absence of a positive inner control in the tissue lymphocytes. The most important IHC results are shown in Tables 3 and 4.

DISCUSSION

Salivary MC is a histologically challenging entity with diverse histology and heterogenous morphologic and IHC features. MC is vaguely defined as a neoplasm that almost exclusively manifests myoepithelial differentiation and is characterized by infiltrative growth pattern, according to the criteria described in the WHO Classification of Tumors of the Head and Neck.[1] MC can arise de novo or in association with a PA component (MC ex-PA). To date, only a few large series have been published describing the histologic features and prognosis of MC of salivary glands.[3–10,20] On the basis of these studies, MC seems to be relatively aggressive with a high risk of recurrence (cumulative recurrence

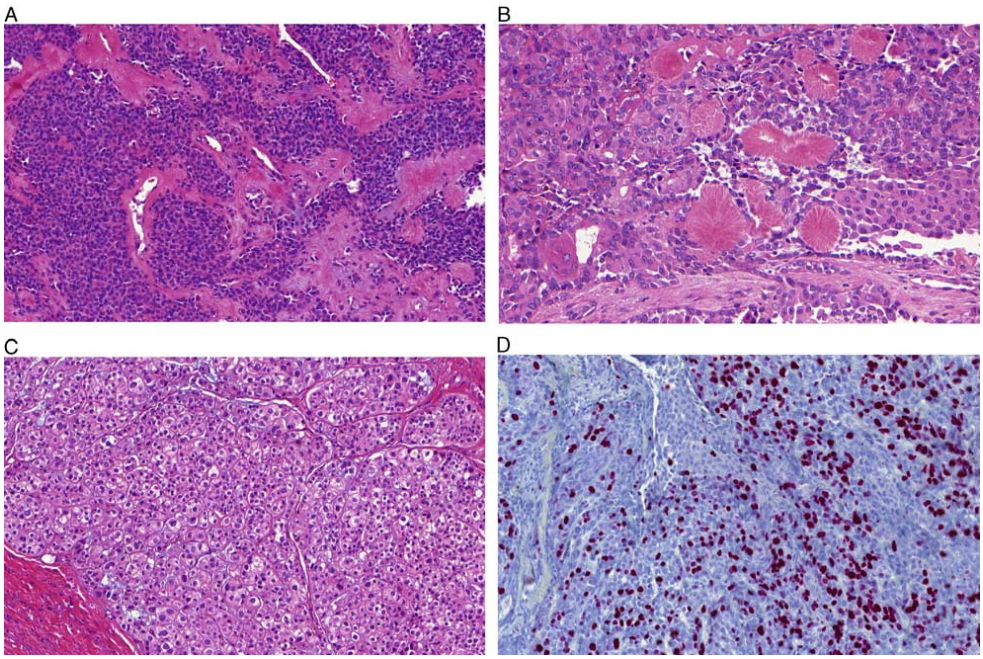

FIGURE 5. Various degrees of hyalinization varying from thickened basement membranes to hyaline stromal deposits accumulate between the cells (A). Collagenous spherulosis-like formations and well-developed collagenous crystalloids are seen (B). Tumor cells show nuclear atypia ranging from bland nuclei to pronounced pleomorphism (C). MIB1 index is slightly higher in tumors with rearranged *EWSR1* compared with tumors with intact *EWSR1* (D).

rate of 43%), including local recurrence (cumulative rate of 35%), lymph node metastases (cumulative rate of 21%), and distant metastases (cumulative rate of 22%).[4] In our prior paper, we have reported that patients with *EWSR1*-rearranged CCMC developed distant and lymph node metastases in 33% and 24%, respectively. Moreover, 8 patients died owing to disseminated cancer (38%), whereas 3 patients were alive with recurrent and/or metastatic disease (14%). The prognosis of CCMC with *EWSR1* rearrangement is rather poor, and it seems that the acquisition of *EWSR1* rearrangement may be the driver of the high-grade malignant phenotype and hence aggressive clinical behavior.[10] There are no active systemic therapies for this cancer, rendering recurrent or metastatic disease generally incurable.

The molecular alterations that would define salivary MC have not been well established.[12–14] In the past decade, molecular studies have suggested that some soft tissue and salivary myoepithelial neoplasms have genetical similarities. Myoepithelial tumors of soft tissue and bone display a heterogenous histologic spectrum, and nearly half of these tumors harbor *EWSR1* gene rearrangements.[15,21–26] In the largest study to date, *POU5F1* and *PBX1* were identified as the most common fusion partners, each reported to occur in up to 16% of the cases.[15,17] Other documented fusion partners of *EWSR1* in soft tissue myoepithelial tumors thus far are *ZNF444*, *KLF17*, *ATF1*, and *PBX3*.[15,22,23,27–29] *EWSR1* rearrangement has also been reported in primary salivary carcinomas having clear cell morphology. Antonescu et al[19] identified a consistent *EWSR1-ATF1* fusion in (hyalinizing) CCC of minor salivary glands. Similar *EWSR1* and *ATF1* gene rearrangements have also been identified in clear cell odontogenic carcinoma, providing molecular evidence of a link between CCC and clear cell odontogenic carcinoma.[30] A novel *EWSR1-CREM* fusion was reported in a subset of salivary CCCs,[31] and finally, *EWSR1* rearrangement has also been reported in a subset of primary salivary MCs having clear cell morphology, although the fusion partners were not identified.[10]

In the present study, rearrangements involving *PLAG1* were detected in salivary MCs that arise both de novo and ex-PA. *PLAG1* gene (PA gene 1) located on 8q12 and encoding a developmentally regulated zinc-finger protein displays common rearrangements in salivary PAs and MCs ex-PA with a function of proto-oncogene.[13] In a recent study on MCs,[14] the most frequent fusion partners of *PLAG1* were *FGFR1* (fibroblast growth factor receptor 1) (18%) and *TGFBR3* (transforming growth factor beta receptor 3) (15%). In contrast, *PLAG1* rearrangements have not been

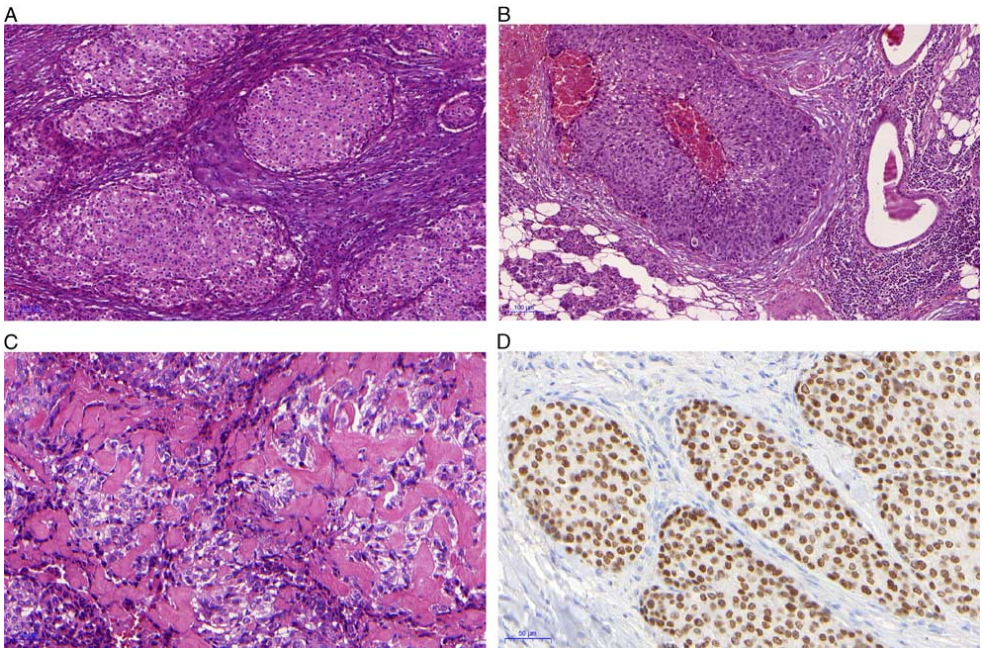

FIGURE 6. Salivary gland tumors with *ATF1* gene rearrangement, reclassified as CCCs, are multilobulated divided by fibrous septa with variable amount of myxoid stroma (A). Four tumors (4/5, 80%) were composed exclusively of clear cells. Growth pattern was suggestive of CCMC with invasive margins, comedo-necroses (B), multiple deposits of hyalinized extracellular matrix (C). Tumors reclassified as CCC are positive for p63 and p40 (D).

identified in soft tissue myoepitheliomas and MCs (that lack tubuloductal differentiation).[32,33] However, alterations of *PLAG1* gene have been described in a subset of skin and soft tissue myoepithelial tumors which morphologically show focal tubuloductal differentiation reminiscent of that seen in salivary PAs.[34]

Herein, we report a subset of *EWSR1*-FISH positive CCMCs harboring *PLAG1* fusions with partners including *CTNNB1* (β-catenin), *LIFR* (leukemia inhibitory factor receptor), and *CHCHD7* (coiled-coil helix-coiled-coil helix domain containing 7). Although *EWSR1* rearrangement was common to a subset of salivary MCs and soft tissue myoepithelial tumors, the prevalence of *PLAG1* fusions in CCMCs but not in the latter highlights the genetic dissimilarities between them. In our study, we have demonstrated that salivary MCs, even if a subset of them harbor the *EWSR1* rearrangement, represent an entity different from MCs of soft tissues. Apparently, occurrence of *PLAG1* fusions reflects the PA-like properties in MCs, whereas *EWSR1* fusions may relate somehow to the clear cell phenotype.

In this study, we report a subset of *EWSR1*-FISH positive CCMCs, but no fusion partners of *EWSR1* were discovered. The reason for such a discrepancy can only be speculated. Evaluation of the FISH results for the *EWSR1* locus could be tricky because of a possibility for occasional artificial separation of FISH signals in FFPE tissue.[35] This cannot be definitely ruled out, although our tumors showed widely separated FISH signals frequent enough for positivity (Table 3). Furthermore, none of our other FISH results suggested artificial separation.

Lack of the *EWSR1* fusion transcript in cases with *EWSR1* gene break could also be due to low quality of RNA from archive materials. A low level of signal in NGS could remain below threshold even if the sample had passed internal controls. However, in our experience, the kit we used can detect fusions down to a few copies. Yet another possibility could be fusion of exons not covered in the panel. This of course cannot be ruled out, although the panel covers all fusion breakpoints in the *EWSR1* gene reported so far.

Another intriguing possibility has been proposed recently.[36] As the *SMARCB1* and *EWSR1* genes are located only 5.5 Mbp apart in bands 22q11.23 and 22q12.2, respectively, it has been speculated that *EWSR1* aberrations could occur secondary to *SMARCB1* deletions. In a recent study, 4 tumors were described, where *SMARCB1* deletions concurred with regional *EWSR1* alterations, mimicking either balanced or unbalanced *EWSR1* rearrangements.[36] Furthermore, 3 case reports describe *SMARCB1*-deficient

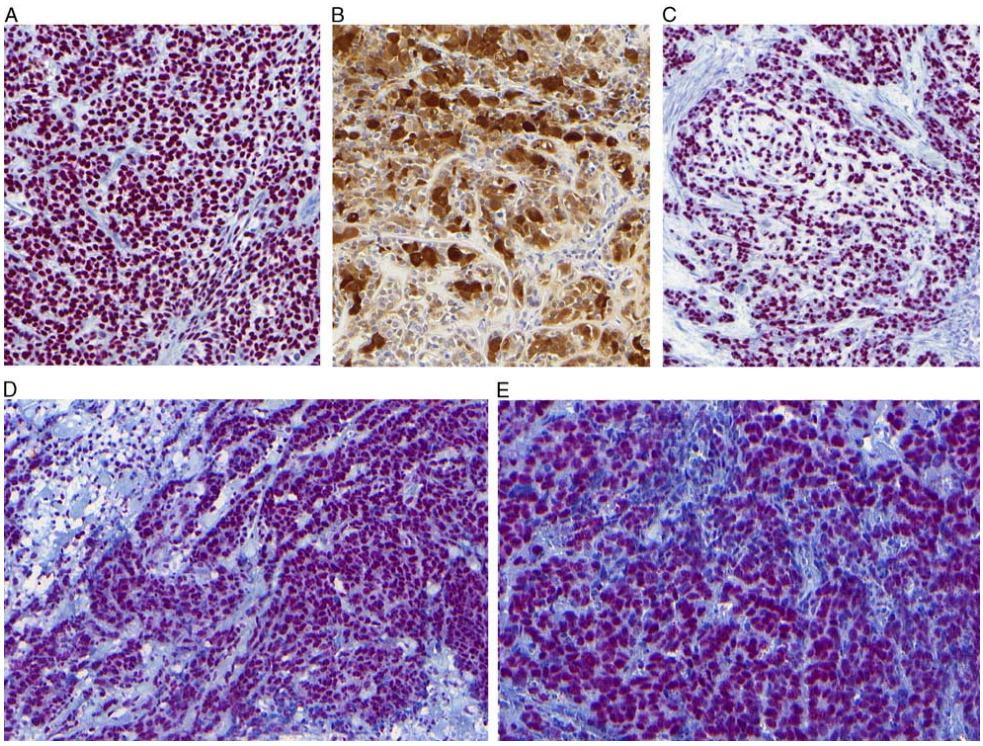

FIGURE 7. CCMCs show positive immunostaining for SOX10 (A), S100 protein (B), and PLAG1 (C). IHC staining for *SMARCB1* (D) and *SMARCA4* showed intact proteins (E).

tumors with *EWSR1* rearrangements, including 2 soft tissue MCs and 1 desmoplastic small round cell tumor.[24,37,38] In our cases (except case 14), a classic FISH pattern of *EWSR1* break was accompanied by a low-level amplification in 6 cases (Table 3). In addition, none of our *EWSR1*-FISH positive CCMCs revealed loss of *SMARCB1* protein. In agreement with our results, *SMARCB1*-deficient MCs and extraskeletal myxoid chondrosarcomas did not reveal a concurrent *EWSR1* rearrangement and *SMARCB1* deletion.[39,40] Thus, codeletion of *SMARCB1* and a part of *EWSR1* locus does not explain findings in our tumors. Having explored a number of alternative possibilities, however, we suspect that our *EWSR1* break without partner might represent just an unproductive passenger mutation.

Six tumors (6/26, 23%) displayed a mild amplification of the *EWSR1* locus. The significance of this finding is unknown. In contrast, a high-level amplification of the 3′ end of the *EWSR1* gene was reported accompanied by fusions, for example, with gene *NFATC2*.[15] However, we saw only mild amplifications not conforming to such findings (fig. 2I[15]).

In conclusion, despite morphologic overlap and an identical immunoprofile, a growing body of evidence indicates that salivary MCs are genetically significantly different from soft tissue myoepithelial tumors. Novel findings in our NGS study suggest that the *EWSR1*-FISH positive CCMC is a fusion-driven disease with prevalent oncogenic *PLAG1* fusions, including *LIFR-PLAG1*, *CTNNB1-PLAG1*, *FGFR1-PLAG1*, and *CHCHD7-PLAG1* in most cases. Cases with *EWSR1* fusion with *ATF1* represent a minority that should be reclassified as CCC. Another novel discovery is a minor subset of CCCs with myoepithelial S100-positive and/or SOX10-positive immunophenotype and an *ATF1* rearrangement. In the rest of CCMCs, an *EWSR1* break may represent a passenger mutation with presumably minor or no oncologic effect.

REFERENCES

1. Bell D, Di Palma S, Katabi N, et al. Myoepithelial carcinoma. In: El-Naggar AK, Chan JKC, Grandis JR, Takata T, Slootweg PJ, eds. *World Health Organization (WHO) Classification of Head and Neck Tumours*, 4th edition. Lyon, France: IARC Press; 2017:174–175.
2. McHugh JB, Visscher DW, Barnes EL. Update on selected salivary gland neoplasms. *Arch Pathol Lab Med*. 2009;133:1763–1774.

3. Savera AT, Sloman A, Huvos AG, et al. Myoepithelial carcinoma of the salivary glands: a clinicopathologic study of 25 patients. *Am J Surg Pathol*. 2000;24:761–774.
4. Xu B, Mneimneh W, Torrence DE, et al. Misinterpreted myoepithelial carcinoma of salivary gland: a challenging and potentially significant pitfall. *Am J Surg Pathol*. 2019;43:601–609.
5. Kong M, Drill EN, Morris L, et al. Prognostic factors in myoepithelial carcinoma of salivary glands: a clinicopathologic study of 48 cases. *Am J Surg Pathol*. 2015;39:931–938.
6. Yang S, Li L, Zeng M, et al. Myoepithelial carcinoma of intraoral minor salivary glands: a clinicopathological study of 7 cases and review of the literature. *Oral Surg Oral Med Oral Pathol Oral Radiol Endod*. 2010;110:85–93.
7. Kane SV, Bagwan IN. Myoepithelial carcinoma of the salivary glands: a clinico-pathologic study of 51 cases in a tertiary cancer center. *Arch Otolaryngol Head Neck Surg*. 2010;136:702–712.
8. Wang C, Zhang Z, Ge Y, et al. Myoepithelial carcinoma of the salivary glands: a clinicopathologic study of 29 patients. *J Oral Maxillofac Surg*. 2015;73:1938–1945.
9. Katabi N, Gomez D, Klimstra DS, et al. Prognostic factors of recurrence in salivary carcinoma ex pleomorphic adenoma, with emphasis on the carcinoma histologic subtype: a clinicopathologic study of 43 cases. *Hum Pathol*. 2010;41:927–934.
10. Skalova A, Weinreb I, Hyrcza M, et al. Clear cell myoepithelial carcinoma of salivary glands showing *EWSR1* rearrangement: molecular analysis of 94 salivary gland carcinomas with prominent clear cell component. *Am J Surg Pathol*. 2015;39:338–348.
11. Michal M, Skalova A, Simpson RH, et al. Clear cell malignant myoepithelioma of the salivary glands. *Histopathology*. 1996;28: 309–315.
12. Vekony H, Roser K, Loning T, et al. Copy number gain at 8q12.1-q22.1 is associated with a malignant tumor phenotype in salivary gland myoepitheliomas. *Genes Chromosomes Cancer*. 2009;48:202–212.
13. Katabi N, Ghossein R, Ho A, et al. Consistent *PLAG1* and *HMGA2* abnormalities distinguish carcinoma ex-pleomorphic adenoma from its de novo counterparts. *Hum Pathol*. 2015;46:26–33.
14. Dalin MG, Katabi N, Persson M, et al. Multi-dimensional genomic analysis of myoepithelial carcinoma identifies prevalent oncogenic gene fusions. *Nat Commun*. 2017;8:1197.
15. Antonescu CR, Zhang L, Chang NE, et al. *EWSR1-POU5F1* fusion in soft tissue myoepithelial tumors. A molecular analysis of sixty-six cases, including soft tissue, bone, and visceral lesions, showing common involvement of the *EWSR1* gene. *Genes Chromosomes Cancer*. 2010;49: 1114–1124.
16. Flucke U, Palmedo G, Blankenhorn N, et al. *EWSR1* gene rearrangement occurs in a subset of cutaneous myoepithelial tumors: a study of 18 cases. *Mod Pathol*. 2011;24:1444–1450.
17. Suurmeijer AJH, Dickson BC, Swanson D, et al. A morphologic and molecular reappraisal of myoepithelial tumors of soft tissue, bone and viscera with *EWSR1* and *FUS* gene rearrangements. *Genes Chromosomes Cancer*. 2020;59:348–356.
18. Skalova A, Vanecek T, Martinek P, et al. Molecular profiling of mammary analogue secretory carcinoma revealed a subset of tumors harboring a novel *ETV6-RET* translocation: report of 10 cases. *Am J Surg Pathol*. 2018;42:234–246.
19. Antonescu CR, Katabi N, Zhang L, et al. *EWSR1-ATF1* fusion is a novel and consistent finding in hyalinizing clear-cell carcinoma of salivary gland. *Genes Chromosomes Cancer*. 2011;50:559–570.
20. Nagao T, Sugano I, Ishida Y, et al. Salivary gland malignant myoepithelioma: a clinicopathologic and immunohistochemical study of ten cases. *Cancer*. 1998;83:1292–1299.
21. Rekhi B, Sable M, Jambhekar NA. Histopathological, immunohistochemical and molecular spectrum of myoepithelial tumours of soft tissues. *Virchows Arch*. 2012;461:687–697.
22. Agaram NP, Chen HW, Zhang L, et al. *EWSR1-PBX3*: a novel gene fusion in myoepithelial tumors. *Genes Chromosomes Cancer*. 2015;54: 63–71.
23. Flucke U, Mentzel T, Verdijk MA, et al. *EWSR1-ATF1* chimeric transcript in a myoepithelial tumor of soft tissue: a case report. *Hum Pathol*. 2012;43:764–768.
24. Thway K, Bown N, Miah A, et al. Rhabdoid variant of myoepithelial carcinoma, with *EWSR1* rearrangement: expanding the spectrum of *EWSR1*-rearranged myoepithelial tumors. *Head Neck Pathol*. 2015;9:273–279.
25. Brandal P, Panagopoulos I, Bjerkehagen B, et al. Detection of a t(1;22)(q23;q12) translocation leading to an *EWSR1-PBX1* fusion gene in a myoepithelioma. *Genes Chromosomes Cancer*. 2008;47: 558–564.
26. Brandal P, Panagopoulos I, Bjerkehagen B, et al. t(19;22) (q13;q12) Translocation leading to the novel fusion gene *EWSR1-ZNF444* in soft tissue myoepithelial carcinoma. *Genes Chromosomes Cancer*. 2009;48:1051–1056.
27. Jo VY, Antonescu CR, Dickson BC, et al. Cutaneous syncytial myoepithelioma is characterized by recurrent *EWSR1-PBX3* fusions. *Am J Surg Pathol*. 2019;43:1349–1354.
28. Yun S, Kim SH, Cho HS, et al. EWSR1-PBX3 fused myoepithelioma arising in metatarsal bone: case report and review of the literature. *Pathol Int*. 2019;69:42–47.
29. Huang SC, Chen HW, Zhang L, et al. Novel *FUS-KLF17* and *EWSR1-KLF17* fusions in myoepithelial tumors. *Genes Chromosomes Cancer*. 2015;54:267–275.
30. Bilodeau EA, Weinreb I, Antonescu CR, et al. Clear cell odontogenic carcinomas show *EWSR1* rearrangements: a novel finding and biologic link to salivary clear cell carcinomas. *Am J Surg Pathol*. 2013;37:1001–1005.
31. Chapman E, Skalova A, Ptakova N, et al. Molecular profiling of hyalinizing clear cell carcinomas revealed a subset of tumors harboring a novel *EWSR1-CREM* fusion. Report of 3 cases. *Am J Surg Pathol*. 2018;42:1182–1189.
32. Hallor KH, Teixeira MR, Fletcher CD, et al. Heterogeneous genetic profiles in soft tissue myoepitheliomas. *Mod Pathol*. 2008;21:1311–1319.
33. Matsuyama A, Hisaoka M, Hashimoto H. *PLAG1* expression in mesenchymal tumors: an immunohistochemical study with special emphasis on the pathogenetical distinction between soft tissue myoepithelioma and pleomorphic adenoma of the salivary gland. *Pathol Int*. 2012;62:1–7.
34. Antonescu CR, Zhang L, Shao SY, et al. Frequent *PLAG1* gene rearrangements in skin and soft tissue myoepithelioma with ductal differentiation. *Genes Chromosomes Cancer*. 2013;52:675–682.
35. Sadri N, Puthiyaveettil R, Zhang PJ. Study of *EWSR1* dual colored probe FISH assay on tumors and tissues not known to have *EWSR1* translocation on paraffin sections: Potential pitfalls in interpretation of FISH signal separation. *Sarcoma Res Int*. 2016;3:1–4.
36. Huang S-C, Zhang L, Sung Y-S, et al. Secondary *EWSR1* gene abnormalities in *SMARCB1*-deficient tumors with 22q11-12 regional deletions: potential pitfalls in interpreting *EWSR1* FISH results. *Genes Chromosomes Cancer*. 2016;55:767–776.
37. Machado I, Lopez-Soto MV, Rubio L, et al. Soft tissue myoepithelial carcinoma with rhabdoid-like features and EWSR1 rearrangement: fine needle aspiration cytology with histologic correlation. *Diagn Cytopathol*. 2015;43:421–426.
38. Soon GS, Petersson F. Beware of immunohistochemistry–report of a cytokeratin-, desmin- and INI-1-negative pelvic desmoplastic small round cell tumor in a 51 year old woman. *Int J Clin Exp Pathol*. 2015;8:973–982.
39. Kohashi K, Oda Y, Yamamoto H, et al. SMARCB1/INI1 protein expression in round cell soft tissue sarcomas associated with chromosomal translocations involving EWS: a special reference to SMARCB1/INI1 negative variant extraskeletal myxoid chondrosarcoma. *Am J Surg Pathol*. 2008;32:1168–1174.
40. Le Loarer F, Zhang L, Fletcher CD, et al. Consistent SMARCB1 homozygous deletions in epithelioid sarcoma and in a subset of myoepithelial carcinomas can be reliably detected by FISH in archival material. *Genes Chromosomes Cancer*. 2014;53:475–486.

1.3 A MINORITY OF CASES OF ACINIC CELL CARCINOMA OF THE SALIVARY GLANDS DRIVEN BY AN *NR4A2* REARRANGEMENT: THE DIAGNOSTIC UTILITY OF THE ASSESSMENT OF *NR4A2* AND *NR4A3* ALTERATIONS IN SALIVARY GLAND TUMORS.

Acinic cell carcinoma (AciCC) constitutes approximately 10% of malignant salivary gland tumors and is the second most common pediatric salivary gland malignancy [2]. Classic low-grade AciCC has a favorable prognosis, with 5-year and 10-year survival rates of 97% and 94%, respectively [21]. However, some cases undergo a high-grade transformation, leading to an aggressive clinical course [22, 23].

Typical AciCC exhibits a solid-microcystic structure with occasional follicular, tubular, and papillary growth patterns [2]. Neoplastic cells show a serous acinic differentiation with PAS-positive cytoplasmic granules. Eosinophilic, clear-cell, or vacuolated neoplastic cells may also be present. The tumor stroma is abundant with lymphoid infiltration and lymphoid follicles with germ centers formation tendency. Areas of transformation into high-grade carcinoma typically represent solid nests, often with central comedo-necrosis. Tumor cells are positive for SOX10, DOG1, negative for p40, p63, and S100. In typical low-grade cases, diagnosis is based on morphology alone, but immunohistochemical methods are helpful in cases with unusual morphology or high-grade transformation.

Genetically, the majority of AciCC cases are driven by t(4;9)(q13;q31) translocation, which leads to the transposition of active enhancer regions from the secretory calcium-binding phosphoprotein cluster of genes to the proximity of the *NR4A3* gene [24]. The result of this alteration is the overexpression of NR4A3 protein which can be detected by immunohistochemistry [25]. Rare cases may show upregulation of the *NR4A2* gene located at chromosome band 2q24.1 [26]. The aberration can also be identified by IHC. Both NR4A3 and NR4A2 immunostains are valuable for the differential diagnosis of AciCC with other salivary gland tumors, with high specificity and sensitivity for AciCC [27].

The authors conducted a study with 128 archival cases of AciCC, including 85 cases of low-grade AciCC, 7 cases of high-grade AciCC, and 36 cases with high-grade transformation (HGT). Low-grade AciCCs displayed a typical solid-microcystic pattern with abundant lymphoid stroma. Thirty-nine cases showed focal cystic or papillary growth patterns associated

with intratumoral hemorrhage. High-grade AciCCs and cases with HGT exhibited moderate to high-grade cytologic atypia, high mitotic activity, and comedo-type necrosis in the majority of cases (95%). One tumor with HGT also showed sarcomatoid dedifferentiation together with adenocarcinoma-like and typical low-grade solid-microcystic components.

We revealed DOG1 and SOX10-positivity by IHC in 98% and 99% of cases, respectively. NR4A3 was at least focally positive in 82% of cases, with comparable proportions in low-grade, HGT, and high-grade AciCC groups. We performed staining to all 23 NR4A3-negative and 33 NR4A3-positive tumors for NR4A2 revealing that 6 NR4A3-immunonegative cases displayed NR4A2-positivity, while none of the NR4A3-positive ones showed NR4A2 immunopositivity. Importantly, NR4A3 positivity was observed in both low-grade and high-grade areas of the tumors.

We assessed the *NR4A3* rearrangement by FISH in 57 cases, including 47 NR4A3-immunopositive and 10 NR4A3-immunonegative cases. *NR4A3* rearrangement was confirmed in 82% of NR4A3-immunopositive analyzable cases. 75% of NR4A3-immunonegative analyzable cases showed no rearrangement, while 25% displayed a positive *NR4A3* split signal. 9 cases were tested for *NR4A2,* including all 6 NR4A2-immunopositive and 3 NR4A2 and NR4A3-double-immunonegative cases. The *NR4A2* break-apart was confirmed in 25% of analyzable cases, while 75% of cases were negative for aberration. All 2 cases with the *NR4A2* rearrangement confirmed by FISH also have NR4A2 expression. The first of these two cases was originally diagnosed as oncocytoma of the parotid gland of a 19-year-old male because of solid-trabecular growth of uniform neoplastic cells with low-grade nuclear features and eosinophilia. The tumor displayed an *NR4A3* break-apart probe negativity. The second case is represented by typical solid-microcystic tumor morphology with HGT occurring in a 61 -year-old male. The *NR4A3* rearrangement was not analyzable by FISH in that case. Overall, 17 cases were negative for both NR4A3 and NR4A2 by IHC. We found *NR4A3* rearrangement by FISH in 2/4 cases which we were able to test in that group.

Previous reports declared 98% of NR4A3-sensitivity of AciCC by IHC [25, 27]. As much as 82% of our cases were NR4A3-immunopositive.

In conclusion, the author recommends using NR4A3, NR4A2, DOG1, and SOX10 immunostains as a cost-effective method for AciCC diagnostics. The NR4A3 was probably highly sensitive to suboptimal processing or old age of FFPE blocks. As for NR4A3-negative

cases, we found the utility of NR4A2-immunostain. From our point of view, both NR4A3 and NR4A2-immunostains are especially useful in small biopsy cases and challenging cases with unusual morphology.

We also suggest conducting a FISH analysis of *NR4A3* rearrangement in all NR4A3 and NR4A2-immunonegative cases. We believe that a negative result of molecular testing does not exclude the possibility of translocation. As reported by Haller et al. [25], some cases with breakpoints of chromosome 9 located higher upstream from the *NR4A3* gene might show normal, non-translocated signals by FISH. qRT-PCR might be employed to detect the *NR4A3* rearrangement for such cases. Further research is needed to explore potential different genetic aberrations in a very minor group of AciCC cases.

Virchows Archiv (2023) 482:339–345
https://doi.org/10.1007/s00428-022-03464-8

ORIGINAL ARTICLE

A minority of cases of acinic cell carcinoma of the salivary glands are driven by an *NR4A2* rearrangement: the diagnostic utility of the assessment of *NR4A2* and *NR4A3* alterations in salivary gland tumors

Natálie Klubíčková[1,2,3] · Petr Grossmann[2] · Petr Šteiner[2] · Martina Baněčková[1,2] · Elaheh Mosaieby[1,2] · Olena Koshyk[4] · Michal Michal[1,2] · Ilmo Leivo[5,6] · Alena Skálová[1,2]

Received: 4 November 2022 / Revised: 18 November 2022 / Accepted: 23 November 2022 / Published online: 5 December 2022

Abstract
Acinic cell carcinoma (AciCC) is a common salivary gland malignancy, typically composed of neoplastic acinic cells with zymogen granules. The vast majority of cases are driven by a t(4;9)(q13;q31) leading to enhancer hijacking and upregulation of the *NR4A3* gene. However, a minority of cases do not display *NR4A3* overexpression on immunohistochemical examination and are negative for the rearrangement involving the *NR4A3* gene when tested by FISH. Such cases overexpress *NR4A2*, and the protein product is detectable by immunohistochemistry. In this study, we aimed to assess the utility of NR4A2 and NR4A3 immunohistochemistry in the differential diagnosis of salivary gland tumors. Eighty-five cases of classic low-grade ACiCC, as well as 36 cases with high-grade transformation (HGT) and 7 high-grade AciCC cases were included in the analysis. NR4A3 was at least focally positive in 105/128 (82%) cases. Out of the 23 cases that were immunohistochemically negative for NR4A3, 6 displayed nuclear immunopositivity with the NR4A2 antibody. The *NR4A3* rearrangement was confirmed by FISH in 38/52 (73%) cases. In addition, this is the first report of an *NR4A2* rearrangement being detected by FISH in 2 AciCC cases that were negative for the *NR4A3* rearrangement. Our analysis confirms that the majority of AciCC, including high-grade cases and cases with HGT, are immunopositive for NR4A3, and suggests that NR4A3 immunohistochemistry is a powerful tool in the differential diagnosis of salivary gland tumors. However, its utility is limited in sub-optimally fixed samples which often display weaker and focal positivity. Our study also indicates that in a minority of cases, AciCC might be negative for NR4A3 immunostaining, because the pathogenic genetic event in these cases is instead a rearrangement involving the *NR4A2* gene.

Keywords Salivary gland · Acinic cell carcinoma · *NR4A3* · *NR4A2* · t(4 · 9)(q13 · q31) translocation · High-grade transformation

Introduction

Acinic cell carcinoma (AciCC) represents about 10% of malignant salivary gland tumors and is also the second most common pediatric salivary gland malignancy [1]. Middle-aged adults, more often female, are the most commonly affected, with the average age of about 50 years, but the age range is considerably wide. While the prognosis for patients with the classic low-grade AciCC is excellent, with 5-year and 10-year survival rates of 97% and 94%,

✉ Natálie Klubíčková
klubickova@biopticka.cz

[1] Department of Pathology, Faculty of Medicine in Pilsen, Charles University, Pilsen, Czech Republic

[2] Bioptical Laboratory, Ltd, Pilsen, Czech Republic

[3] Biomedical Center, Faculty of Medicine in Pilsen, Charles University, Pilsen, Czech Republic

[4] Medical Laboratory CSD, Kiev, Ukraine

[5] Institute of Biomedicine, Pathology, University of Turku, Turku, Finland

[6] Department of Pathology, Turku University Hospital, Turku, Finland

respectively [2], some cases display a transformation into high-grade, aggressively behaving neoplasms with unfavorable outcomes [3–5].

In typical low-grade cases, the neoplastic cells display a serous acinic differentiation with PAS-positive cytoplasmic granules. However, some neoplastic cells can also have eosinophilic, clear-cell or vacuolated cytoplasm. The most common architectural pattern is solid-microcystic, often with abundant lymphoid stroma, including well-formed lymphoid follicles with germ centers in some cases. Cribriform and cystic architecture is often associated with intratumoral hemorrhage. Follicular, tubular, and papillary growth patterns are less common and might pose a diagnostic challenge in some instances. Areas with transformation into high-grade carcinoma usually grow as solid nests, often with central comedonecrosis. Tumor cells are positive for SOX10 and DOG1, with the latter antibody usually showing an apical/canalicular pattern of staining. Conversely, p40, p63, and S100 markers are negative in AciCC. Even though the diagnostic process in acinic cell carcinoma is usually straight-forward, the immunohistochemical markers might be of benefit in challenging cases such as zymogen granule-poor and other rare morphological variants including clear-cell changes, tumors with high-grade transformation or unusually located tumors. In fine-needle aspiration cytology specimens, immunohistochemistry might aid to differentiate among zymogen granule-rich neoplastic cells of acinic cell carcinoma and normal acinic cells.

Genetically, the vast majority of AciCC are driven by t(4;9)(q13;q31), leading to the hijacking of strong enhancer regions from the secretory calcium-binding phosphoprotein cluster of genes (*SCPP*) to the proximity of *NR4A3* (*Nor1*) gene [6]. This causes the overexpression of *NR4A3* which might in turn detected by immunohistochemistry [7]. Rare cases that are negative for the translocation might display upregulation of another gene from the same group of nuclear receptors called *NR4A2* (*Nurr1*), located at chromosome band 2q24.1 [8]. Recently, immunohistochemical markers NR4A3 and, rarely, NR4A2 have been gaining importance in the differential diagnosis of salivary glands tumors, being highly specific and sensitive for AciCC [7–9].

Materials and methods

Case selection

For the current study, 128 AciCC cases were collected from institutional files of Biopticka laboratory. The diagnosis was confirmed by two pathologists (NK and AS) based on histomorphology and immunohistochemistry, in accordance with the current WHO classification of head and neck tumors [1]. Classic low-grade AciCC cases as well as cases with high-grade features or high-grade transformation (HGT) were included. Tumors with HGT were defined by the presence of a transformed area consisting of poorly differentiated carcinoma with high-grade features (with high mitotic activity and/or necrosis), within an otherwise well-defined, low-grade AciCC. The diagnosis of high-grade AciCC (without HGT) was rendered if areas with increased mitotic activity (> 5 mitotic figures/10 HPF (2.4 mm^2)) and/or necrosis were present in the tumor, without the presence of a classic low-grade area, in accordance with a grading system proposed by Xu et al. [3]. Similarly to previous studies [7], these high-grade cases were included based on the concordant immunohistochemistry and clinicopathological correlation, as most of the samples represented recurrent tumors, metastases, or probatory biopsy specimens.

Histology and immunohistochemistry

For conventional microscopy, the excised tissues were fixed in formalin, processed routinely, embedded in paraffin (FFPE), cut, and stained with hematoxylin & eosin. For the DOG1, SOX10, NR4A3, and NR4A2 immunohistochemistry, the 4-µm-thick sections cut from paraffin blocks were processed in accordance with institutional standard on BenchMark ULTRA (Ventana Medical Systems, Tucson, AZ). All primary antibodies with their respective epitope retrieval method used in this study are summarized in Table 1. Visualization was performed using the ultraView Universal DAB Detection Kit (Roche, Tucson, AZ) and ultraView Universal Alkaline Phosphatase Red Detection Kit (Roche, Tucson, AZ). The slides were counterstained with Mayer's hematoxylin. Appropriate controls were employed.

NR4A3 immunohistochemical examination was recognized as positive if moderate to strong nuclear staining was present at least focally (≥5% tumor cells). Cytoplasmic or membranous staining was considered non-specific and was not counted as positive. NR4A2 immunohistochemical stain displayed a strong background affinity to multiple, even non-neoplastic structures. Consequently, only strong diffuse nuclear staining was regarded as positive.

FISH

For the detection of *NR4A2* and *NR4A3* rearrangements, custom-design SureFISH *NR4A2* break-apart probe (SureFISH/Agilent Technologies, Santa Clara, CA, USA) and ZytoLight

Table 1 Antibodies used in the study

	Dilution	Clone	Source
DOG1	RTU	SP31	Ventana
NR4A2	1:100	N1404	Abcam
NR4A3	1:50	H-7	Santa Cruz
SOX10	RTU	SP267	Ventana

RTU, ready to use

SPEC *NR4A3* Dual Color Break Apart Probe (ZytoVision Gmbh, Bremerhaven, Germany) were used. Chromosomal locations (build Human Genome version hg19) used for custom *NR4A2* break-apart probe oligos were chr2:156,780,798–157,181,092 and chr2:157,198,713–157,599,007. The FISH procedure and interpretation of the results were performed as described previously [10].

Results

Demographic and clinical characteristics

The clinicopathological data for the 128 AciCC cases are summarized in Table 2. Eighty-five cases of low-grade AciCC, 7 cases of high-grade AciCC, and 36 cases with HGT were included in the study. The patients' age ranged from 11 to 86 years (mean = 56, median = 61). Patients with HGT and high-grade tumors were more than a decade older than patients with low-grade AciCC (mean = 65, median = 68 vs. mean = 52, median = 56). Whereas 72% of patients with low-grade AciCC were female, both sexes were affected almost equally in the HGT and high-grade groups. One hundred and sixteen cases were primary tumors, most commonly occurring in the parotid gland, while 1 case each originated from the sublingual gland, submandibular gland, and small salivary gland in the parapharyngeal space. Location was unknown in 1 case. In addition, 9 cases represented recurrences, and 3 metastases

Table 2 Clinical data and molecular-genetic features of the cases

128 AciCC cases		*n*	%
Clinical features			
	Sex		
	Female	84	66%
	Male	44	34%
	Age, median (range)	61 (11–86)	
	Primary tumor	116	91%
	Parotid gland	112	
	Submandibular gland	1	
	Sublingual gland	1	
	Minor salivary gland	1	
	Recurrence	9	7%
	Metastatic lesion	3	2%
Pathologic features			
	Size, median (range) (cm)	2.3 (0.4–9)	
	Mitotic figures/10 HPF (2.4 mm^2)		
	0–4	87	68%
	≥ 5	41	32%
	HG and HGT	43	34%
	Necrosis	41	32%
	Architecture		
	Solid-microcystic	115	90%
	Cystic/cystopapillary	39	30%
	Cribriform	16	13%
	Follicular	3	2%
	Clear-cell change	33	26%
	Eosinophilic/oncocytoid cytoplasm	2	2%
Immunohistochemistry			
	DOG1	126	98%
	SOX10	127	99%
	NR4A3	105	82%
NR4A3 break-apart by FISH			
	Total	38/52 analyzable cases	73%
	NR4A3-immunopositive cases	36/44 analyzable cases	82%
	NR4A3-immunonegative cases	2/8 analyzable cases	25%

AciCC, acinic cell carcinoma; *FISH*, fluorescence in situ hybridization; *HG*, high-grade; *HGT*, high-grade transformation; *HPF*, high-power field

in the lung, pleura, and omentum, respectively, were sampled. Tumor size ranged from 4 to 90 mm (mean 26.1, median 23).

Histopathologic and molecular-genetic features

Various architectural patterns were seen on microscopic examination, with the solid-microcystic pattern (Fig. 1A) being most prevalent ($n = 115$), commonly accompanied by abundant lymphoid stroma surrounding the neoplastic cell nests. Solid growth was present in 4% of low-grade AciCC cases ($n = 3$), while all cases with high-grade features contained at least minor parts with solid growth pattern. Occasionally, cystic or cystopapillary growth patterns were present ($n = 39$), often associated with intratumoral hemorrhage, with erythrocytes located in the lumina (Fig. 1B). Cribriform and follicular areas were revealed in 16 and 3 cases, respectively. Clear-cell change was frequent in both grade groups ($n = 33$), while oncocytoid or eosinophilic cytoplasm was observed in 2 cases with HGT. A collision with Warthin tumor was seen in 1 case of a parotid lesion of an 83-year-old female.

The high-grade cases and the high-grade areas in cases with HGT displayed moderate to high-grade cytologic atypia with larger round to oval, often vesicular nuclei, and well-visible nucleoli. The mitotic activity was moderate to high, reaching up to 69 mitotic figures/10 HPF (2.4 mm^2). In addition, necrotic areas were revealed in 95% of these cases ($n = 41$), usually in the form of comedo-type necrosis (Fig. 1C-D). In some cases, larger areas of geographic necrosis were revealed. Conversely, no necrotic foci were present and no more than 4 mitotic figures/10 HPF (2.4 mm^2) were counted in the low-grade cases.

One case with HGT revealed further sarcomatoid dedifferentiation. The tumor, arising in the parotid gland of a 78-year-old male, contained three components: a small typical low-grade solid-microcystic components, larger sarcomatoid component consisting of pleomorphic spindled cells growing in short fascicular and vaguely storiform patterns on the background of hyalinized fibrous stroma, and a tubular to cribriform adenocarcinoma-like component with high-grade nuclear atypia growing in nests inside the sarcomatoid area. The mitotic activity was similar in both the tubular and sarcomatoid regions, reaching 14 and 11 mitotic figures/10 HPF (2.4 mm^2), respectively, while no mitosis was revealed in the low-grade area. Small necrotic foci were present in the tubular component. On immunohistochemical examination, both the low-grade and the tubular-to-cribriform component were positive for NR4A3 but the sarcomatoid component was negative. FISH examination of an NR4A3 rearrangement was negative in all parts of the analyzed slide.

DOG1 immunomarker was positive in 126/128 (98%) cases (Fig. 2A), while SOX10 displayed nuclear positivity in 127/128 (99%) cases (Fig. 2B). NR4A3 was at least focally positive in 105/128 (82%) cases (Fig. 2C-D). A similar proportion (82% vs. 81% vs. 86%) of NR4A3-positive cases were revealed in the low-grade, HGT, and high-grade groups of AciCC.

Out of the 23 cases that were immunohistochemically negative for NR4A3 (Fig. 2E), all were positive for both DOG1 and SOX10. All NR4A3-negative and 33 NR4A3-positive cases were subsequently stained for NR4A2 ($n = 56$). Six of the NR4A3-immunonegative cases displayed unequivocal nuclear immunopositivity with the NR4A2 antibody (Fig. 2F), while all the 33 NR4A3-immunopositive cases tested negative for NR4A2 on immunohistochemistry (Table 3).

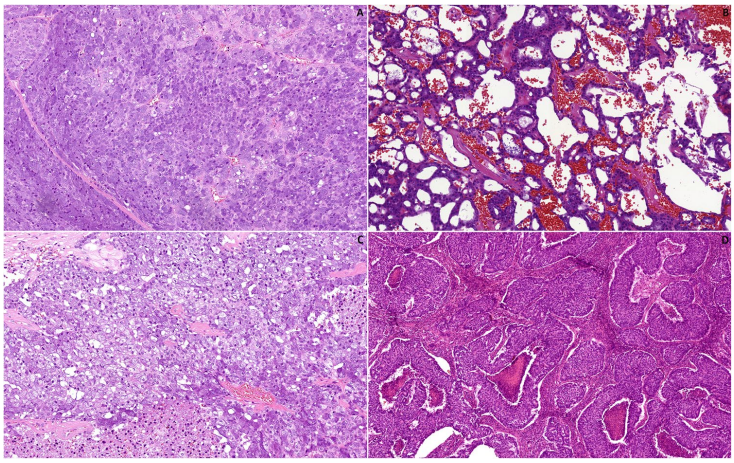

Fig. 1 Histomorphologic features of AciCC. **A** Neoplastic acinic cells with zymogen granules organized in a solid-microcystic pattern were the most common finding (case LG9). **B** Cystic-hemorrhagic pattern in low-grade AciCC (case LG15). **C** Clear cell change and necrotic foci in a case with HGT (case HGT9). **D** High-grade area with foci of comedonecrosis and high mitotic activity (case HGT3)

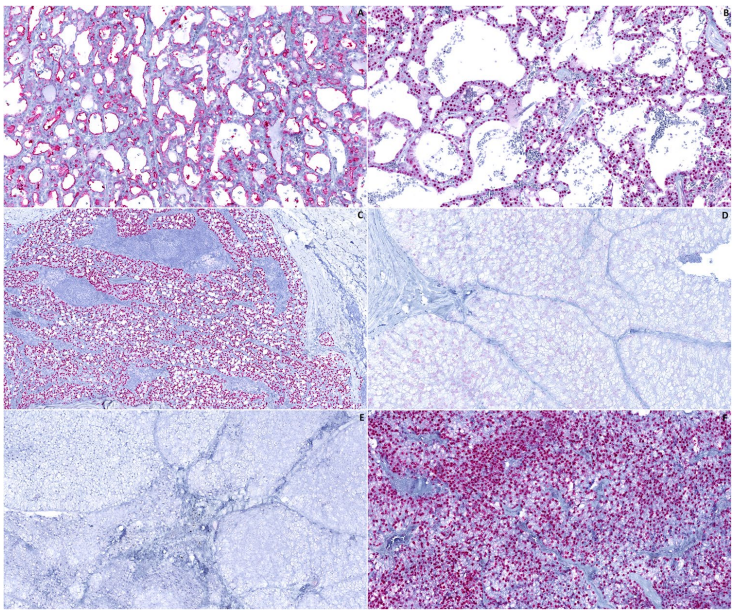

Fig. 2 Immunohistochemical findings Immunohistochemical staining for DOG1 (**A**) and SOX10 (**B**) was positive in 126/128 (98%) and 127/128 (99%) cases, respectively (case LG15). NR4A3 immunostaining revealed strong (**C**) (case LG10) to moderate (**D**) (case HGT9) nuclear positivity in 105/128 (82%) cases. Twenty-four cases did not stain for NR4A3 (**E**) (case LG13), six of which showed strong nuclear immunopositivity for NR4A2 (**F**) (case HGT23)

The *NR4A3* rearrangement was analyzed by FISH in 57 cases. Firstly, 47 NR4A3-immunopositive cases were tested. The rearrangement was verified in 23/28 (82%) low-grade AciCC cases, 11/14 (79%) cases with HGT, and 2/2 (100%) high-grade AciCC cases. In total, *NR4A3* rearrangement was confirmed by FISH in 36/44 (82%) NR4A3-immunopositive analyzable cases, while 8/44 (18%) cases were negative for the aberration. Secondly, 10 NR4A3-immunonegative cases were assessed, with 6/8 (75%) analyzable cases being negative on the FISH examination and 2/8 (25%) cases displaying a positive *NR4A3* split signal. Out of the whole cohort, 5 cases were not able to be analyzed by FISH.

Finally, we assessed the presence of a rearrangement involving *NR4A2* using a custom FISH break-apart probe (Table 3). In total, 9 cases were tested, including the 6 NR4A2-immunopositive cases and 3 cases that were negative for both NR4A2 and NR4A3 by immunohistochemistry. The *NR4A2* break-apart was confirmed in 2/8 (25%) analyzable cases, while 6/8 (75%) analyzable cases were negative and 1 case was not analyzable. Both cases with the *NR4A2* rearrangement confirmed by FISH were also positive for the NR4A2 immunohistochemical marker (Fig. 3B-C). The first case that harbored the break was an unusual low-grade AciCC affecting the parotid gland of a 19-year-old male. It displayed a solid-trabecular growth of uniform neoplastic cells with abundant eosinophilic and occasionally clear cytoplasm and was therefore originally diagnosed as oncocytoma (Fig. 3A). FISH analysis of an *NR4A3* break-apart was negative in this case. The second case was a tumor with HGT occurring in a 61-year-old male. The low-grade areas with solid-microcystic architecture gradually devolved into high-grade solid tumor displaying a conspicuous cytoplasmic clearing, nuclear atypia, and central necrosis. The *NR4A3* rearrangement was not analyzable by FISH.

Overall, 17 cases were immunohistochemically negative for both NR4A3 and NR4A2 markers. Four of these were able to be tested for the NR4A3 rearrangement by FISH, and the break was confirmed in 2/4 (50%) cases. The NR4A2 break-apart was further analyzed by FISH in 3 of these cases, with a negative result in all of them.

Table 3 NR4A2 immunohistochemistry and FISH analysis in acinic cell carcinoma

	Number of positive cases	Number of analyzed cases
NR4A2 immunohistochemistry		
Total	6	56
NR4A3-immunonegative cases	6	23
NR4A3-immunopositive cases	0	33
NR4A2 break-apart by FISH	2	8

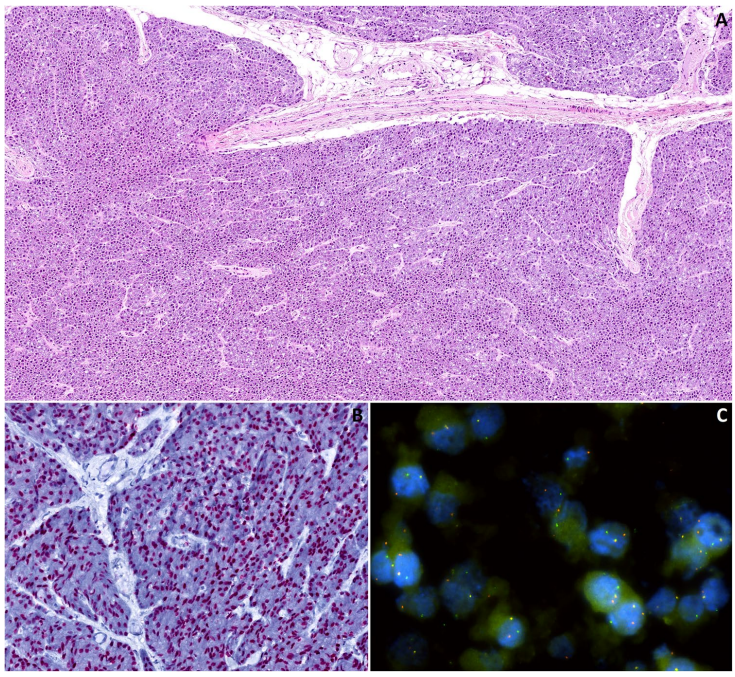

Fig. 3 *NR4A2*-rearranged case of AciCC (caseLG42). **A** The low-grade tumor was composed of uniform cells with eosinophilic cytoplasm organized in a solid-trabecular pattern. **B** Diffuse nuclear NR4A2 immunostaining. **C** FISH analysis utilizing a *NR4A2* break-apart probe was clearly positive

Discussion

In this study, we present an extensive analysis of the immunohistochemical and molecular genetic features of AciCC, a common malignant salivary gland tumor driven in most cases by t(4;9)(q13;q31) leading to upregulation of the *NR4A3* gene. NR4A3 immunostain is a powerful tool in differential diagnostics in AciCC cases. As much as 82% of cases were positive for NR4A3 in our series. However, previous reports documented an even higher proportion (up to 98%) of AciCC cases to be immunopositive for NR4A3 with a homogenous diffuse nuclear pattern [7, 9]. The discordance was likely caused by the inclusion of archival, sub-optimally fixed samples, which were slightly more prevalent in the low-grade cohort. The NR4A3 antigenicity was probably limited or completely lost in such cases, and the NR4A3 immunohistochemistry was apparently highly sensitive to sub-optimal processing in our laboratory. Although FISH analysis of the *NR4A3* rearrangement might be informative in some of these troublesome cases, a negative result of the molecular-genetic examination does not necessarily exclude the possibility of the t(4;9)(q13;q31) being present. As indicated by Haller et al. [7], some cases with chromosomal breakpoints of chromosome 9 located higher upstream from the *NR4A3* gene might show apparently normal, non-translocated fluorescence signals. Other methods might thereafter be employed to reveal the *NR4A3* overexpression (qRT-PCR) and the exact location of the chromosome breaks involved in the rearrangement, especially in rare cases with unusual morphology that might render the diagnostic process exceptionally difficult. Notably, since the mechanism of oncogenesis in acinic cell carcinoma is enhancer hijacking which upregulates *NR4A3*, and not a gene fusion that would code for an active fusion oncoprotein, no fusion transcript is detectable by RT-PCR or RNA-sequencing.

Importantly, both low-grade and high-grade (including cases with HGT) cases were able to be stained with the NR4A3 antibody. In cases with HGT, nuclear positivity for NR4A3 was observed in both low-grade and transformed areas. NR4A3 immunostaining might therefore be utilized in challenging cases, i.e., small samples containing poorly differentiated high-grade areas only, fine-needle aspiration cytology specimens [11, 12], tumors with unusual morphology etc.

In addition, AciCC might sporadically be driven by overexpression of *NR4A3* paralog *NR4A2*. Both genes code for proteins belonging to the steroid-thyroid hormone retinoid receptor family that act as transcription factors when activated by their respective ligands. The carcinogenetic process in tumors with the *NR4A2* rearrangement is therefore likely analogous to the enhancer hijacking described in *NR4A3*-rearranged acinic cell carcinomas. While *NR4A3*

locates to 9q31, *NR4A2* is found at 2q24. In this study, 6 NR4A3-immunonegative cases displayed a strong nuclear positivity with the NR4A2 antibody. NR4A2 immunoexpression was shown to correlate with *NR4A2* upregulation in AciCC in a recent study [8]. This is the first report of a rearrangement involving *NR4A2* being confirmed by FISH in 2 cases of AciCC. Interestingly, both cases displayed unusual morphologic features, with the first low-grade tumor resembling oncocytoma and the second tumor containing abundant clear-cell areas. Solid growth pattern was observed in both cases, similarly to the case reported by Haller et al. [8]. Further studies might contribute further evidence to clarify whether the *NR4A2* rearrangement occurs more frequently in AciCC cases with less usual morphology.

Lastly, a small cohort of our cases was negative for both NR4A2 and NR4A3 immunomarkers. FISH analysis of the *NR4A3* rearrangement proved more sensitive in two of these double-immunonegative cases, and they were finally classified as acinic cell carcinoma with an *NR4A3* rearrangement. However, rearrangements of *NR4A2* nor *NR4A3* were not detected by FISH in some of these double-immunonegative cases. Members of this group may represent cases where both detection methods used in this study failed, and the tumors in fact harbor *NR4A2* or *NR4A3* rearrangements. Some cases may nonetheless belong to a very minor group of AciCC cases whose pathogenesis is based on a different genetic aberration, whether it is, for example, the rearrangement of other genes from the nuclear receptor subfamily 4A, or another alteration of a completely unrelated gene.

In summary, we present a first report of an *NR4A2* rearrangement in a subset of acinic cell carcinoma cases. This genetic aberration was present in cases that were negative for the NR4A3 marker and positive for the NR4A2 marker on immunohistochemical examination. *NR4A2* and *NR4A3* code for highly similar, paralogous proteins; we therefore propose a similar pathogenetic process being involved in acinic cell carcinomas with the *NR4A2* rearrangement that has been proposed previously in tumors with the *NR4A3* break-apart. NR4A2 and NR4A3 are reliable immunohistochemical markers for acinic cell carcinoma whose importance is highlighted especially in challenging, less typical cases.

Author contribution All authors contributed to the study conception and design. Material preparation, data collection, and analysis were performed by NK and AS. The first draft of the manuscript was written by NK, and all authors commented on previous versions of the manuscript. There are two senior authors of this manuscript (IL and AS) with equal contribution.

Funding This study was supported by study grant SVV 260539 from the Ministry of Education, Czech Republic (NK). This work was supported by the Cooperatio Program, research area SURG (NK).

Data Availability Data supporting the findings of this study are available within the article. The complete datasets generated during and/or analyzed during the current study are available from the corresponding author upon reasonable request.

Declarations

Conflict of interest The authors declare no competing interests.

Informed consent Informed consent was not required for the study.

References

1. WHO classification of tumours editorial board (2022) Head and neck tumours, 5th edn. IARC Press, Lyon, France
2. Patel NR, Sanghvi S, Khan MN, Husain Q, Baredes S, Eloy JA (2014) Demographic trends and disease-specific survival in salivary acinic cell carcinoma: an analysis of 1129 cases. Laryngoscope 124(1):172–178
3. Xu B, Saliba M, Ho A, Viswanathan K, Alzumaili B, Dogan S, Ghossein R, Katabi N (2022) Head and Neck Acinic Cell Carcinoma: A New Grading System Proposal and Diagnostic Utility of NR4A3 Immunohistochemistry. Am J Surg Pathol 46(7):933–941
4. Thompson LD, Aslam MN, Stall JN, Udager AM, Chiosea S, McHugh JB (2016) Clinicopathologic and immunophenotypic characterization of 25 cases of acinic cell carcinoma with high-grade transformation. Head Neck Pathol 10(2):152–160
5. Skálová A, Sima R, Vanecek T et al (2009) Acinic cell carcinoma with high-grade transformation: a report of 9 cases with immunohistochemical study and analysis of TP53 and HER-2/neu genes. Am J Surg Pathol 33(8):1137–1145
6. Haller F, Bieg M, Will R et al (2019) Enhancer hijacking activates oncogenic transcription factor NR4A3 in acinic cell carcinomas of the salivary glands. Nat Commun 10(1):368
7. Haller F, Skálová A, Ihrler S et al (2019) Nuclear NR4A3 immunostaining is a specific and sensitive novel marker for acinic cell carcinoma of the salivary glands. Am J Surg Pathol 43(9):1264–1272
8. Haller F, Moskalev EA, Kuck S et al (2020) Nuclear NR4A2 (Nurr1) immunostaining is a novel marker for acinic cell carcinoma of the salivary glands lacking the classic NR4A3 (NOR-1) upregulation. Am J Surg Pathol 44(9):1290–1292
9. Wong KS, Mariño-Enriquez A, Hornick JL, Jo VY (2021) NR4A3 Immunohistochemistry reliably discriminates acinic cell carcinoma from mimics. Head Neck Pathol 15(2):425–432
10. Šteiner P, Andreasen S, Grossmann P et al (2018) Prognostic significance of 1p36 locus deletion in adenoid cystic carcinoma of the salivary glands. Virchows Arch 473(4):471–480
11. Millan N, Tjendra Y, Zuo Y, Jorda M, Garcia-Buitrago M, Velez-Torres JM, Gomez-Fernandez C (2022) Utility of NR4A3 on FNA cytology smears and liquid-based preparations of salivary gland. Cancer Cytopathol. https://doi.org/10.1002/cncy.22632. Online ahead of print.
12. Skaugen JM, Seethala RR, Chiosea SI, Landau MS (2021) Evaluation of NR4A3 immunohistochemistry (IHC) and fluorescence in situ hybridization and comparison with DOG1 IHC for FNA diagnosis of acinic cell carcinoma. Cancer Cytopathol 129(2):104–113

1.4. SCLEROSING POLYCYSTIC ADENOMA OF THE SALIVARY GLAND. A NOVEL NEOPLASM CHARACTERIZED BY *PI3K-AKT* PATHWAY ALTERATIONS – NEW INSIGHTS INTO A CHALLENGING ENTITY.

Sclerosing polycystic adenoma (SPA) is a rare salivary gland neoplasm that shows characteristic histologic features, which are reminiscent of sclerosing adenosis and various intraductal epithelial proliferations in the breast [2]. Initially, it was hypothesized that SPA is a non-neoplastic lesion analogous to fibrocystic disease of the breast [28]. The later data assumed that it is a genuine neoplasm [29,30,31,32,33]. SPA often contains solid and cribriform intraductal proliferation of apocrine ductal cells with nuclear atypia up to dysplasia/carcinoma in situ surrounded by an intact or partially disrupted myoepithelial cell layer [29]. In addition, SPA is reported to have a significant risk of local recurrence [2]. Moreover, a single study utilizing polymorphisms of the androgen receptor (AR) reported X-chromosome inactivation in all SPA cases suggesting that SPA is a clonal neoplastic process [32]. Bishop et al. found *PTEN, PI3KCA*, and *PIK3R1* mutations in a subset of SPA cases [34]. Thereby, the term "sclerosing polycystic adenoma" seems to reflect the neoplastic nature of neoplasm [35].

In our 36 case series, all cases fulfilled the characteristic histological criteria of SPA, such as lobulated well-circumscribed growth pattern, focal hyalinized stromal sclerosis, presence of large abnormal acinar cells with brightly eosinophilic intracytoplasmic granules, variably sized and shaped ducts lined by flattened, cylindrical, or apocrine epithelium. Ductal components are represented by foamy, vacuolated, apocrine, mucous, clear, squamous, columnar, and oncocyte-like cells. Foci of intraluminal solid and cribriform intercalated duct-like epithelial proliferation with variable degrees of dysplasia were observed in every case. In our work, we present for the first time diagnostic criteria for low and high-grade dysplasia in the solid and cribriform epithelial proliferations in SPA.

By IHC, ductal epithelial proliferations were positive for S100 protein, SOX10, and mammaglobin and have intact layers of myoepithelial cells on the periphery (IDC-type) in 58% of cases. They showed an ummunophenotype of intercalated ducts and were negative for AR and GATA3. 39% of cases had focal intraductal cribriform and micropapillary apocrine-type dysplastic epithelial structures composed of AR-positive and S100/SOX10 negative cells (apocrine type). All cases were negative for DOG1, PLAG1, and NOR1. HER2/neu overexpression and amplification were tested in 2 cases negative.

In our case series, we found two cases with overt malignant features ranging from high-grade intraductal carcinoma to invasive carcinoma with an apocrine ductal phenotype.

Our results of molecular testing were comparable with the observations of Bishop et al.[34] and Hernandez-Prera et al. [33]. We found that 92% of SPA cases had *PIK3CA* gene c.3140A > G, p.(His1047Arg) or c.1624G > A, p.(Glu542Lys) mutations. Morphologically all tumors with *PIK3CA* mutation are represented by focal solid and cribriform proliferation of epithelium with IDC-like phenotype and mild to moderate dysplasia. In contrast, the cases with detected *HRAS* and *AKT1* mutations displayed extensive apocrine solid and cribriform dysplastic components with severe atypia. Our index case of apocrine IDC with invasive SDC component arising from SPA showed an identical mutation in the *PIK3CA* gene in benign and both malignant components. Moreover, we found an additional *HRAS* mutation only in the malignant component. None of the *HRAS* and *AKT1* gene mutations has been documented in SPA previously. We didn't also find any gene fusions in our case series.

The *PI3K/Akt* pathway regulates cell survival, cell metabolism, and cell growth through the control of apoptosis, cell proliferation, and cell cycle [36]. The aberrant activation of the PI3K pathway might be caused either by activating mutations in *AKT1, PIK3CA*, and *mTOR* genes or by inactivating mutations in the *PTEN* gene [37]. Somatic mutations in the *AKT1* gene stimulate downstream signaling and are responsible for oncogenic transformation [37].

The alterations of *HRAS* and *PI3K* pathways in SPA with apocrine IDC component are identical to alterations detected in SDC and a subset of apocrine IDC [38]. Many studies emphasize important roles for *PI3K/AKT/mTOR* signaling in the tumorigenesis of SDC [39,40,41,42,43].

In our work, we presented a unique case of a salivary gland apocrine IDC with transformation to SDC, arising from SPA which harbored a mutation in PI3K/Akt pathway in all tumor components.

In total, our findings suggest a close relationship between SPA, apocrine IDC, and invasive SDC. SPA may represent a precursor lesion for the apocrine IDC and sometimes invasive SDC.

Sclerosing Polycystic Adenoma of Salivary Glands

A Novel Neoplasm Characterized by PI3K-AKT Pathway Alterations—New Insights Into a Challenging Entity

Alena Skálová, MD, PhD,† Martina Baněčková, MD, PhD,*† Jan Laco, MD, PhD,‡ Silvana Di Palma, MD,§ Abbas Agaimy, MD,‖ Nikola Ptáková, MSc,¶ Valérie Costes-Martineau, MD, PhD,# Bengt F. Petersson, MD, PhD,** Mari F.C.M. van den Hout, MD, PhD,†† Gisele de Rezende, MD,‡‡ Natálie Klubíčková, MD,*† Miroslav Koblížek, MD,§§ Olena Koshyk, MD,‖‖ Tomáš Vaneček, PhD,¶ and Ilmo Leivo, MD, PhD¶¶*

Abstract: Sclerosing polycystic adenoma (SPA) is a rare salivary gland neoplasm originally thought to represent a non-neoplastic lesion. Recently we have encountered an index case of apocrine intraductal carcinoma of parotid gland of 62-year-old man with invasive salivary duct carcinoma component arising from SPA, a combination of tumor entities that has never been published so far. Here, we further explore the nature of SPA by evaluating 36 cases that were identified from the authors' consultation files. The patients were 25 females and 11 males aged 11 to 79 years (mean, 47.8 y). All tumors originated from the parotid gland. Their size ranged from 11 to 70 mm (mean, 28 mm). Histologically, all cases revealed characteristic features of SPA, such as lobulated well-circumscribed growth, focal hyalinized sclerosis, presence of large acinar cells with abundant brightly eosinophilic intracytoplasmic granules, and ductal components with variable cytomorphologic characteristics, including foamy, vacuolated, apocrine, mucous, clear/ballooned, squamous, columnar and oncocyte-like cells. In all cases, there were foci of intraluminal solid and cribriform intercalated duct-like epithelial proliferations with variable dysplasia which were positive for S100 protein and SOX10, and fully enveloped by an intact layer of myoepithelial cells. In addition, 14/36 cases (39%) had focal intraductal cribriform and micropapillary apocrine-type dysplastic epithelial structures composed of cells positive for androgen receptors and negative for S100/SOX10. The intraductal proliferations of both types showed focal mild to severe dysplasia in 17 cases (17/36; 47%). Two cases showed overt malignant morphology ranging from high-grade intraductal carcinoma to invasive carcinoma with an apocrine ductal phenotype. Next generation sequencing using ArcherDX panel targeting RNA of 36 pan-cancer-related genes and/or a TruSight Oncology 170/500 Kit targeting a selection of DNA from 523 genes and RNA from 55 genes was performed. Tumor tissue was available for molecular analysis in 11 cases, and 9 (9/11; 82%) of them harbored genetic alterations in the PI3K pathway. Targeted sequencing revealed *HRAS* mutations c.37G > C, p.(Gly13Arg) (2 cases) and c.182A > G, p.(Gln61Arg) (2 cases), and *PIK3CA* mutations c.3140A > G, p.(His1047Arg) (3 cases), c.1633G > A, p.(Glu545Lys) (1 case), and c.1624G > A, p.(Glu542Lys) (1 case). Moreover, mutations in *AKT1* c.49G > A, p.(Glu17Lys) and c.51dup, p.(Tyr18ValfsTer15); c.49_50delinsAG, p.(Glu17Arg) (as a double hit) were found (2 cases). In addition, germinal and somatic mutation of *PTEN* c.1003C > T, p.(Arg335Ter); c.445C > T, p.(Gln149Ter), respectively, were detected. Gene fusions were absent in all cases. These prevalent molecular alterations converging on one major cancer-related pathway support the notion that SPA is a true neoplasm with a significant potential to develop intraluminal epithelial proliferation with apocrine and/or intercalated duct-like phenotype. The name SPA more correctly reflects the true neoplastic nature of this enigmatic lesion.

Key Words: sclerosing polycystic adenoma, sclerosing polycystic adenosis, salivary gland neoplasm, parotid gland, *PIK3CA-AKT* pathway

(*Am J Surg Pathol* 2022;46:268–280)

From the *Department of Pathology, Charles University, Faculty of Medicine in Plzen; †Bioptic Laboratory Ltd; ¶Molecular and Genetic Laboratory, Bioptic Laboratory Ltd, Plzen; ‡The Fingerland Department of Pathology, Charles University, Faculty of Medicine and University Hospital Hradec Kralove, Hradec Králové; §§Department of Pathology and Molecular Medicine, 2nd Faculty of Medicine in Prague, Prague, Charles University and Motol University Hospital, Prague, Czech Republic; §Department of Histopathology, Division of Clinical Medicine, University of Surrey, Royal Surrey County Hospital, Guildford, Surrey, UK; ‖Institute of Pathology, University Hospital Erlangen, Friedrich-Alexander University Erlangen-Nürnberg (FAU), Comprehensive Cancer Center (CCC) Erlangen-EMN, Erlangen, Germany; #Department of Pathology, CHU Gui de Chauliac, Montpellier, France; **Department of Pathology, National University Health System, Singapore, Singapore; ††Department of Pathology, Research Institute GROW, Maastricht University Medical Center, Maastricht, The Netherlands; ‡‡Department of Anatomic Histopathology and Cytogenetics, Department of Laboratory Medicine, Niguarda Cancer Center, Milan, Italy; ‖‖Medical Laboratory CSD, Kyiv, Ukraine; and ¶¶Institute of Biomedicine, Pathology, University of Turku, and Turku University Hospital, Turku, Finland.

Conflicts of Interest and Source of Funding: Supported in part by study grant SVV 22639 from the Ministry of Education, Czech Republic and the Finnish Cancer Society, Helsinki. The authors have disclosed that they have no significant relationships with, or financial interest in, any commercial companies pertaining to this article.

Correspondence: Alena Skálová, MD, PhD, Sikl's Department of Pathology, Faculty of Medicine in Pilsen, Charles University, E. Benese 13, 305 99 Pilsen, Czech Republic (e-mail: skalova@fnplzen.cz).

Sclerosing polycystic adenoma (SPA) previously known as sclerosing polycystic adenosis, is a rare salivary gland neoplasm that was first described in 1996 by Smith et al.[1] SPA reveals a characteristic combination of histologic features, some of which are reminiscent of histopathologic changes that occur in the mammary gland, such as fibrocystic disease/sclerosing adenosis and intraductal epithelial proliferations of various types.[2] In their initial description of SPA, Smith et al[1] hypothesized that SPA represented a non-neoplastic, reactive lesion analogous to fibrocystic disease of the breast. However, SPA frequently harbors intraluminal epithelial solid and papillary proliferations that have been described earlier as dysplasia ranging from mild to severe/carcinoma in situ.[3–8] In addition, a single study utilizing polymorphisms of the human androgen receptor (AR) on 6 cases of SPA reported X-chromosome inactivation in all informative cases suggesting that SPA is a clonal neoplastic process.[9] In a recent study, Bishop et al[10] reported recurrent *PTEN* mutation and *PI3K* pathway alteration in 4 cases of SPA. Report of *PTEN* mutation and *PI3K* pathway alteration in additional 2 cases, and an association with Cowden syndrome in 1 patient[11] represents further evidence to support that these lesions are neoplastic and more appropriately referred to as "sclerosing polycystic adenoma" (SPA). This name has been proposed earlier[12] and it is used in this manuscript.

Recently, we have encountered an index case of parotid gland tumor composed of apocrine intraductal carcinoma (IC) and invasive salivary duct carcinoma (SDC) arising from conventional SPA, a combination of tumor entities that has never been published so far. IC is the current designation used by the World Health Organization (WHO) Classification of Head and Neck Tumors for a rare salivary gland neoplasm[13] that has previously also been referred to as "low-grade (LG) SDC" and "LG cribriform cystadenocarcinoma."[14] IC is conceptually believed to be similar to ductal carcinoma in situ (DCIS) of the breast. Although IC is one entity in the current WHO Classification of Head and Neck Tumors,[13] recent studies have suggested that at least 3 subtypes exist: a LG intercalated duct cell (IDC)-like variant with frequent *RET* rearrangements,[15–17] a LG apocrine and mixed IC with frequent *TRIM27-RET* fusion,[16–18] and an apocrine and mixed IC with SDC-like genetics.[19] Like SPA, apocrine IC may harbor molecular alterations similar to high-grade (HG) SDC with frequent *HRAS* and PI3K pathway mutations.[19] SDC is a highly aggressive carcinoma that recapitulates invasive ductal breast cancer and it constitutes up to 10% of all salivary gland carcinomas.[20] SDC is characterized by heterogenous molecular abnormalities involving predominantly inactivation of tumor suppressor genes, such as *TP53*, *PTEN*, and activation of genes of the PI3K/AKT/mTOR pathway (such as *PIK3CA*, *HRAS*, and *AKT1*).[21–24] It has been suggested earlier that apocrine IC and SPA may be related entities.[19] Here, we present an index case of apocrine IC of parotid gland with transformation to SDC arising from SPA. To further explore the nature of SPA and to learn how SPA, apocrine IC and SDC are associated, we decided to study molecular, immunohistochemical and histologic features of 36 cases of SPA, the largest series in the literature so far.

MATERIALS AND METHODS

Case Selection

Recently the authors (J.L. and A.S.) encountered an index case of a parotid gland tumor in a 62-year-old male patient with a unique combination of 3 components, SPA, apocrine IC, and invasive HG SDC. A total of 36 cases of SPA were selected from the authors' consultation files. All cases were reviewed by the corresponding author (A.S.) and another head and neck pathologist (M.B.), and were confirmed to meet the diagnostic criteria of SPA as described previously,[1,3,4] and detailed in the 2017 WHO Classification of Head and Neck Tumors.[2] Thirty-six cases were identified that met these inclusion criteria. Three and 12 of these SPA cases were included in 2 previous studies, Skalova et al[3] and Skalova et al,[9] respectively.

All available H&E sections from each case were reviewed, and the histologic features, including intraductal epithelial cribriform and papillary apocrine proliferations and the spectrum of dysplastic changes were tabulated. Focal epithelial proliferations were classified into 2 categories according to their histomorphology and immunophenotype as IDC-type composed of S100 protein/SOX10 positive and AR negative epithelial cells, and apocrine type composed of AR positive and S100 protein/SOX10 negative cells. LG dysplasia was defined by mild (G1) or moderate (G2) nuclear features and by a solid/tubular growth pattern with mild irregularities in cell shape and by occasional back-to-back arrangements with intraluminal protrusions (Figs. 1A, B). HG dysplasia was defined by moderate (G2) and severe (G3) atypical nuclear features and by a complex growth pattern characterized by solid/cribriform and intraluminal protrusions of micropapillary structures and rigid bridging (Figs. 1C, D).

Where available, clinical follow-up was obtained from the patients, their physicians, or referring pathologists.

Histology and Immunohistochemistry

For conventional microscopy, the excised tissues were fixed in formalin, processed routinely, embedded in paraffin (formalin fixed paraffin embedded), cut, and stained with hematoxylin and eosin.

For immunohistochemistry, 4-μm-thick sections were cut from paraffin blocks and mounted on positively charged slides (TOMO, Matsunami Glass IND, Osaka, Japan). Sections were processed on a BenchMark ULTRA (Ventana Medical Systems, Tucson, AZ), deparaffinized and subjected to heat-induced epitope retrieval by immersion in a CC1 solution (pH 8.6) at 95°C and for NOR1 antibody in a CC2 solution (pH 6.0) at 92°C. All primary antibodies used in this study are summarized in Table 1.

Visualization was performed using the ultraView Universal DAB Detection Kit (Roche, Tucson, AZ) and ultraView Universal Alkaline Phosphatase Red Detection Kit (Roche). The slides were counterstained with Mayer hematoxylin. Appropriate positive and negative controls were employed.

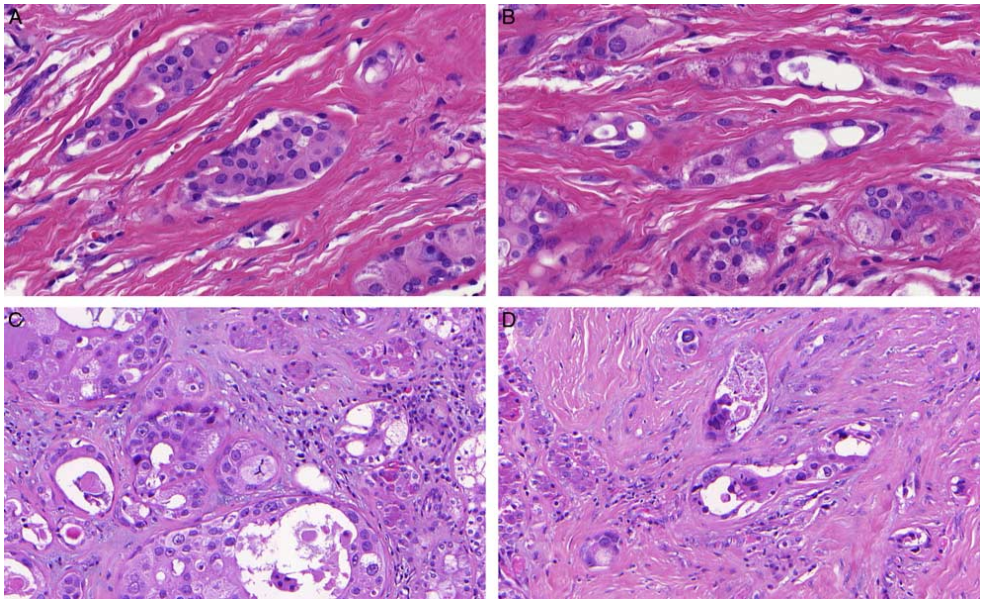

FIGURE 1. LG dysplasia was defined by mild (G1) or moderate (G2) nuclear features and by a solid/tubular growth pattern with mild irregularities in cell shape and by occasional back-to-back arrangements with intraluminal protrusions (A, B). HG dysplasia was defined by moderate (G2) and severe (G3) atypical nuclear features and by a complex growth pattern characterized by solid/cribriform and intraluminal protrusions of micropapillary structures and rigid bridging (C, D).

Molecular Studies: Next Generation Sequencing and Fluorescence in Situ Hybridization (FISH) Testing

Sample Preparation for Next Generation Sequencing

Two to 3 formalin fixed paraffin embedded sections (10 μm thick) were macrodissected to isolate tumor rich regions. Samples were extracted for total nucleic acid using Agencourt FormaPure Kit (Beckman Coulter, Brea, CA). Integrity of RNA was evaluated using PreSeq RNA QC Assay as previously described.[25]

Next Generation Sequencing and Analysis

Comprehensive Thyroid and Lung Kit

FusionPlex Comprehensive Thyroid and Lung Kit (ArcherDX Inc., Boulder, CO) was used to construct cDNA library for the detection of fusion transcripts and hotspot mutations in 36 genes. All steps were performed according to the manufacturer's protocol (version of the protocol LA135.G), and the library was sequenced on an Illumina platform as described previously.[25] Fusion and mutation detection was performed using the Archer Analysis software (v6.2; ArcherDX Inc.). Fusion parameters were set to a minimum of 5 valid fusion reads with a minimum of 3 unique start sites within the valid fusion reads.

TruSight Oncology 500 and 170 Kits

A DNA library was prepared using the TruSight Oncology 170/500 Kit (Illumina), targeting a selection of DNA from 523 genes of interest, and RNA from 55 genes, according to the manufacturer's protocol, except for the enzymatic fragmentation of DNA using KAPA FragKit (KAPA Biosystems, Washington, MA). Sequencing was performed on the NextSeq. 550 sequencer (Illumina) following the manufacturer's recommendations. Data analysis (DNA variant filtering and annotation) was performed using the Omnomics next generation sequencing (NGS) analysis software (Euformatics, Finland). Custom variant filter was set up including only nonsynonymous variants with coding consequences, read depth greater than 50, and benign variants according to the ClinVar database[26] were excluded. The remaining subset of variants was checked visually, and suspected artefactual variants were excluded.

Detection of PLAG1 Break by FISH

Briefly, a 4 μm thick section on a positively charged slide was routinely deparaffinized, incubated in the 1× Target Retrieval Solution Citrate pH 6 (Dako, Glostrup, Denmark) for 40 minutes at 95°C and digested in protease solution with Pepsin (0.5 mg/mL) (Sigma Aldrich, St. Louis, MO) in 0.01 M HCl at 37°C for 30 minutes. The slide was then dehydrated in a series of ethanol solutions (70%, 85%, 96%). Probe Sure FISH 8q12.1 PLAG1 Break

TABLE 1. Antibodies Used for The Immunohistochemical Study

Antibody	Clone	Dilution	Antigen Retrieval/Time	Source
p63	DAK-p63	RTU	EnVision low pH/30 min	Dako
AE1-AE3	AE1/AE3	RTU	EnVision high pH/30 min	Dako
CK7	OV-TL 12/30	RTU	EnVision high pH/30 min	Dako
Calponin	EP798Y	RTU	CC1/36 min	Ventana
S100 protein	Polyclonal	RTU	EnVision high pH/30 min	Dako
Mammaglobin	304-1A5	RTU	EnVision high pH/30 min	Dako
SOX10	SP267	RTU	CC1/64 min	Cell Marque
DOG1	SP31	RTU	CC1/36 min	Cell Marque
NOR-1	H-7	1:50	CC2/68 min	Ventana
PLAG1	3B7	1:100	CC1/64 min	Sigma Aldrich
AR	SP107	RTU	CC1/64 min	Cell Marque
Ki-67	MIB1	RTU	EnVision high pH/30 min	Dako
GATA3	L50-823	1:200	CC1/52 min	BioCareMedical

CC1 indicates EDTA buffer, pH 8.6, 95°C; CC2, citrate buffer, pH 6.0, 92°C; EnVision High pH, pH 9,0, 97°C; EnVision low pH, pH 6.0, 97°C; RTU, ready to use.

Apart Probe Kit (Agilent Technologies, Santa Clara, CA) was used for the detection of *PLAG1* rearrangement and was mixed of both probes (each color was delivered in a separated well), deionized water and LSI/WCP (Locus-Specific Identifier/Whole Chromosome Painting) hybridization buffer (Vysis/Abbott Molecular Diagnostics, Des Plaines, IL) in a 1:1:1:7 ratio, respectively. The slide with the applied probe was incubated in the ThermoBrite instrument (StatSpin/Iris Sample Processing, Westwood, MA) with codenaturation parameters at 85°C for 8 minutes and hybridization parameters at 37°C for 16 hours. After hybridization the slide was washed in a post-hybridization wash solution (2×SSC/0.3% NP-40) at 72°C for 2 minutes, air-dried in the dark, counterstained with 4′,6-diamidino-2-phenylindole DAPI (Vysis) and examined immediately.

The section was examined with an Olympus BX51 fluorescence microscope (Olympus Corporation, Tokyo, Japan) using a ×100 objective and filter sets Triple Band Pass (DAPI/SpectrumGreen/SpectrumOrange), Dual Band Pass (SpectrumGreen/SpectrumOrange) and Single Band Pass (SpectrumGreen and SpectrumOrange). One hundred randomly selected nonoverlapping tumor cell nuclei were examined for the presence of yellow (normal) or green and orange (chromosomal breakpoint) fluorescent signals. Cutoff value was set to > 10% of nuclei with chromosomal breakpoint signals (mean+3 SD in normal non-neoplastic control tissues).

RESULTS

Demographic and Clinical Features

The clinicopathologic data for the 36 identified SPA cases are summarized in Table 2. The patients were 25 females and 11 males aged 11 to 79 years with a mean of 47.8 years. All tumors originated in the parotid gland. Tumor size ranged from 11 to 70 mm (mean 28 mm). Follow-up was available for 33 patients (33/36; 92%), however, patient information was lost in the cohorts (14/36; 39%) published earlier (Table 2). Complete follow-up information was available for a total of 19 cases (19/26; 53%) (range, 2 mo to 15 y; mean 42.7 mo).

Clinically, the tumors manifested as slowly growing and well-circumscribed, palpable masses with a duration of a few months to 10 years. Tenderness or intermittent pain was recorded in 3 patients.

Treatment was complete excision in all cases, performed with different surgical modalities (Table 2).

Five cases (5/36;14%) have recurred with a mean period before the first recurrence of 38 months. In 2 patients, there were multiple recurrences; in case 9, SPA recurred twice, at 6 and 13 years, and in case 19, SPA recurred 3 times at 6 and 18 months and at 13 years. The latter patient, at the age of 32, was treated by extended radical parotidectomy followed by radiotherapy. At follow-up of 13 years after the latest surgery, she was without evidence of disease, and was then lost to follow-up.

Two patients suffered from prior malignancy. In case 28, a 65-year-old female patient had a history of bone marrow transplantation for Hodgkin lymphoma 19 years before diagnosis of SPA. In case 32 (index case), a 62-year-old male patient who quit smoking 2 years before presented with a history of clear cell renal cell carcinoma. The kidney tumor was treated by left-sided nephrectomy. Ten months after surgery, the patient developed lung and liver metastases, and he was treated with PD-L1 immune checkpoint inhibitors. Four years after the kidney surgery, the patient presented with a slowly growing painless mass in the left parotideo-masseteric area of 9 months duration. On palpation, a mildly tender swelling was covered by skin with a violet discoloration. No symptoms of facial nerve paresis were observed. A tumor of the left parotid gland, 25 mm in diameter, was extirpated and a diagnosis of apocrine IC with a positive margin was rendered. Radical parotidectomy and lymph node dissection was performed, followed by radiotherapy. There was a well-circumscribed focus of SPA, measuring 21×20×12 mm, that extended into the resection margin. The parotidectomy specimen also included a small benign lymphoepithelial cyst, and residual structures of the apocrine IC with a focal invasive component of SDC close to the surgical margin (tumor-free resection margin was 0.6 mm). Perineural or lymphovascular invasions were not observed. The removed lymph nodes were negative (0/23). The patient is alive without evidence of any neoplastic disease 8 months after his latest surgery.

TABLE 2. Clinicopathologic Features of Current and Previously Reported SPAs

Case No.	Age/ Sex	Size (mm)	Presentation	IDC-like Proliferation (%)/Nuclear Grade	Apocrine Proliferation (%)/Nuclear Grade	Outcome (Follow-up) (mo, y)	Previously Published
1	27/female	45	Slowly growing painless mass	5	0	NED at 4 y, LOF	Skálová et al[3] case 2 Skálová et al[9] case 7
2	31/female	16	Slowly growing tender mass, 2 y	20	30/G3	NED at 3 y, LOF	Skálová et al[3] case 1 Skálová et al[9] case 8
3	35/female	22	Painless mass	5	0	NA	Skálová et al[9] case 1
4	24/female	25	Parotid mass suggestive of malignancy	5	5	NED at 2 y, LOF	Skálová et al[9] case 2
5	64/female	43	Parotid mass suggestive of malignancy	10	0	NA	Skálová et al[9] case 3
6	72/male	30	Parotid mass	40	0	NED at 3 y, LOF	Skálová et al[9] case 4
7	35/male	35	Slowly growing mass			NED at 3 y, LOF	Skálová et al[9] case 5
8	46/female	32	Firm circumscribed mass	< 5	50/G3	NED at 5 y, LOF	Skálová et al[9] case 6
9	35/female	50	Mass for 18 mo, sometimes painful	< 5	20	2 RE—at 6 y and at 13 y, LOF	Skálová et al[3] case 3 Skálová et al[9] case 9
10	33/female	20	Swelling of parotid gland, 2 mo	30	0	NED 2 y, LOF	Skálová et al[9] case 10
11	51/female	30	Parotid mass, features suggestive of neoplasm by FNA	< 5	0	NED at 7 y, LOF	Skálová et al[9] case 11
12	58/male	15	Parotid mass	10	0	NED at 2 y, LOF	Skálová et al[9] case 12
13	60/female	18	Solid well-circumscribed mass of parotid with mucinous cysts	20	< 5	NA	
14	26/female	48	Multinodular parotid mass with multiple satellite nodules	5	0	RE at 5 y; NED at 14 y	
15	57/male	30	Long lasting painless firm nodule of parotid removed by enucleation	20	0	NED at 13 y	
16	NA/male	NA	Multinodular well-defined nodule in parotid	30	5	NED at 15 y	
17	47/female	40	Slowly growing mass, 2 y	20/G2	20/G2	RE at 2 y, removed by conservative PE, NED at 15 y	
18	45/female	14	Well-demarcated solid nodule in parotid, removed by SPE	10/G3	10/G3	NED at 14 mo, LOF	
19	32/female	12	1st recurrence—diagnosed as PA 2nd—recurrence—conservative PE 3rd recurrence—extended RPE and RT	20/G2	0	3 RE—at 6 mo, 18 mo and 10 y NED at 13 y	Manojlović et al[6] case 1
20	33/female	40	8 y slowly growing mass suggestive of benign tumor; SPE	10	0	NED at 4 y, LOF	Manojlović et al[6] case 2
21	42/female	70	10 y slowly growing mass	30/G1	0	NED at 7 y	
22	71/male	30	Solitary nodule of hard consistency, 1 y	20	0	NED at 7 y	
23	69/female	22	2 y growing tough movable mass	20	15	NED at 6 y	
24	25/male	NA	5 y tough resistance	10	0	NED at 6 y	
25	36/female	NA	Solitary nodule of hard consistency	10/G1	0	NED at 5 y	
26	11/female	40	Slowly growing left-sided neck mass removed by SPE	20	0	NED at 10 mo; LOF	
27	51/female	22	6 mo swelling, feeling of pressure and intermittent pain below right ear	10	30/G3	NED 31 mo	
28	65/female	25	Slowly growing painless mass; SPE History of Hodgkin lymphoma 19 y ago	20/G2	0	NED at 3 y	
29	66/male	20	Palpable mass growing slowly for several months	0	30/G2	NED at 18 mo	

TABLE 2. (*continued*)

Case No.	Age/ Sex	Size (mm)	Presentation	IDC-like Proliferation (%)/Nuclear Grade	Apocrine Proliferation (%)/Nuclear Grade	Outcome (Follow-up) (mo, y)	Previously Published
30	64/female	24	12 mo painless mass, watering eye, lying ear; PPE	10/G2	< 5	NED at 12 mo	
31	48/male	11	Solitary nodule hard in consistency, palpable mass 1 y, total PE	40/G1	5	NED at 11 mo	
32	62/male	25	9 mo slowly growing painless mass treated by simple enucleation; Followed by RPE, LN dissection and RT History of CCRCC with lung and liver mets 3 y ago	15/G1	30/G1 apocrine IC invasive SDC	AWD at 12 mo	
33	63/female	25	RPE	20/G1	30/G1	NED at 8 mo	
34	52/female	13	24 mo preauricular edema, PE and LN dissection Recurrence treated by simple extirpation	30/G1	10	RE at 13 mo NED at 43 mo	
35	79/male	22	RPE and cervical dissection	40/G1	5	NED at 2 mo	
36	59/female	22	Solitary nodule, PE	5	40/G2	NED at 36 mo	

AWD indicates alive with disease; CCRCC, clear cell renal cell carcinoma; LN, lymph node; LOF, lost of follow-up; NA, not available; NED, no evidence of disease; PA, pleomorphic adenoma; PE, parotidectomy; PPE, partial parotidectomy; RE, recurrence; RPE, radical parotidectomy; RT, radiotherapy; SPE, superficial parotidectomy.

Histologic and Immunohistochemical Features

All 36 tumors in this series revealed characteristic diagnostic features of SPA, showing a circumscribed epithelial proliferations of ducts and acini, mostly arranged in nodular or multinodular patterns without capsule, but sometimes displaying an incomplete pseudocapsule. Most commonly, the cellular components in SPA were embedded in a sharply delineated, dense, sclerotic-collagenous stroma often with focal lymphoid aggregates (Fig. 2A). A highly characteristic feature of SPA was a lobular pattern of variably sized and shaped ducts lined by flattened, cylindrical, or apocrine epithelium separated by bands of hyalinized fibrous stroma. Frequently the ductal epithelium had a foamy cell appearance and sometimes the lumen of the ducts was filled by foamy cells (Fig. 2B). The epithelial component featured variably arranged and sized acini, tubules and ducts with heterogenous cytomorphologic characteristics of the lining epithelium, including foamy, vacuolated (sebaceous-like), apocrine, mucous, clear/"ballooned," squamous and oncocyte-like cells. The hallmark of SPA was the occurrence of numerous acini with abnormal acinar cells displaying brightly eosinophilic cytoplasmic granules/globules of varying sizes (Fig. 2C). The epithelial component of SPA was either cystic or solid. The cysts were often lined by a bilayered epithelium with luminal apocrine cells with apical snouts and an abluminal layer of myoepithelial cells (Fig. 2D). The ductal structures were in places surrounded by periductal concentric layers of hyalinized stroma (Fig. 2E). A less common feature was focal fibromyxoid (pleomorphic adenoma-like) stroma (Fig. 2F) sometimes intermixed with foci of mature adipose tissue.

SPA frequently harbored focal intraductal epithelial proliferations with foamy cell or oncocytic metaplasia vaguely resembling atypical ductal hyperplasia of the breast (Fig. 3A). These intraluminal epithelial ductal structures often displayed solid (Fig. 3B), cribriform (Fig. 3C), or micropapillary growth patterns with variable degrees of cytologic atypia.

Foci (< 5% to 40%, Table 2) of homogenous solid, micropapillary, and cribriform intraductal epithelial proliferations reminiscent of an IDC variant of IC were observed in most cases. The intraductal proliferations showed rigid bridging and cribriform patterns, and were composed of IDC-like epithelium positive for S100 protein, mammaglobin and SOX10 (Fig. 3D), and negative for AR (Fig. 3E). These structures were surrounded by a complete layer of myoepithelial cells decorated by positive staining for calponin (Fig. 3F). Less common findings were solid and cribriform intraductal epithelial proliferations with a pronounced apocrine morphology. The apocrine structures were present in 14/36 (39%) of cases ranging from small foci that made up <5% and up to 50% of the tumor (Table 2). In most cases of SPA, a variably prominent dilated ductal and cystic component was present (Fig. 4A). The cysts were divided by a prominent hyalinized stroma with focal lymphoid infiltrates. The cysts were lined by a cuboidal and/or attenuated epithelium with intercalated duct phenotype intermingled with foamy epithelial cells (Fig. 4B). Other dilated ducts were lined and partly filled by dysplastic epithelial proliferations with an apocrine morphology (Fig. 4C) and cells positive for AR (Fig. 4D).

In all cases, there were foci of homogenous intraductal solid and cribriform intercalated duct-like epithelial proliferations with variable degrees of dysplasia (Figs. 5A, B) and positivity for S100 protein and SOX10 (Fig. 5C), fully enveloped by an intact layer of myoepithelial cells. In addition, 9/36 cases (25%) had focal intraductal cribriform and micropapillary apocrine type variably dysplastic epithelial structures composed of cells positive for AR (Figs. 5D, E) and negative for S100/SOX10 (Fig. 5F). The

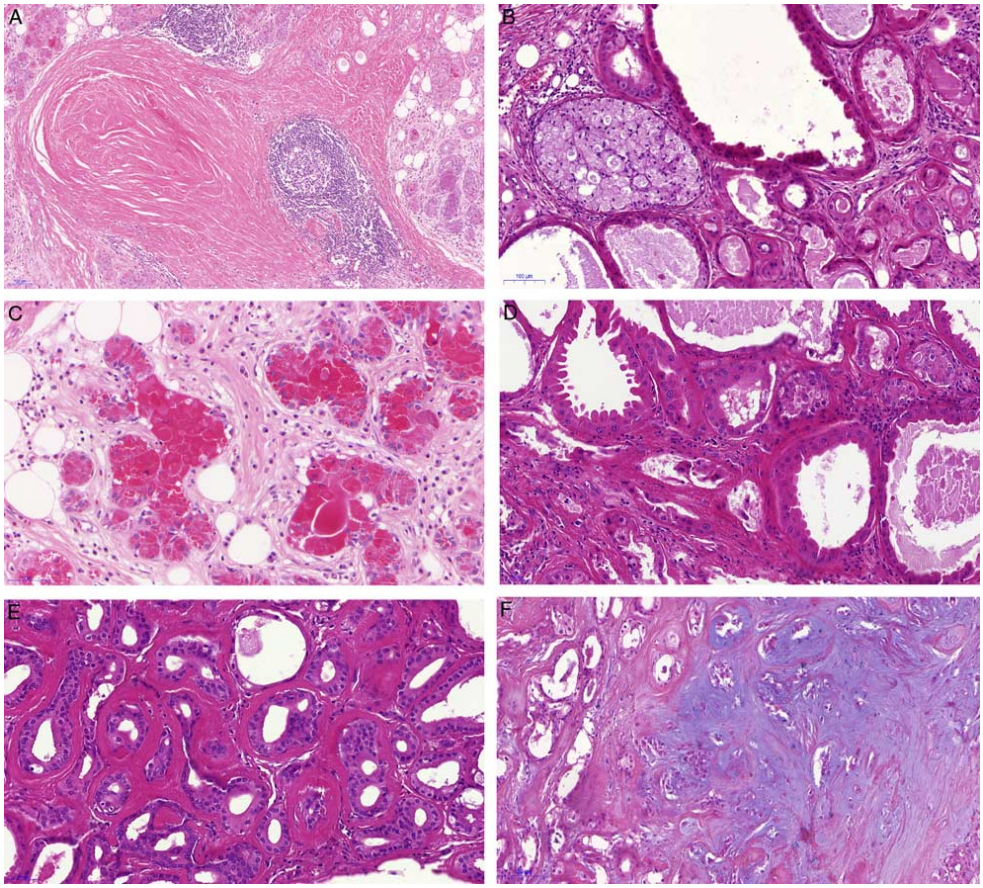

FIGURE 2. SPA is embedded in a sharply delineated, dense, sclerotic-collagenous stroma often with focal lymphoid aggregates (A). Frequently the lining ductal epithelium had a foamy cell appearance and sometimes the lumen of the ducts was completely filed by foamy cells (B). Acini were composed of abnormal acinar cells with brightly hyper-eosinophilic cytoplasmic granules/globules of varying size (C). The cysts were often lined by bilayered epithelium with inner luminal apocrine epithelium with apical snouts and abluminal myoepithelial layer (D). Ductal structures were surrounded by periductal concentric layers of stromal hyalinization (E). Less common feature was a focal presence of fibromyxoid (pleomorphic adenoma-like) stroma (F) sometimes intermixed with foci of mature adipose tissue.

intraductal proliferations showed focal mild to severe dysplasia in 17 cases (17/36; 47%). Two cases showed overt malignant morphologies ranging from HG IC to invasive carcinoma with apocrine ductal phenotype.

Index case: tumor of the left parotid gland, 25 mm in diameter, was composed of 3 closely associated components. The first lesion was a well-circumscribed predominantly polycystic tumor with features fully compatible with a diagnosis of SPA, conventional variant (Fig. 6A, right lower part of the picture), separated from the parotid gland by a fibrous pseudocapsule. The second lesion was composed of densely packed solid, cribriform (Fig. 6B), and intraluminal micropapillary epithelial proliferations. Tumor cysts were lined by large apocrine cells with cytoplasmic snouts (Fig. 6C). The cells had an apocrine morphology with abundant, granular eosinophilic cytoplasm, and large nuclei with mild polymorphism (Fig. 6D). The third lesion was found next to the apocrine IC and it was a frankly invasive SDC composed of HG tumor cells (Fig. 6E). By immunohistochemistry, the apocrine neoplastic cells of both apocrine IC and invasive SDC were strongly and uniformly positive for AR (Fig. 6F).

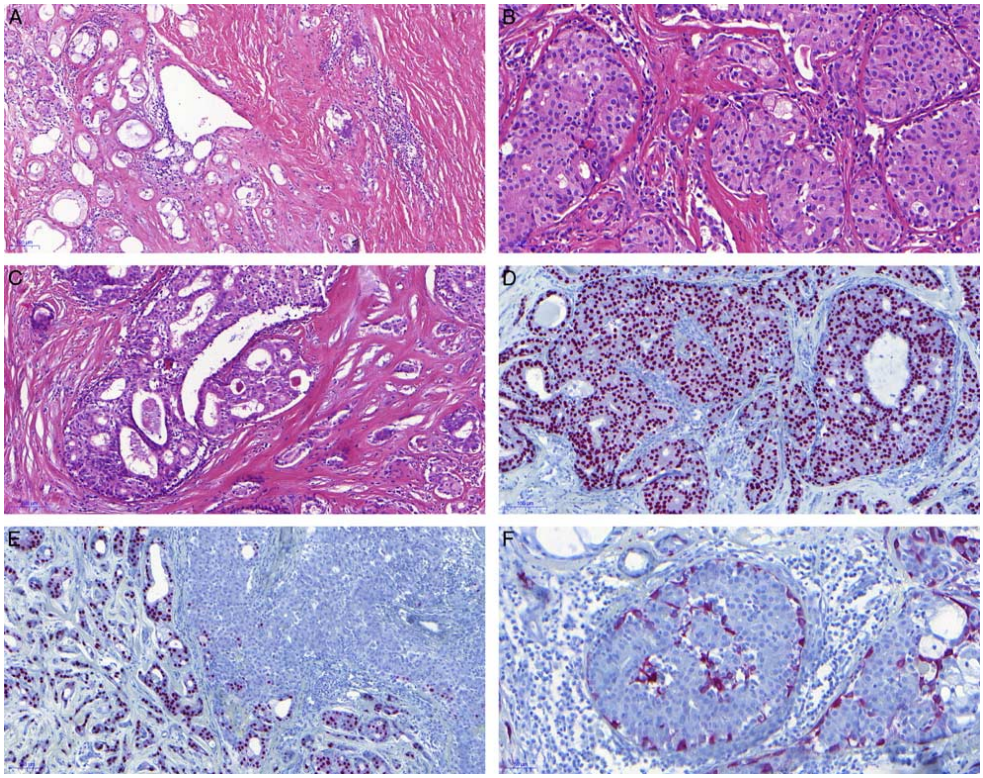

FIGURE 3. SPA frequently harbors intraductal epithelial proliferations with apocrine metaplasia and intraluminal proliferations resembling atypical ductal hyperplasia of the breast (A). These intraluminal epithelial ductal structures often display solid (B), cribriform (C), or micropapillary growth patterns with variable degree of cytologic atypia. The epithelial structures were composed of intercalated duct-like epithelium positive for S100 protein, mammaglobin and SOX10 (D) and negative for AR (E). These structures are surrounded by complete myoepithelial layer, here decorated by positive staining for calponin (F).

Immunohistochemistry

For purposes of this study, the immunohistochemical investigation was performed in 21 cases (21/36; 58%) in which tissue was available. Both ductal and acinar cells were positive for broad spectrum cytokeratins (AE1 to AE3) and cytokeratin CK7. The luminal epithelium in cystically dilated ducts was variably positive for S100, SOX10, and mammaglobin and negative for AR and GATA3, consistent with intercalated duct phenotype. In apocrine foci, in contrast, the luminal epithelium was stained with AR while it was negative for S100 and SOX10. In SPA, antibodies to p63, p40, and calponin variably decorated the abluminal myoepithelial cells in the periphery of the acini and ducts. Myoepithelial cells were also present occasionally and somewhat discontinuously around the solid, cribriform, and micropapillary intraductal and intracystic epithelial proliferations of both IC-like and apocrine types. Cell proliferation was predominantly low with an average MIB1 index of 3.2%. All cases were negative with DOG1, PLAG1, and NOR1 antibodies. HER2/neu overexpression and amplification was tested in 2 cases negative.

Molecular Testing

Results of targeted NGS are summarized in Table 3. A The Comprehensive Thyroid and Lung panel was used in 8 cases. In addition, TruSight Oncology 170/500 Kits were used in 7 cases (Table 3). Of 11 tumors with tissue available for molecular analysis, 9 (9/11; 82%) harbored genetic alterations in the PI3K pathway. One case was negative for mutation, one was unanalyzable due to low quality NGS data. The remaining 25 cases could not be sequenced due to inadequate DNA and RNA quality due to the age of the tissue blocks. In analyzable cases, targeted sequencing revealed HRAS mutations c.37G>C, p.(Gly13Arg) (2 cases) and c.182A>G, p.(Gln61Arg) (2 cases), and PIK3CA mutations c.3140A>G, p.(His1047Arg) (3 cases), c.1633G>A, p.(Glu545Lys) (1 case),

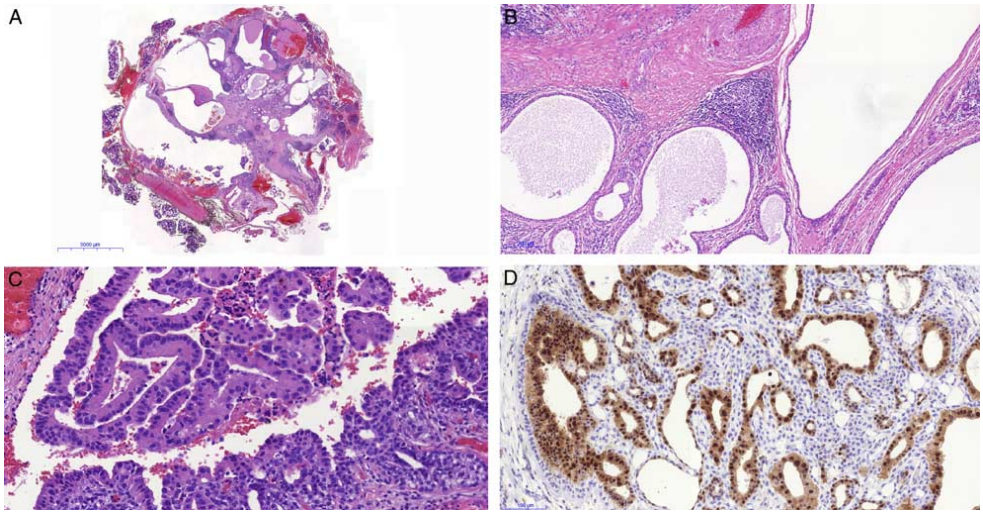

FIGURE 4. In most cases of SPA, a variably prominent, dilated ductal and cystic component is present (A). The cysts are divided by prominent hyalinized stroma with focal lymphoid infiltrate. Cyst are lined by cuboid and/or attenuated epithelium with intercalated duct phenotype intermingled with foamy epithelial cells (B). Other dilated duct in the same tumor are lined and partly filled by dysplastic epithelial proliferations with apocrine morphology (C) and lined by cells positive for AR (D).

and c.1624G > A, p.(Glu542Lys) (1 case). Moreover, mutations in AKT1 c.49G > A, p.(Glu17Lys) and c.51dup, p.(Tyr18ValfsTer15); c.49_50delinsAG, p.(Glu17Arg) (as a double hit) were found (2 cases). Additionally, germinal and somatic mutation of PTEN c.1003C > T, p.(Arg335Ter); c.445C > T, p.(Gln149Ter), respectively, were detected. Gene fusions were not found by RNA sequencing in any of the cases, in particular, genes *PLAG1* and *HMGA2* were found intact. All cases were negative for *PLAG1* alterations by FISH.

DISCUSSION

SPA is a rare benign salivary gland lesion that usually arises from the parotid gland. SPA has been an enigmatic entity since its initial description, and it was originally interpreted to be a non-neoplastic alteration of salivary glands analogous to fibrocystic disease of the breast.[1] In fact, it is still classified as such in the 2017 WHO Classification of Head and Neck Tumors.[2] Nevertheless, SPA has many characteristics that suggest that it is a genuine neoplasm. First, SPA often contains intraductal proliferation of apocrine ductal cells in solid and cribriform patterns surrounded by an intact or partially disrupted myoepithelial cell layer. These epithelial structures are composed of cells with a spectrum of nuclear atypia resembling that of the apocrine intraductal neoplasia of the breast and focally severe enough to fulfill the criteria of dysplasia or carcinoma in situ.[3] In addition, SPA is reported to have a significant risk of local recurrence (up to 20%).[7]

Recently, Bishop and colleagues analyzed 4 cases of SPA by targeted NGS and discovered mutations in genes that are well established drivers in human neoplasms. Such mutations were found in *PTEN* (4 of 4 cases), *PIK3CA* (2 of 4 cases) and *PIK3R1* (2 of 2 cases), all of which are members of the PI3K pathway of cell cycle regulation.[10] Hernandez-Prera et al[11] detected *PTEN* and *PIK3R1* mutations in additional 2 cases. Moreover, a patient with 2 different *PTEN* alterations had clinical stigmata of Cowden syndrome which was confirmed with germline genetic testing.[11]

In this study, we confirmed and expanded the observations of Bishop et al[10] and Hernandez-Prera et al.[11] In our series, we found that 92% of our SPA cases had a mutation in the PI3K/Akt pathway, in particular 1 of 2 mutations in *PIK3CA* gene c.3140A > G, p.(His1047Arg) or c.1624G > A, p.(Glu542Lys). All 5 tumors harboring *PIK3CA* mutation have shown focal solid and cribriform proliferation of epithelium with IDC-like phenotype and mild to moderate dysplasia. Interestingly, in contrast the 2 mutations in *HRAS* gene c.37G > C, p.(Gly13Arg) and c.182A > G, p.(Gln61Arg) were detected in 3 cases of SPA, all of them displaying intermediate to severe dysplastic changes of apocrine epithelial proliferations. In addition, the mutations of gene *AKT1* c.49G > A, p.(Glu17Lys) and *AKT1* c.51dup, p.(Tyr18ValfsTer15); AKT1 c.49_50delinsAG, p.(Glu17Arg) were discovered in 2 cases of SPA with extensive apocrine solid and cribriform dysplastic component. Our index case of apocrine IC with invasive SDC component arising from

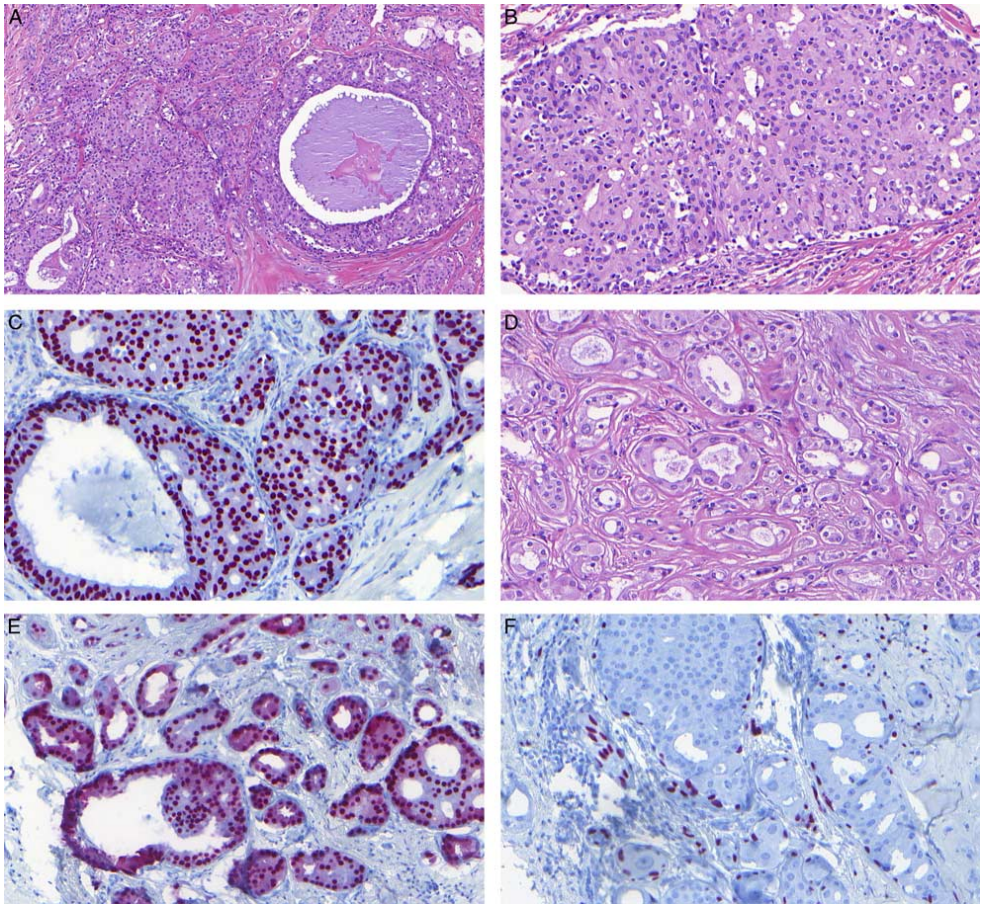

FIGURE 5. IDC-like dysplasia: complex solid and cribriform cystic epithelial proliferations (A); displaying mild nuclear atypia (B), SOX10 is positive (C) while AR negative. Apocrine dysplasia: closely attached solid, tubular and cribriform epithelial proliferations composed of the cells with mild nuclear atypia and finely granular cytoplasm (D), positive or AR (E), and negative for SOX10. Nuclear grade 3 (F).

SPA harbors an identical mutation in *PIK3CA* c.1624G > A, p.(Glu542Lys) in the conventional SPA component as well as in the malignant components of apocrine IC and invasive SDC. Moreover, when performing macrodissection we found a mutation in *HRAS* only in the malignant component. This is a novel finding as none of above mentioned mutations in *HRAS* and *AKT1* genes have been documented in SPA so far.

The PI3K/Akt pathway is involved in tumorigenesis, particularly influencing cell growth, cell cycle progression and cell survival. The aberrant activation of the PI3K pathway might be caused either by activating mutations in *AKT1*, *PIK3CA*, and *mTOR* genes or by inactivating mutations in *PTEN* gene.[27] Somatic mutations in *AKT1* gene resulting in the substitution of glutamic acid with lysine at amino acid 17 (E17K) alter electrostatic interactions of a lipid-binding pocket in the plasma membrane forming a hydrogen bond with a phosphoinositide ligand stimulating downstream signaling and is responsible for oncogenic transformation.[27]

The alterations of *HRAS* and *PI3K* pathways in SPA with apocrine IC component are identical to alterations detected in SDC. Many studies imply important roles for PI3K/AKT/mTOR signaling in the tumorigenesis of SDC.[21–24,28,29] Mutation rates in SDC were estimated at 18% for *PIK3CA*, 16% for *HRAS* and 1.5% for *AKT1* gene.[28] Mutations in *PTEN* and *AKT1* in SDC have been

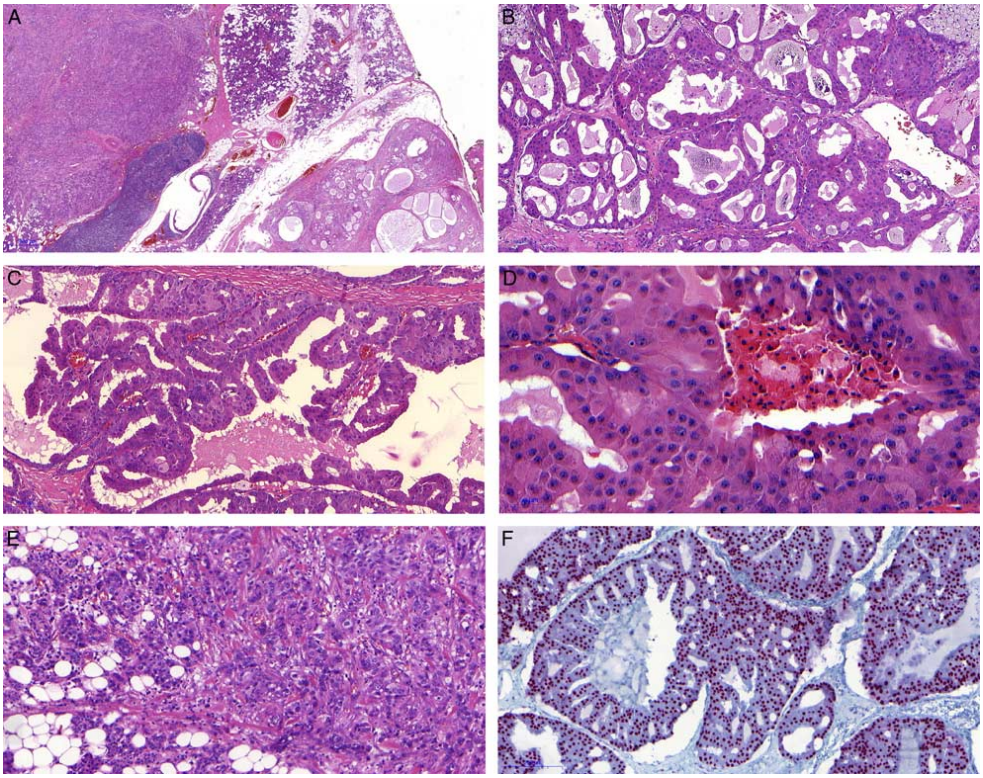

FIGURE 6. Index case: the tumor is composed of 3 closely related components. First lesion is a well-circumscribed predominantly polycystic SPA (A, right lower part of the picture) divided from parotid gland by fibrous pseudocapsule. The second component iss composed of densely packed solid, cribriform (B), and intraluminal micropapillary epithelial structures. The tumor cysts are lined by large apocrine cells with cytoplasmic snouts (C). The cells have apocrine morphology with abundant, granular eosinophilic cytoplasm and large nuclei with mild polymorphism (D). The third component found next to apocrine IC is frankly invasive SDC composed of HG cells (E). By immunohistochemistry, the apocrine neoplastic cells of both apocrine IC and invasive SDC are uniformly strongly positive for AR (F).

identified in other studies.[21–24] Interestingly, similar SDC-like genetic alterations of PI3K pathway including *PTEN*, *PIKCA*, and *PIK3R1* have been observed not only in SPA[10,11] but also in a subset of apocrine IC.[19]

SPA frequently harbors intraductal epithelial proliferations which may display atypia and morphologic features of DCIS.[3,9,30] Some degree of intraductal epithelial proliferations in SPA has been reported in at least 50% of SPA cases.[7] However, the proportion of cases of SPA with epithelial proliferations that reasonably fulfill the criteria for HG DCIS does not exceed 10% of reported cases.[7] Petersson[7] in his excellent review compared the intraductal epithelial proliferations in SPA with atypical ductal hyperplasia/DCIS of the mammary gland and concluded that "there is no reason to postulate that various categories of epithelial proliferations, for example, hyperplasia, atypical hyperplasia and LG DCIS are morphologically identical or biologically similar in SPA as those in the breast."[7] The authors of the current study agree with that conclusion. Here, we present for the first time diagnostic criteria for LG and HG dysplasia in the solid and cribriform epithelial proliferations in SPA. First, the IDC-type is characterized by mild to moderate dysplasia, S100 protein/SOX10 positive and AR negative immunophenotype harboring *PIK3CA* mutations. Second, the apocrine epithelial proliferations with intermediate to severe dysplasia, S100/SOX10 negative and AR positive immunophenotype harboring *HRAS* and *AKT1* mutations. It is important to emphasize that despite morphologic and immunohistochemical similarities with IC, none of our cases of SPA harbored any translocation.

Although no patient with SPA has developed metastases or died of disease, reports indicate that 2

TABLE 3. Molecular Genetic Findings in 11 Selected Cases of SPA (Using NGS Technologies)

Case No.	NGS Technology	*HRAS*	*PIK3CA*	*AKT1*	Other
21	Archer CTL; TS170		c.1633G > A, p. (Glu545Lys)		PTEN c.445C > T, p.(Gln149Ter) (somatic) PTEN c.1003C > T, p.(Arg335Ter) (germline)
23	TS500	NA	NA	NA	
27	Archer CTL	c.37G > C, p. (Gly13Arg)			
29	Archer CTL	c.182A > G, p. (Gln61Arg)		c.49G > A, p.(Glu17Lys)	
30	TS170; TS500 Archer CTL	Negative	Negative	Negative	
31	Archer CTL		c.3140A > G, p. (His1047Arg)		
32	TS170 TS500 SPA		c.1624G > A, p. (Glu542Lys)		
	IC apocrine/SDC invasive	c.37G > C, p. (Gly13Arg)	c.1624G > A, p. (Glu542Lys)		Isoform of the AR gene
33	Archer CTL		c.3140A > G, p. (His1047Arg)		
34	TS500		c.3140A > G, p. (His1047Arg)		
35	Archer CTL; TS500			c.51dup, p. (Tyr18ValfsTer15); c.49_50delinsAG, p. (Glu17Arg)	
36	Archer CTL; TS500	c.182A > G, p. (Gln61Arg)			

TS170, TruSight Oncology 1700 Panel; TS500, TruSight Oncology 500 Panel.

previous patients had invasive carcinoma with apocrine ductal phenotype arising from SPA.[11,30] Here, we present a unique case of a parotid gland tumor arising from SPA and composed of apocrine IC with transformation to SDC, and which harbored a mutation in PI3K/Akt pathway in all tumor components. This combination of tumor entities has not been published so far. Taken together, our findings not only strongly support that SPA is a neoplastic disease, but suggest a close relationship between SPA, apocrine IC and HG invasive SDC. SPA may represent a precursor lesion for the development of apocrine IC and sometimes even invasive SDC.

REFERENCES

1. Smith BC, Ellis GL, Slater LJ, et al. Sclerosing polycystic adenosis of major salivary glands: a clinicopathologic analysis of nine cases. *Am J Surg Pathol*. 1996;20:161–170.
2. Seethala R, Gnepp DR, Skálová A, et al. Sclerosing polycystic adenosis. In: El-Naggar AK, Chan JKC, Grandis JR, Takata T, Slootweg PJ, eds. *WHO Classification of Head and Neck Tumours*. Lyon, France: IARC Press; 2017:195.
3. Skalova A, Michal M, Simpson RHW, et al. Sclerosing polycystic adenosis of parotid gland with dysplasia and ductal carcinoma in situ: report of three cases with immunohistochemical and ultrastructural examination. *Virchows Arch*. 2002;440:29–35.
4. Gnepp DR, Wang LJ, Brandwein-Gensler M, et al. Sclerosing polycystic adenosis of the salivary gland. *Am J Surg Pathol*. 2006;30:154–164.
5. Fulciniti F, Losito NS, Ionna F, et al. Sclerosing polycystic adenosis of the parotid gland: report of one case diagnosed by fine-needle cytology with in situ malignant transformation. *Diagn Cytopathol*. 2010;38:368–373.
6. Manojlović S, Virag M, Milenovič A, et al. Sclerosing polycystic adenosis of parotid gland: a unique report of two cases occurring in two sisters. *Pathol Res Pract*. 2014;210:342–345.
7. Petersson F. Sclerosing polycystic adenosis of salivary glands: a review with some emphasis on intraductal epithelial proliferations. *Head Neck Pathol*. 2013;7(suppl 1):S97–S106.
8. Petersson F, Tan PH, Hwang JSG. Sclerosing polycystic adenosis of parotid gland: report of a bifocal, paucicystic variant with ductal carcinoma in situ and pronounced stromal distortion mimicking stromal invasion. *Head Neck Pathol*. 2011;5:188–192.
9. Skalova A, Gnepp DR, Simpson RHW, et al. Clonal nature of sclerosing polycystic adenosis of salivary glands demonstrated by using the polymorphism of the human androgen receptor locus (HUMARA) as a marker. *Am J Surg Pathol*. 2006;30:939–944.
10. Bishop JA, Gagan J, Baumhoer D, et al. Sclerosing polycystic "adenosis" of salivary glands: a neoplasm characterized by PI3K pathway alterations more correctly named sclerosing polycystic adenoma. *Head Neck Pathol*. 2020;14:63–636.
11. Hernandez-Prera J, Heidarian A, Wenig B. Sclerosing polycystic adenoma: conclusive clinical and molecular evidence of its neoplastic nature. *Mod Pathol*. 2021;34(suppl 2):773–774.
12. Skalova A, Bishop J, Ferlito A, et al. Newly described entities in salivary gland pathology. *Am J Surg Pathol*. 2017;41:e33–e47.
13. Loening T, Leivo I, Simpson RHW, et al. Intraductal carcinoma. In: El-Naggar AK, Chan JKC, Grandis JR, Takata T, Slootweg PJ, eds. *WHO Classification of Head and Neck Tumours*. Lyon, France: IARC Press; 2017:170–171.
14. Brandwein-Gensler M, Gnepp DR. Low-grade cribriform cystadenocarcinoma. In: Barnes L, Eveson JW, Reichart P, Sidransky D, eds. *Pathology and Genetics of Head and Neck Tumours: World Health Organization Classification of Tumours*. Lyon, France: IARC; 2005:430.

15. Weinreb I, Bishop JA, Chiosea SI, et al. Recurrent *RET* gene rearrangements in intraductal carcinomas of salivary gland. *Am J Surg Pathol*. 2018;42:442–452.
16. Skalova A, Vanecek T, Uro-Coste E, et al. Molecular profiling of salivary gland intraductal carcinoma revealed a subset of tumor harboring *NCOA4-RET* and novel *TRIM27-RET* fusions: report of 17 cases. *Am J Surg Pathol*. 2018;42:1445–1455.
17. Skalova A, Ptáková N, Santana T, et al. *NCOA4-RET* and *TRIM27-RET* are characteristic gene fusions in salivary intraductal carcinoma, including invasive and metastatic tumors. Is "intraductal" correct? *Am J Surg Pathol*. 2019;43:1303–1313.
18. Lu H, Graham RP, Seethala R, et al. Intraductal carcinoma of salivary glands harboring *TRIM27-RET* fusion with mixed low grade and apocrine types. *Head Neck Pathol*. 2020;14:239–245.
19. Bishop JA, Gagan J, Krane JF, et al. Low-grade apocrine intraductal carcinoma: expanding the morphologic and molecular spectrum of an enigmatic salivary gland tumor. *Head Neck Pathol*. 2020;14:869–875.
20. Nagao T, Licitra L, Loening T, et al. Salivary duct carcinoma. In: El-Naggar AK, Chan JKC, Grandis JR, Takata T, Slootweg PJ, eds. *WHO Classification of Head and Neck Tumours*, 4th ed. Lyon, France: IARC Press; 2017:173–174.
21. Chiosea SI, Williams L, Griffith CC, et al. Molecular characterization of apocrine salivary duct carcinoma. *Am J Surg Pathol*. 2015;39:744–752.
22. Dalin MG, Desrichard A, Katabi N, et al. Comprehensive molecular characterization of salivary duct carcinoma reveals actionable targets and similarity to apocrine breast cancer. *Clin Cancer Res*. 2016;22:4623–4633.
23. Wang K, Russell JS, McDermott JD, et al. Profiling of 149 salivary duct carcinomas, carcinoma ex pleomorphic adenomas, and adenocarcinomas, not otherwise specified reveals actionable genomic alterations. *Clin Cancer Res*. 2016;22:6061–6068.
24. Santana T, Andrle P, Martinek P, et al. Biomarker immunoprofile and molecular characteristics in salivary duct carcinoma: clinicopathological and prognostic implications. *Hum Pathol*. 2019;93:37–47.
25. Skalova A, Vanecek T, Martinek P, et al. Molecular profiling of mammary analogue secretory carcinoma revealed a subset of tumors harboring a novel *ETV6-RET* translocation: report of 10 cases. *Am J Surg Pathol*. 2018;42:234–246.
26. Landrum MJ, Lee JM, Benson M, et al. ClinVar: improving access to variant interpretations and supporting evidence. *Nucleic Acids Res*. 2018;46:D1062–D1067.
27. Yang J, Nie J, Ma X, et al. Targeting PI3K in cancer: mechanisms and advances in clinical trials. *Mol Cancer*. 2019;18:1–28.
28. Shimura T, Yuichiro Tada Y, Hirai H, et al. Prognostic and histogenetic roles of gene alteration and the expression of key potentially actionable targets in salivary duct carcinomas. *Oncotarget*. 2018;9:1852–1867.
29. Griffith CC, Seethala RR, Luvison A, et al. *PIK3CA* mutations and *PTEN* loss in salivary duct carcinomas. *Am J Surg Pathol*. 2013;37:1201–1207.
30. Canas Marques R, Felix A. Invasive carcinoma arising from sclerosing polycystic adenosis of the salivary gland. *Virchows Arch*. 2014;464:621–625.

2. PART – MESENCHYMAL SINONASAL TUMORS

2.1 BIPHENOTYPIC SINONASAL SARCOMA WITH *PAX3::MAML3* FUSION TRANSFORMING INTO HIGH-GRADE RHABDOMYOSARCOMA: REPORT OF AN EMERGING RARE PHENOMENON

In this paper, we discussed a rare case of high-grade rhabdomyosarcoma originating from biphenotypic sinonasal sarcoma (BSNS). BSNS is a low-grade sarcoma with neural and myogenic features [44]. Tumors involve the sinonasal tract exclusively. Clinically, these tumors usually are indolent with frequent recurrences but no metastases [44,45,46]. Histologically, BSNS is an infiltrative hypercellular tumor that consists of the fascicles of uniform spindle cells, with palely eosinophilic cytoplasm, ovoid nuclei, fine chromatin, and small basophilic nucleoli. The surface epithelium is hyperplastic and entrapped within the tumor. Mitotic activity is usually low. Immunohistochemically, tumors co-express smooth muscle (SMA, desmin) and neural markers (S100 protein). Only a minority of cases may exhibit skeletal muscle differentiation [44, 45,46]. The skeletal muscle phenotype of BSNS is in line with its molecular alterations. The latter is most commonly represented by *PAX3::MAML3* fusions or (less commonly) *PAX3::FOXO1* or *PAX3::NCOA1*. Very rarely, other fusions may be present, including *RREB::MRTFB* (*MKL2*) [46,47,48,49,50,51].

We present a unique case of aggressive high-grade rhabdomyosarcoma (RMS) originating from a typical BSNS of the right ethmoid, maxillary, and frontal sinuses. Partly, the tumor had typical morphology of BSNS; partly it was represented by a high-grade sarcoma with rhabdoid features, high mitotic activity, and necrosis.

Immunohistochemically, the conventional BSNS areas showed expression of typical neural and myogenic markers, there was also a diffuse strong positivity with PAX7 and patchy expression of MyoD1, while desmin and myogenin were completely negative. In contrast, the high-grade areas were completely negative for S100 protein and SMA, patchy positive with PAX7, whereas the diffuse positivity of desmin, MyoD1, and myogenin were observed. PAX7 and MyoD1 regulate earlier stages of myogenesis than myogenin [53], and these transcriptional factors are expressed earlier in myogenesis than the desmin [54]. This suggests that the BSNS with skeletal muscle differentiation more frequently express MyoD1 compared to the expression of desmin and myogenin [46,47,54].

NGS revealed *PAX3*(exon7)*:: MAML3*(exon2) fusion which was confirmed by FISH, using *MAML3* (4q31.1) and *PAX3* (2q36.1) break-apart probes in both the conventional and high-grade components.

It is well known that during development, the *PAX3* gene is required for melanocytic, neuronal, and skeletal muscle differentiation and regulates normal myogenesis and muscular regeneration [48,49,52], while the *MAML3* gene has been shown as a transactivator of *PAX3* response elements [49]. So, *PAX3* has been implicated in the pathogenesis of tumors originating from these tissues, including RMS, melanoma, and neuroblastoma [49]. *PAX3::FOXO1* and *PAX3::NCOA1* fusions have also been described in rare cases of alveolar RMS [48]. In this regard, it has been suggested that the differences in clinicopathological features between BSNS and alveolar RMS are likely determined by the cell of origin, cellular environment, as well as additional genetic aberrations [47].

Of interest, BSNS with rhabdomyoblastic differentiation and *RREB1::MRTFB* fusion showed histological features and molecular alteration potentially overlapping with ectomesenchymal chondromyxoid tumors (EMCMT) [50,51].

The differential diagnosis of BSNS includes various neoplasms with uniform spindle cell morphology such as cellular schwannoma, synovial sarcoma, sinonasal glomangiopericytoma, spindle cell RMS, malignant peripheral nerve sheath tumor, solitary fibrous tumor. However, the distinction is usually possible using immunohistochemical staining [44,45,46,47]. The rhabdomyosarcomatous component in our case should be differentiated with embryonal and RMS, malignant Triton-tumor, sarcomas with *EWSR1::POU2AF3*-rearrangement, EMCMT.

In small biopsies when the conventional BSNS component is absent, we consider a molecular genetic study for accurate diagnosis. It will be especially helpful in cases with evident rhabdomyoblastic differentiation. Moreover, the investigation of more cases is mandatory to delineate the morphological spectrum and the biological behavior of this rare entity.

Virchows Archiv (2023) 482:777–782
https://doi.org/10.1007/s00428-023-03501-0

BRIEF REPORT

Biphenotypic sinonasal sarcoma with *PAX3::MAML3* fusion transforming into high-grade rhabdomyosarcoma: report of an emerging rare phenomenon

Anders Meyer[1] · Natálie Klubíčková[2,3] · Elaheh Mosaieby[2,3] · Petr Grossmann[3] · Antonina Kalmykova[2,4] · Olena Koshyk[2,4] · Michael Michal[2,3]

Received: 26 December 2022 / Revised: 24 January 2023 / Accepted: 25 January 2023 / Published online: 31 January 2023

Abstract
We report a case of a 67-year-old male patient with a sinonasal tumor that showed areas of classic biphenotypic sinonasal sarcoma (BSNS) which in some sections sharply transitioned into high-grade rhabdomyosarcoma. Immunohistochemically, the conventional BSNS parts showed S100 protein, SMA, PAX7, and focal MyoD1 expression, whereas desmin and myogenin were negative. In contrast, the cells in high-grade areas expressed desmin, MyoD1, myogenin, and PAX7, while being negative for S100 protein and SMA. Using the Archer FusionPlex assay, the classical *PAX3::MAML3* gene fusion was detected. FISH for *PAX3* and *MAML3* confirmed a break of these genes in both components. Despite aggressive therapy, the tumor progression resulted in the patient's death. The herein presented case, together with 2 previously published cases of BSNS with high-grade transformation, helps to better understand this novel phenomenon. Although the risk for such transformation appears low, it has important clinical and diagnostic implications which are discussed.

Keywords Biphenotypic sinonasal sarcoma · Rhabdomyosarcoma · High-grade transformation · PAX3::MAML3

Introduction

Biphenotypic sinonasal sarcoma (BSNS) was initially described by Lewis et al. in 2012 as a low-grade sarcoma with neural and myogenic features [1]. Clinically, these tumors usually follow an indolent course with frequent recurrences but no reported metastases and only exceptional disease-related mortality [1–4]. Morphologically, BSNS typically consists of an infiltrative hypercellular proliferation of uniform spindle cells arranged in fascicles, often with a herringbone pattern and frequent invaginations of hyperplastic surface mucosa. Mitotic activity is usually minimal. The vast majority of cases co-express smooth muscle actin (SMA) and S100 protein, while a minority of cases may also exhibit morphological and/or immunohistochemical signs of skeletal muscle differentiation [1, 3–5]. Fusions of *PAX3* gene are the molecular hallmark of BSNS, with *MAML3* being the fusion partner in the majority of cases [3, 4, 6]. Herein, we present a unique case of high-grade rhabdomyosarcoma (RMS) emerging from a typical BSNS with an aggressive clinical course.

Case presentation

The patient was a 67-year-old male with Parkinson's disease and a history of septoplasty, bilateral frontal sinusotomy, and removal of right middle turbinate concha bullosa 3 years before presenting with nasal congestion and epiphora. MRI showed a soft tissue mass involving the right ethmoid, maxillary, and frontal sinuses and invading the extraconal orbit causing mild asymmetric right-sided ocular proptosis (Fig. 1A,B). Endoscopic evaluation revealed a soft tissue mass measuring 4.4 × 3.4 × 2.2 cm which obscured the nasal airway and centered around the

✉ Michael Michal
michael.michal@biopticka.cz

[1] Department of Pathology, University of Kansas, KS, Kansas City, USA

[2] Department of Pathology, Faculty of Medicine, Charles University, Medical Faculty and Charles University Hospital Plzen, Alej Svobody 80, 323 00, Plzen, Czech Republic

[3] Bioptical Laboratory, Ltd., Plzen, Czech Republic

[4] Medical Laboratory CSD Health Care, Ltd., Kyiv, Ukraine

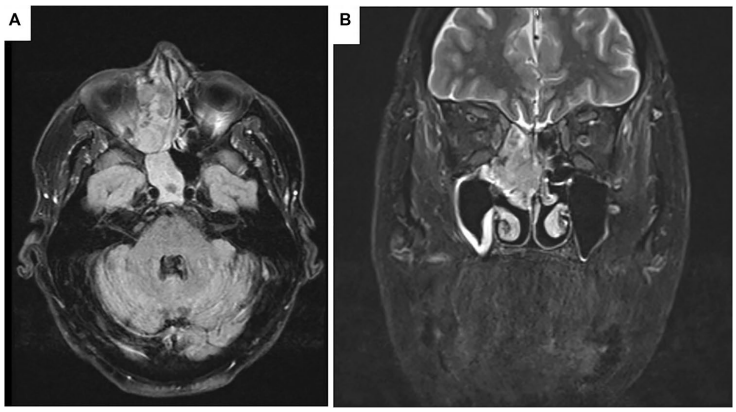

Fig. 1 MRI on axial flair (**A**) and on coronal T2 short tau inversion recovery (**B**) showed a soft tissue mass involving the right ethmoid, maxillary, and frontal sinuses and invading the extraconal orbit causing mild asymmetric right-sided ocular proptosis

middle turbinate. Biopsy revealed a high-grade sarcoma with myogenic differentiation by immunohistochemistry, diagnosed as embryonal RMS. Staging PET was negative for metastatic disease. The patient initiated neoadjuvant chemotherapy with vincristine-dactinomycin-cytoxan. Repeated imaging after three cycles showed local progression and increased FDG avidity without metastatic disease.

The resection specimen showed a proliferation of uniform spindled cells with moderate to high cellularity, occasional fascicular arrangement, minimal atypia, and no mitotic activity (Fig. 2B). In some areas, invaginations of the hyperplastic surface mucosa were enveloped by the tumor cells (Fig. 2A). No rhabdoid differentiation was noted by morphological examination in this area. However, in some sections, this typical BSNS morphology sharply transitioned

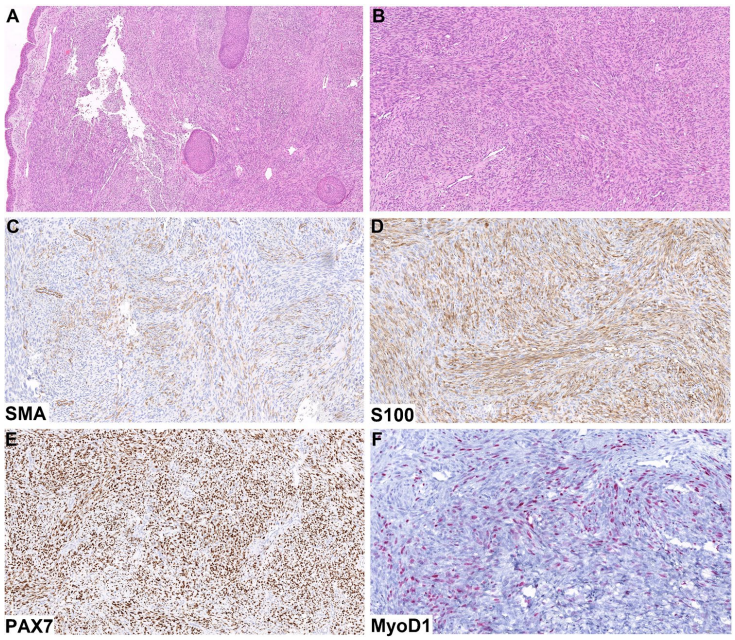

Fig. 2 The resection specimen showed a proliferation of uniform spindled cells with moderate to high cellularity, occasional fascicular arrangement, minimal atypia and no mitotic activity (**B**). In some areas, invaginations of the hyperplastic surface mucosa were enveloped by the tumor cells (**A**). Immunohistochemically, the conventional BSNS areas showed patchy SMA (**C**) and diffuse S100 protein (**D**) expression. There was also a diffuse strong positivity with PAX7 (**E**) and patchy expression of MyoD1 (**F**)

to a high-grade sarcoma with rhabdoid features, very high mitotic activity, and areas of necrosis (Fig. 3A,B).

Immunohistochemically, the conventional BSNS areas showed patchy SMA (Fig. 2C) and diffuse S100 protein (Fig. 2D) expression. There was also a diffuse strong positivity with PAX7 (Fig. 2E) and patchy expression of MyoD1 (Fig. 2F), while desmin and myogenin were completely negative. In contrast, the high-grade areas were completely negative for S100 protein and SMA, and there was only patchy positivity with PAX7 (Fig. 3D), whereas the expression of desmin (Fig. 3C), MyoD1 (Fig. 3E), and myogenin (Fig. 3F) was diffuse in these parts.

Based on the presence of the typical BSNS areas, molecular studies were performed using Archer FusionPlex assay as described previously [7]. This analysis revealed *PAX3*(exon7)*::MAML3*(exon2) fusion which was confirmed by FISH, using *MAML3* (4q31.1) and *PAX3* (2q36.1) break-apart probes (both from SureFISH, Agilent). Of note, the FISH analysis confirmed the presence of the rearrangement (with a cut-off defined as at least 10% cells with a break) in both the conventional and high-grade components.

Postoperatively, the patient received 5040 cGy in 28 fractions. Imaging studies 4 months after resection demonstrated recurrence along the right medial orbital wall and orbital floor. He was initiated on vincristine-urinotecan-temozolamide. Imaging after three cycles again showed local progression. Clinically, the tumor caused total vision loss in the right eye and started to protrude from the right nare. Due to continued progression on maximal therapy, the patient transitioned to hospice and died 15 months after his initial diagnosis.

Discussion

BSNS with morphologically evident rhabdomyoblastic differentiation has been described in approximately 10% of cases [1–3, 5]. However, as the 2 largest studies have shown, at least focal immunohistochemical expression of desmin or MyoD1 is common, with the percentage of immunopositive cases ranging from 35 to 66% and 26 to 91%, respectively. Myogenin expression is the least frequent and is encountered in only 20% of cases [3, 4]. PAX7 expression in BSNS has not been extensively studied but was noted previously as well [8]. The skeletal muscle phenotype of BSNS is in line with its molecular background, which is most commonly characterized by fusions of *PAX3* with either *MAML3* or (less commonly) with *FOXO1* or *NCOA1*. Very rarely, other fusions partners may be involved, including *RREB::MRTFB* (*MKL2*) [3–6, 9–11]. However, the nosological classification of the latter as BSNS is somewhat controversial as identical gene fusions have been described in other head and

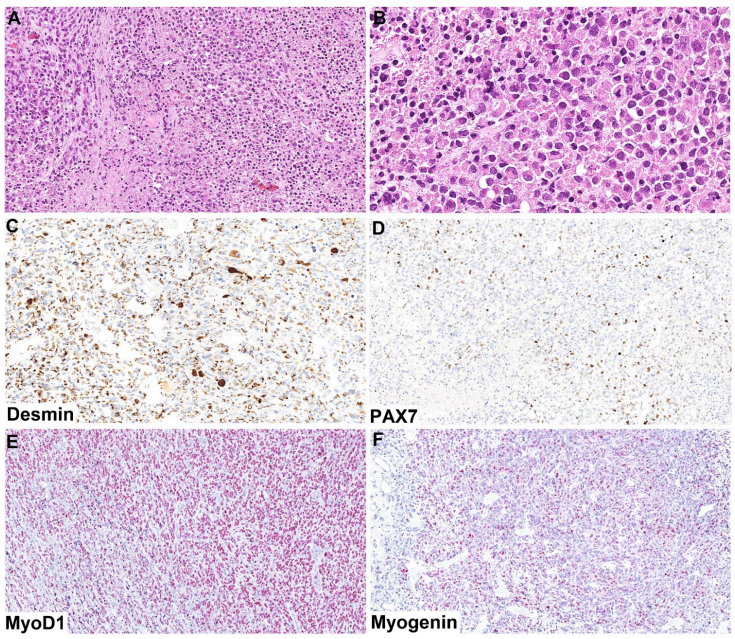

Fig. 3 In some sections, this typical BSNS morphology sharply transitioned to a high-grade sarcoma with rhabdoid features, very high mitotic activity, and areas of necrosis (**A, B**). There was only patchy positivity with PAX7 (**D**), whereas the expression of desmin (**C**), MyoD1 (**E**), and myogenin (**F**) was diffused in these parts

neck mesenchymal tumors [10–12]. During development, PAX3 determines the cell fate of melanocytic, neuronal, and skeletal muscle differentiation and regulates normal myogenesis and postnatal muscular regeneration [5, 6, 13], while MAML3 has been shown to function as a potent transactivator of PAX3 response elements [6]. Gene expression profiling of BSNS with *PAX3::MAML3* fusion also showed altered expression of several genes and signaling networks involved in neural crest, skeletal system, and general embryonic development, including the myogenic genes *MYOCD* and *MYOD1* [6]. Interestingly, the *PAX3::FOXO1* and *PAX3::NCOA1* fusions were also described in rare cases of alveolar RMS [5]. It has been speculated that the differences in clinicopathological features between BSNS and alveolar RMS are probably determined by the cell of origin and cellular environment and by additional genetic aberrations [4].

Nevertheless, the case we are presenting herein shows that a very small subset of BSNS may progress towards a high-grade RMS. After review of the literature, we found 2 recently reported cases of molecularly confirmed BSNS with high-grade transformation, their clinicopathological features together with our case are summarized in Table 1. From the available description and figures, it seems that both cases showed a high-grade spindle cell morphology without the rhabdoid features detected in our case. Unfortunately, the first case was not tested for skeletal muscle markers at all [14], and the other was tested only for desmin and myogenin, both of which were focally positive in the high-grade areas of this case, suggesting differentiation into spindle cell RMS [15].

The differential diagnosis of ordinary BSNS includes a list of other neoplasms with uniform spindle cell morphology occurring in this anatomic area such as malignant peripheral nerve sheath tumor (including malignant Triton tumor when rhabdomyoblastic differentiation is present), cellular schwannoma, monophasic fibrous synovial sarcoma, sinonasal glomangiopericytoma, and solitary fibrous tumor. However, the distinction is usually possible using a carefully selected panel of immunohistochemical stains [1–4]. In contrast, the rhabdomyosarcomatous component in our case could be mistaken for embryonal RMS or pleomorphic RMS. If this area is sampled without the conventional BSNS component (as happened in the initial probatory biopsy in our case), the distinction is impossible without molecular genetic methods. Since the clinical behavior and/or response to treatment of embryonal and pleomorphic RMS might differ from RMS arising from BSNS, we believe it is reasonable that molecular investigation of such cases in the sinonasal area with either *PAX3* FISH probe or preferably using an adequate RNA-sequencing panel is carried out. Significant prognostic differences have already been noted between several molecular subgroups of spindle cell RMS. For example,

Table 1. Clinicopathological features of BSNS cases with high-grade progression

	Case 1 (Bell D et al[11])	Case 2 (Hasnie S et al[12])	Current case
Age/sex	66/M	72/F	67/M
Size (cm)	3.0 × 2.4 × 2.0	NA	4.4 x 3.4 x 2.2
Course of disease	BSNS recurring as high-grade sarcoma in superior extraconal orbit with intracranial extension 15 years later.	2-year history of progressive nasal obstruction with epistaxis and headaches. Resection of a "polyp" which was diagnosed as BSNS. Then resection of a skull base lesion encompassing the entirety of both sinonasal cavities.	History of septoplasty, bilateral frontal sinusotomy, and removal of right middle turbinate concha bullosa 3 years before presenting with nasal congestion and epiphora. MRI showed a soft tissue mass involving the right ethmoid, maxillary, and frontal sinuses and invading the extraconal orbit causing mild asymmetric right-sided ocular proptosis
Treatment and outcome	Primary tumor – resection, radiotherapy, chemotherapy. Recurrence – resection, irradiation. No evidence of disease (10 months)	Resection. Died on complications related to surgery 4.5 months after the resection with no signs of tumor recurrence	Neoadjuvant chemotherapy, resection, irradiation. Died 15 months after diagnosis on tumor progression
Morphology	High-grade spindle cell sarcoma	High-grade spindle cell sarcoma	High-grade rhabdomyosarcoma
IHC of the high-grade areas	Patchy SMA and S100 expression, myogenic markers not tested	Focal desmin and myogenin	Desmin, PAX7, MyoD1, Myogenin positive
Molecular genetics	*PAX3::MAML3* fusion	*PAX3* gene break, copy number alterations of 9p and 22	*PAX3::MAML3* fusion

spindle cell RMS with *VGLL2* and *VGLL3* fusions has a relatively favorable prognosis which is in contrast to the very aggressive subset harboring *MYOD1* mutations [16]. Importantly, spindle cell RMS with *VGLL3* fusions and *MYOD1* mutations has a predilection for the head and neck area [16]. As the other published case of BSNS with high-grade transformation featured spindle cell RMS pattern, a comprehensive molecular investigation for this morphological variant of RMS is warranted as well. Lastly, the herein presented case emphasizes the importance of careful follow-up of patients with BSNS and a throughout sampling of every case to prevent a delayed detection of high-grade transformation.

With regard to the case presented herein, it is interesting to note the significantly different expression of skeletal muscle markers in the conventional BSNS areas compared to the high-grade areas. Even though the former areas were diffusely positive for PAX7 and MyoD1, they were completely negative for desmin and myogenin. In contrast, the high-grade areas were moderately to diffusely positive for all these markers. Both PAX7 and MyoD1 regulate earlier stages of mammalian myogenesis than myogenin [17], and all these 3 transcriptional factors are expressed significantly earlier in myogenesis than the structural protein desmin [18]. This suggests that the cells in conventional BSNS areas were arrested at earlier stages of myogenesis which would be also in line with a generally more frequent expression of MyoD1 compared to the expression of desmin and myogenin in the previous studies [3, 4]. In contrast, possibly due to additional molecular aberrations, the cells in the high-grade areas, although being highly anaplastic, were apparently able to differentiate further along the myogenic pathway as also evidenced by their rhabdoid morphology.

In conclusion, we presented a unique case of BSNS with transformation into high-grade RMS which together with 2 previously published cases of BSNS with high-grade transformation helps to better understand this novel phenomenon. Although the risk for high-grade transformation of BSNS appears low, it has important clinical and diagnostic implications. Besides advocating for a careful follow-up of patients with BSNS and a throughout sampling of every case, we believe that molecular profiling of sinonasal RMS of any type is warranted.

Author contributions

Anders Meyer, M.D.: diagnosed the case, performed histological analyses, wrote parts of the manuscript, and edited the manuscript.

Natálie Klubíčková, M.D.: wrote parts of the manuscript and edited the manuscript.

Elaheh Mosaieby, MsC.: NGS sequencing, edited molecular genetic section.

Petr Grossmann: FISH analysis, edited molecular genetic section.

Antonina Kalmykova, M.D.: literature review and preparation of the table, edited the manuscript.

Olena Koshyk, M.D.: prepared manuscript figures, edited the manuscript.

Michael Michal, M.D., PhD.: performed histological analyses, wrote parts of the manuscript and edited the manuscript.

Funding Open access publishing supported by the National Technical Library in Prague. This study was supported by study grant SVV 260539 from the Ministry of Education, Czech Republic (NK, EM), and by the Cooperatio program, research area SURG.

Declarations

Ethical approval and consent to participate The study was conducted following the rules set by the Faculty Hospital in Pilsen Ethics Committee. Informed consent was not required for the study.

Conflict of interest The authors declare no competing interests.

References

1. Lewis JT, Oliveira AM, Nascimento AG, Schembri-Wismayer D, Moore EA, Olsen KD et al (2012) Low-grade sinonasal sarcoma with neural and myogenic features: a clinicopathologic analysis of 28 cases. Am J Surg Pathol 36:517–525
2. Carter CS, East EG, McHugh JB (2018) Biphenotypic sinonasal sarcoma: a review and update. Arch Pathol Lab Med 142:1196–1201
3. Le Loarer F, Laffont S, Lesluyes T, Tirode F, Antonescu C, Baglin AC et al (2019) Clinicopathologic and molecular features of a series of 41 biphenotypic sinonasal sarcomas expanding their molecular spectrum. Am J Surg Pathol 43:747–754
4. Fritchie KJ, Jin L, Wang X, Graham RP, Torbenson MS, Lewis JE et al (2016) Fusion gene profile of biphenotypic sinonasal sarcoma: an analysis of 44 cases. Histopathology 69:930–936
5. Huang SC, Ghossein RA, Bishop JA, Zhang L, Chen TC, Huang HY et al (2016) Novel PAX3-NCOA1 fusions in biphenotypic sinonasal sarcoma with focal rhabdomyoblastic differentiation. Am J Surg Pathol 40:51–59
6. Wang X, Bledsoe KL, Graham RP, Asmann YW, Viswanatha DS, Lewis JE et al (2014) Recurrent PAX3-MAML3 fusion in biphenotypic sinonasal sarcoma. Nat Genet 46:666–668
7. Michal M, Rubin BP, Kazakov DV, Michalova K, Steiner P, Grossmann P et al (2020) Inflammatory leiomyosarcoma shows frequent co-expression of smooth and skeletal muscle markers supporting a primitive myogenic phenotype: a report of 9 cases with a proposal for reclassification as low-grade inflammatory myogenic tumor. Virchows Arch 477:219–230
8. Georgantzoglou N, Green D, Stephen SA, Kerr DA, Linos K (2022) Biphenotypic sinonasal sarcoma with PAX7 expression. Int J Surg Pathol 30:642–645

9. Nichols MM, Alruwaii F, Chaaban M, Cheng YW, Griffith CC (2022) Biphenotypic sinonasal sarcoma with a novel PAX3::FOXO6 fusion: a case report and review of the literature. Head Neck Pathol. https://doi.org/10.1007/s12105-022-01479-w
10. Mechtersheimer G, Andrulis M, Delank KW, Volckmar AL, Zhang L, von Winterfeld M et al (2021) RREB1-MKL2 fusion in a spindle cell sinonasal sarcoma: biphenotypic sinonasal sarcoma or ectomesenchymal chondromyxoid tumor in an unusual site? Genes Chromosom Cancer 60:565–570
11. Siegfried A, Romary C, Escudie F, Nicaise Y, Grand D, Rochaix P et al (2018) RREB1-MKL2 fusion in biphenotypic "oropharyngeal" sarcoma: new entity or part of the spectrum of biphenotypic sinonasal sarcomas? Genes Chromosom Cancer 57:203–210
12. Agaimy A, Din NU, Dermawan JK, Haller F, Melzer K, Denz A et al (2023) RREB1::MRTFB fusion-positive extra-glossal mesenchymal neoplasms: a series of five cases expanding their anatomic distribution and highlighting significant morphological and phenotypic diversity. Genes Chromosom Cancer 62:5–16
13. Buckingham M, Relaix F (2007) The role of Pax genes in the development of tissues and organs: Pax3 and Pax7 regulate muscle progenitor cell functions. Annu Rev Cell Dev Biol 23:645–673
14. Bell D, Phan J, DeMonte F, Hanna EY (2022) High-grade transformation of low-grade biphenotypic sinonasal sarcoma: radiological, morphophenotypic variation and confirmatory molecular analysis. Ann Diagn Pathol 57:151889
15. Hasnie S, Glenn C, Peterson JEG, El Rassi ET, McKinney KA (2022) High-grade biphenotypic sinonasal sarcoma: a case report. J Neurol Surg Rep 83:e105–e109
16. Agaimy A, Dermawan JK, Leong I, Stoehr R, Swanson D, Weinreb I et al (2022) Recurrent VGLL3 fusions define a distinctive subset of spindle cell rhabdomyosarcoma with an indolent clinical course and striking predilection for the head and neck. Genes Chromosom Cancer 61:701–709
17. Charville GW, Varma S, Forgo E, Dumont SN, Zambrano E, Trent JC et al (2016) PAX7 Expression in rhabdomyosarcoma, related soft tissue tumors, and small round blue cell neoplasms. Am J Surg Pathol 40:1305–1315
18. Folpe AL (2002) MyoD1 and myogenin expression in human neoplasia: a review and update. Adv Anat Pathol 9:198–203

2.2 *EWSR1::POU2AF3(COLCA2)* SARCOMA: AN AGGRESSIVE, POLYPHENOTYPIC SARCOMA WITH A HEAD AND NECK PREDILECTION

The group of small round cell tumors has always been extremely challenging for histopathological diagnosis due to its high heterogeneity, encompassing a wide spectrum of tumors such as neuroendocrine tumors, sarcomas, and lymphomas. Each of these tumor groups lacks clear morphological features that could be useful for an accurate histopathological diagnosis, ultimately leading to the correct treatment. Therefore, the diagnosis of such tumors requires a comprehensive range of different investigations, from immunohistochemistry to molecular genetic studies

Within the group of sarcomas with small round cell and spindle cell morphology affecting the head and neck, there are various tumors, including rhabdomyosarcoma, Ewing's sarcoma, sarcomas with *CIC* and *BCOR*-rearrangements, small cell osteosarcoma, etc.

EWSR1::POU2AF3 (*COLCA2*) sarcomas are a recently identified group of undifferentiated round/spindle cell neoplasms with a predilection for the head and neck region.

This type of sarcoma has only been described in two studies, where 5 and 6 cases of small round cell/spindle cell sarcoma with a novel *POU2AF3* rearrangement were presented [55,56]. This rearrangement was first reported in the literature as a putative colorectal cancer predisposition gene [57], previously known as the *colorectal cancer-associated 2* gene (*COLCA2*). It is now renamed as *POU class 2 homeobox associating factor 3* (*POU2AF3*). *EWSR1::POU5F1* fusion has been identified in myoepithelial tumors of soft tissues and skin [22,23,24,25]. *FUS* and *EWSR1* are members of the FET family of RNA-binding proteins that are involved in splicing and transcription [59,60]. Chromosomal translocations lead to the fusion of a FET family member to the DNA binding domain of a transcription factor in a variety of tumors [60], especially in soft tissue sarcomas.

Considering its clinically aggressive course, a histopathological diagnosis for tumors with *POU2AF3* rearrangements should be made accurately. In our study, we evaluated a total of 19 cases. We analyzed 8 cases collected by us and combined them with 11 from previous studies. The presence of the *POU2AF3* rearrangement was observed in all cases. We provided the histopathological and immunohistochemical features, including molecular genetic alterations.

Previous studies described that the tumor is predilected to the head and neck [55]. However, our study confirmed the observation of the Hiemenz et al. group [56] that the tumor is not limited to this localization and can affect peripheral soft tissues and bones of the limbs and trunk, including internal organs such as the lungs.

In the Agamy and Hiemenz studies [55,56] the tumors had obviously high-grade morphology. In our cohort, however, patients were represented with both high-grade and low-grade morphology, which unfortunately had no impact on the clinical course of this type of tumor. The age of patients ranged from 16 to 74 years and did not play a role in the clinical course of the disease.

Although all tumors with *POU2AF3* rearrangement consisted of relatively uniform spindled to round cells, we found two distinct morphologic subgroups. The first one had low-grade morphology and consisted of relatively bland, spindled/stellate cells in a fibromyxoid stroma, with mild to moderate nuclear atypia, low mitotic activity, and absent necrosis.

The second, larger subgroup consisted predominantly of highly cellular sheets and fascicles of malignant-appearing spindled and round cells, with somewhat biphasic architecture. Mitotic activity was high and small areas of necrosis were present. Stroma was relatively scarce, abundant myxoid or collagenized. Some cases contained numerous hyalinized small vessels. The most distinctive feature of this second subgroup was the presence of nests or loose dispersed sheets of cells with “neuroendocrine” morphology. In individual cases, we noted true epithelial glands containing Alcian-blue-positive mucin clear cells, foci of osteogenic and rhabdomyoblastic differentiation.

We did not find a specific immunophenotype for this type of tumor. The most commonly expressed immunohistochemical markers were GFAP, SATB2, keratins, and S100 protein. Sometimes, tumors display an unusual immunophenotype with a frequent expression of epithelial (pan-keratins and/or EMA expression) or neuroendocrine differentiation markers (CD56, synaptophysin, chromogranin, and INSM1) [55,56]. Polyphenotypic immunoprofile (variable expression of epithelial, rhabdomyogenic, and neurogenic markers) is partially reminiscent of the recently reported *EWSR1::PATZ1* fusion sarcomas [58].

The molecular genetic data included fusions with genomic breakpoints in exons 9, 10, 14, 15, or 16 of *EWSR1,* and only breakpoints in exon 2 of the *POU2AF3* gene were detected.

Some cases had a break of *EWSR1* which was confirmed by FISH. Only two cases harbored *FUS* rearrangement has been found in our cohort.

In summary, the nosology of these neoplasms has yet to be clarified. These 19 reported cases showed the polyphenotypic immunoprofile, which may be consistent with the violation of cell differentiation pathways downstream of the fusion transcript. The morphological differences between described two subgroups raise the question of whether all tumors presented in this study belong to the same entity or are two fundamentally different neoplasms sharing the same genetic event, the *EWSR1/FUS::POU2AF3* fusion. We believe that several cases in our study provided evidence of a single entity with a wide morphological spectrum. Since most of these tumors show an aggressive clinical behavior the use of molecular methods is strongly recommended to achieve an early detection, enabling optimal treatment.

Modern Pathology

EWSR1::POU2AF3(COLCA2) Sarcoma: An aggressive, polyphenotypic sarcoma with a head and neck predilection

--Manuscript Draft--

Manuscript Number:	
Full Title:	EWSR1::POU2AF3(COLCA2) Sarcoma: An aggressive, polyphenotypic sarcoma with a head and neck predilection
Article Type:	Research Article
Section/Category:	
Keywords:	sinonasal tract; soft tissue; EWSR1::POU2AF3 fusion; COLCA2; spindle and round cell sarcoma; synovial sarcoma; neuroendocrine-like; Ewing-like sarcoma
Corresponding Author:	Michael Michal, Ph.D., M.D. Charles University Faculty of Medicine in Pilsen Plzen, Other CZECH REPUBLIC
Corresponding Author Secondary Information:	
Corresponding Author's Institution:	Charles University Faculty of Medicine in Pilsen
Corresponding Author's Secondary Institution:	
First Author:	Olena Koshyk
First Author Secondary Information:	
Order of Authors:	Olena Koshyk
	Carina A. Dehner
	Mari F.C.M. van den Hout
	Isabelle Vanden Bempt
	Raf Sciot
	Hsuan-Ying Huang
	Abbas Agaimy
	Nasir Ud Din
	Natálie Klubíčková
	Elaheh Mosaieby
	Alena Skálová
	Květoslava Michalová
	Patrick Schöffski
	Andre M. Oliveira
	Kevin C Halling
	Sounak Gupta
	John M. Gross
	Johanna W.M. Nin
	Michal Michal
	Kemal Kosemehmetoglu
	Andrew L. Folpe

	Jorge Torres-Mora
	Michael Michal, Ph.D., M.D.
Order of Authors Secondary Information:	
Manuscript Region of Origin:	CZECH REPUBLIC
Abstract:	EWSR1::POU2AF3 (COLCA2) sarcomas are a recently identified group of undifferentiated round/spindle cell neoplasms with a predilection for the head and neck region. Herein we report our experience with 8 cases, occurring in 5 men and 3 women (age range: 37-74 years; median 60 years). Tumors involved the head/neck (4 cases), and one each the thigh, thoracic wall, fibula and lung. Seven patients received multimodal therapy, one patient was treated only with surgery. Clinical follow-up (8 patients; range 4-122 months; median: 32 months) showed 5 patients with metastases (often multifocal, with a latency ranging from 7-119 months), 3 of them along with local recurrence. The median local recurrence-free and metastasis-free survival rates were 24 months and 29 months, respectively. Of the 8 patients, 1 died of an unknown cause, 4 were alive with metastatic disease, 1 was alive with unresectable local disease and 2 were without disease. The tumors comprised of 2 morphologic subgroups: 1) relatively bland tumors consisting of spindled to stellate cells with varying cellularity and fibromyxoid stroma (2 cases) and 2) overtly malignant tumors comprised of nests of “neuroendocrine-appearing” round cells surrounded by spindled cells (6 cases). Individual cases in the 2nd group showed glandular, osteogenic or rhabdomyoblastic differentiation. Immunohistochemical results included: CD56 (4/4 cases), GFAP (5/8) SATB2 (4/6), keratin (AE1/AE3) (5/8) and S100 protein (4/7). RNA sequencing identified EWSR1:: POU2AF3 gene fusion in all cases. EWSR1 gene rearrangement was confirmed by FISH in 5 cases. Our findings confirm the head/neck predilection and aggressive clinical behavior of EWSR1::POU2AF3 sarcomas, and widen the morphologic spectrum of these rare lesions to include relatively bland spindle cell tumors and tumors with divergent differentiation.
Suggested Reviewers:	
Opposed Reviewers:	
Additional Information:	
Question	**Response**

Dear editor, July 24th, 2023

we are submitting our paper named **" *EWSR1::POU2AF3(COLCA2)* Sarcoma: An aggressive, polyphenotypic sarcoma with a head and neck predilection"** which we would like to publish in Modern Pathology.

Compliance with Ethical Standards: The study was conducted following the rules set by the Faculty Hospital in Pilsen Ethics Committee. Informed consent was not required for the study.

Ethics and conflict of interest: The authors have no conflict of interest to disclose.

With best regards,

Michael Michal M.D., PhD.

Department of Pathology, Charles University, Medical Faculty and Charles University Hospital Plzen, Alej Svobody 80, 323 00 Pilsen, Czech Republic. Email: michael.michal@biopticka.cz, cellular phone: +420603792671

EWSR1::POU2AF3(COLCA2) Sarcoma: An aggressive, polyphenotypic sarcoma with a head and neck predilection

Running title: *EWSR1::POU2AF3-rearranged sarcoma*

Olena Koshyk[1,2#], Carina A. Dehner[3,4#], Mari F.C.M. van den Hout[5], Isabelle Vanden Bempt[6], Raf Sciot[7], Hsuan-Ying Huang[8], Abbas Agaimy[9], Nasir Ud Din[10], Natálie Klubíčková[1,11], Elaheh Mosaieby[1,11], Alena Skálová[1,11], Květoslava Michalová[1,11], Patrick Schöffski[13], Andre M. Oliveira[3], Kevin C Halling[3], Sounak Gupta[3], John M. Gross[14], Johanna W.M. Nin[15], Michal Michal[1,11], Andrew L. Folpe[3], Kemal Kosemehmetoglu[16], Jorge Torres-Mora[3*] Michael Michal[1,11*]

#Co-first authorship

*Co-senior authorship

[1]Department of Pathology, Charles University, Faculty of Medicine in Plzen, Czech Republic

[2]Medical Laboratory CSD, Ltd., Kyiv, Ukraine

[3]Department of Laboratory Medicine and Pathology, Mayo Clinic, Rochester, MN, USA

[4]Department of Pathology, Indiana University School of Medicine, Indianapolis, IN, USA

[5]Department of Pathology, GROW School for Oncology and Developmental Biology, Maastricht University Medical Center, Maastricht, The Netherlands.

[6]Department for Human Genetics, University Hospitals Leuven, KU Leuven, Leuven, Belgium

[7]Department of Pathology, University Hospitals Leuven, KU Leuven, Leuven, Belgium

[8]Department of Anatomical Pathology, Kaohsiung Chang Gung Memorial Hospital and Chang Gung University College of Medicine, Kaohsiung City, Taiwan

[9]Institute of Pathology, Friedrich- Alexander University Erlangen- Nürnberg, University Hospital, Erlangen, Germany

[10]Section of Histopathology, Department of Pathology and Laboratory Medicine, Aga Khan University Hospital, Karachi, Pakistan

[11]Bioptical Laboratory, Ltd., Plzen, Czech Republic

[12] Department of General Medical Oncology, University Hospitals Leuven, Leuven Cancer Institute

[13] Department of Oncology, KU Leuven, Laboratory of Experimental Oncology, Leuven, Belgium

[14] Departments of Pathology, The Johns Hopkins Medical Institutions, Baltimore, Maryland, USA

[15]Department of Internal Medicine, Maastricht University Medical Center, Maastricht, The Netherlands

[16]Department of Pathology, Hacettepe University, Ankara, Turkey

Address for correspondence: Michael Michal M.D., PhD., Department of Pathology, Charles University, Medical Faculty and Charles University Hospital Plzen, Alej Svobody 80, 323 00 Plzen, Czech Republic. Email: michael.michal@biopticka.cz

Abstract

EWSR1::POU2AF3 (*COLCA2*) sarcomas are a recently identified group of undifferentiated round/spindle cell neoplasms with a predilection for the head and neck region. Herein we report our experience with 8 cases, occurring in 5 men and 3 women (age range: 37-74 years; median 60 years). Tumors involved the head/neck (4 cases), and one each the thigh, thoracic wall, fibula and lung. Seven patients received multimodal therapy, one patient was treated only with surgery. Clinical follow-up (8 patients; range 4-122 months; median: 32 months) showed 5 patients with metastases (often multifocal, with a latency ranging from 7-119 months), 3 of them along with local recurrence. The median local recurrence-free and metastasis-free survival rates were 24 months and 29 months, respectively. Of the 8 patients, 1 died of an unknown cause, 4 were alive with metastatic disease, 1 was alive with unresectable local disease and 2 were without disease.

The tumors comprised of 2 morphologic subgroups: 1) relatively bland tumors consisting of spindled to stellate cells with varying cellularity and fibromyxoid stroma (2 cases) and 2) overtly malignant tumors comprised of nests of "neuroendocrine-appearing" round cells surrounded by spindled cells (6 cases). Individual cases in the 2nd group showed glandular, osteogenic or rhabdomyoblastic differentiation. Immunohistochemical results included: CD56 (4/4 cases), GFAP (5/8) SATB2 (4/6), keratin (AE1/AE3) (5/8) and S100

protein (4/7). RNA sequencing identified *EWSR1:: POU2AF3* gene fusion in all cases. *EWSR1* gene rearrangement was confirmed by FISH in 5 cases. Our findings confirm the head/neck predilection and aggressive clinical behavior of *EWSR1::POU2AF3* sarcomas, and widen the morphologic spectrum of these rare lesions to include relatively bland spindle cell tumors and tumors with divergent differentiation.

Key Words: sinonasal tract, soft tissue, sarcoma, *EWSR1*, *POU2AF3*, COLCA2, gene fusion, spindle cell sarcoma, synovial sarcoma, neuroendocrine-like, rhabdomyosarcoma, osteosarcoma, Ewing-like sarcoma

Introduction

With the widespread application by pathologists of sophisticated molecular genetic techniques such as next-generation sequencing, an ever-increasing number of new, distinctive entities are now recognized within the group of undifferentiated round and/or spindle cell sarcomas. One of the most recently identified categories comprises aggressive, histologically undifferentiated spindle cell/round cell sarcomas harboring *EWSR1/FUS::POU2AF3(COLCA2)* gene fusions, first reported by Agaimy et al in a series of 5 sinonasal tumors[1], and more recently by Hiemenz et al, in a series of 6 cases predominantly (but not exclusively) involving soft tissue and bone locations in the head/neck [2]. Herein we present our experience with 8 additional examples of *EWSR1/FUS::POU2AF3* sarcoma, further expanding the clinical, morphological and immunohistochemical spectrum of these rare malignant neoplasms.

Materials and methods

Review of our collective consultation archives identified 8 cases known to harbor *EWSR1/FUS::POU2AF3* fusions. Clinical information was obtained from the medical records. Statistical analysis, including survival analyses, were performed with Bluesky Statistics software (ver 7.40).

Immunohistochemistry for each case was performed at several different laboratories based on the original differential diagnostic considerations (staining protocols and antibody sources are available upon request). Some markers (i.e. GFAP, SATB2, neuroendocrine markers) were added in selected cases for the purposes of this study. In cases 1 and 6 both the primary and recurrent or metastatic tumor, respectively, were available for analysis. RNA sequencing in cases 1, 3, 4, 6 and 7 was performed using various customized versions of FusionPlex assay (Archer, Inc). Case 2 was analyzed using TruSight RNA Fusion panel (Illumina Inc.), while DNA and RNA sequencing in case 8 case was performed using TruSight Oncology 500 kit (Illumina Inc.). Cases 5 and 6 were sequenced using a targeted, custom designed, amplicon-based panel, utilizing QIAGEN's (Germantown, MD) QIAseq chemistry. In 6 cases, *EWSR1* FISH break-apart probe was used for confirmation of the gene rearrangement. All methods have been described in more detail previously[3-7]. Molecular data from case 5 have been previously reported[7].

Results

Clinical findings

The clinical features are summarized in Table 1. There were 5 male and 3 female patients aged 37-74 years (median: 60 years; mean: 57 years). The head and neck area was involved in 4 cases (frontal bone, nasopharynx and 2 cases in

the sinonasal area), one case each affected the thigh, thoracic wall, fibula and lung.

Imaging studies were available for four patients (cases 1-3 and 8). CT scan in case 1 revealed a tumor involving left ethmoidal and frontal sinuses with a soft tissue component and with destruction of bilateral cribriform plates and left sphenoidal ala. MRI revealed a T1 isointense and T2 hyperintense mass with contrast enhancement and diffusion restriction involving the left ethmoid sinus, left sphenoid wing, and bilateral frontal sinuses. CT scan in case 2 showed a lytic tumor in the right frontal bone (Fig. 1D) while an infiltrative, variably calcified lesion of soft tissue density, involving the right nasal cavity and frontal, ethmoid and maxillary sinuses was found in case 3 (Fig. 2A). The initial tumor in case 8 affected the left part of the thoracic wall around 5th rib with lytic bone involvement on CT scan.

All patients underwent surgical resection of their primary tumors with either R0, R1 or R2 margins (for details see Table 1). One patient received neoadjuvant chemo/radiotherapy; adjuvant chemotherapy and radiation therapy were administered to 4 and 6 patients, respectively. One patient (case 6) was treated with surgery only. Clinical follow-up (8 patients; range 4 to 122 months; median: 32 months; mean: 39 months) showed 5 patients with metastases (unconfirmed by biopsy in case 1), 3 of them along with local recurrence. Of the 8 patients, 1 died of an unknown cause, 4 were alive with metastatic disease, 1

was alive with unresectable local disease and 2 were without disease. The metastases occurred with a latency ranging from 7 to 119 months, were often multifocal and involved bone (n=3) and pleura, base of the skull and lymph nodes (1 case each). The median local recurrence-free and metastasis-free survival rates were 24 months and 29 months, respectively.

Submitting diagnostic considerations from referring pathologists included Ewing-like sarcoma (2x), osteosarcoma (2x), "spindle cell sarcoma", ossifying fibromyxoid tumor, desmoplastic fibroma, intranodal palisaded myofibroblastoma, atypical carcinoid, synovial sarcoma, myoepithelial tumor and neuroendocrine carcinoma.

Morphological findings

Microscopically, 6 cases grew in an infiltrative fashion into surrounding soft tissue and bone, whereas cases 5 and 6 appeared relatively well-circumscribed. Although all tumors consisted of relatively uniform spindled to round cells, two distinct morphologic groups could be discerned. The first of these, illustrated by cases 1 and 2, displayed variable cellularity and consisted of relatively bland, spindled to stellate cells in a fibromyxoid stroma; nuclear atypia was mild to moderate, mitotic activity was low, not exceeding 2 mitoses per 10 high-power fields (HPF) and necrosis was absent (Fig. 1). In case 1, the primary tumor showed predominantly low cellularity (Fig. 1A), with only a small focus having more cellular, round cell features (Fig. 1B); the recurrent tumor consisted

chiefly of more cellular spindled proliferation. (Fig. 1C). Similarly, case 2 was predominantly hypocellular (Fig. 1E), with scattered small to medium-sized nests having a more cellular, round cell appearance (Fig. 1E-G). The initial tumor in case 1 had a striking arborizing capillary vasculature (Fig. 1A), whereas small, hyalinized vessels predominated in the recurrence and in case 2 (Fig. 1E).

The second, larger subgroup consisted predominantly of highly cellular sheets and fascicles of overtly malignant-appearing spindled and round cells, with somewhat biphasic architecture (Fig. 2-5). Mitotic activity ranged from 4-24 mitoses per 10 HPF and small areas of necrosis were identified in 2 cases. Stroma was relatively scarce in cases 3, 4, 6 and 7 (Fig. 3B), whereas cases 4 and 5 contained foci with abundant myxoid stroma, in which the tumor cells grew in cord-like, pseudopapillary, pseudoglandular, and cribriform formations (Fig. 3A, C, E). Relatively hypocellular zones with hyalinized collagen were variably present (Fig. 3D, 5A-C). Some cases contained numerous hyalinized small vessels (Fig. 3A, B), whereas others had an inconspicuous vasculature. Perhaps the most distinctive feature of this second subgroup (found in 4 cases) was the presence of nests or loose dispersed sheets of round cells with basophilic nuclei with finely stippled chromatin ("neuroendocrine"), sometimes with peripheral palisading, surrounded by zones with more spindled cells having lighter and more evenly dispersed chromatin (Fig. 3D, 4B, C, G, 5A-C).

One prominent pinpoint nucleolus was typically present in both types of cells (Fig. 2D, 5C)

Unusual features, noted in individual cases, included keratin 7-positive glands containing Alcian-blue-positive mucin (case 8) (Fig. 5D), clear cells (cases 7 and 8) (Fig. 4H), osteogenic differentiation with production of osteoid matrix (case 3) (Fig. 2E), and rhabdomyoblastic differentiation including rhabdomyoblasts with visible cross-striations (case 6) (Fig. 4D). Interestingly, rhabdomyoblasts were absent in the metastasis from this tumor.
Scanned whole slide images for most cases are available online at the hyperlinks listed in the Supplementary file 1. No correlation was found between any of the histologic features studied and the clinical course of the disease.

Immunohistochemical findings

The immunohistochemical results are summarized in Table 2. The most commonly expressed markers were GFAP (5/8 cases; 63%) (Fig. 5F), SATB2 (4/6 cases; 67%) (Fig. 2F, 4F), keratins (AE1/AE3) (5/8 cases; 63%) (Fig. 5G) and S100 protein (4/7 cases; 57%) (Fig. 5E). In general, expression of these markers was more pronounced in the round cell nodules, as compared with the spindled cells (Fig. 4F, 5E-G). Expression of CD56 (4/4 cases) (Fig. 3F), synaptophysin, chromogranin and INSM1 (collectively 3/7; 43%) also tended to

be restricted to these round cell areas (Fig. 5H, I). As expected, more robust SATB2 expression was seen in case 3 with overt osteoblastic differentiation as compared with undifferentiated spindle cell zones in other cases (Fig. 2F, 4F). In case 6, markers of rhabdomyoblastic differentiation (e.g., desmin, myogenin, MyoD1) were seen in differentiating rhabdomyoblasts as well as in morphologically undifferentiated cells (Fig. 4E). More limited expression of these markers was present in the metastasis as well. A wide variety of other markers, tested on an ad hoc basis in individual cases, were negative or non-contributory (listed in Table 2).

Molecular genetic findings

The molecular genetic data is summarized in Table 2. Fusions with genomic breakpoints in exons 9, 10, 14, 15 or 16 of *EWSR1* were noted across the cohort, while only breakpoints in exon 2 of *POU2AF3* gene were detected. Case 2 showed 3 co-existing breakpoint-defined subclones affecting adjacent exons 14-16 of *EWSR1*. Notably, the *EWSR1* genomic breakpoints in all 4 sinonasal cases were located in exons 14-16, while all extrasinonasal cases had breakpoints in exons 9 or 10. In cases 1-3, 5, 7 and 8, a break of *EWSR1* was confirmed by FISH. In case 8, DNA sequencing did not detect any pathogenic mutations and the tumor mutation burden was low (3.9/Mb). No case harbored *FUS* rearrangement.

Discussion

Including the original description by Agaimy et al followed by the Hiemenz et al´s series, and our current cases, a total of 19 neoplasms carrying the *EWSR1/FUS::POU2AF3* (formerly *COLCA2*) fusion have been well documented (clinicopathological features of all cases are summarized in the supplementary Table 1).[1,2] A single case mentioned in one fusion detection methodological study (included in the current study as case 5) lacked any clinical or anatomic data [7].

Clinically, these tumors show a striking predilection for the head and neck area (13/19 cases), particularly for the sinonasal tract (9/19 cases), but they may occur at other sites including soft tissue and bone. They affect predominantly middle-aged to older adults without gender predilection. *EWSR1/POU2AF3*-rearranged neoplasms reported so far mostly behaved as high-grade sarcomas irrespective of their morphology. Half of published cases (9/18) developed metastases (as late as 10 and 23 years after diagnosis hence warranting a lifelong follow-up) with or without recurrence and additional 3 patients experienced either recurrence or progressive tumor growth. The 5-year local recurrence-free survival and metastasis-free survival were 48% and 54%, respectively, after combining the available clinical data from these three studies. While only 1/18 patients died of disseminated disease, most remaining patients were alive with disease despite multimodal therapy. However, 5 patients were

without evidence of disease at last follow-up and all 4 with available treatment information received a multimodal therapy.

The previously emphasized morphological features including the presence of undifferentiated round and spindled cells with fine chromatin and prominent nucleoli [1, 2] and frequent biphasic arrangement of spindled and round/epithelioid cells, often mimicking synovial sarcoma[2] were observed in our cases as well. The reported cases did not exhibit any consistent morphological evidence of epithelial, mesenchymal or other specific lines of differentiation, apart from single cases in our study exhibiting glandular, osteoblastic and rhabdomyoblastic differentiation, respectively. However, they seem to display an unusual immunophenotype with frequent expression of markers associated with epithelial (pankeratins and/or EMA expression) or neuroendocrine differentiation [1, 2].

New findings in our study include the presence of 2 morphologically different subgroups. The first consisted of relatively uncharacteristic low-grade appearing spindle cell tumors with mild to moderate atypia and variable cellularity with occasional foci showing round cells, while the second encompassed hypercellular neoplasms with predominantly high-grade round and spindle cell morphology. A very characteristic and frequent microscopic feature of this latter group was the presence of distinctly biphasic arrangement of the tumor cells with the formation of round cell nests on a predominantly

spindle cell background reminiscent of biphasic synovial sarcoma but lacking true gland formation (apart from a single case). The round cells often contained more basophilic staining nuclei with more stippled chromatin, imparting a neuroendocrine appearance. Notably, it was these round cells that preferentially showed expression of keratins and various neuroendocrine markers we tested. Novel findings also included the identification of true glands with mucin production, and rhabdomyoblastic and osteogenic differentiation found in one case each.

The exact nosology of these neoplasms remains to be further delineated. Data from these 19 reported cases are in line with a sarcoma showing polyphenotypic (ambiguous) immunoprofile. Their morphological heterogeneity precludes putting them into any of the defined epithelial or mesenchymal neoplastic categories, despite their focal overlap with basaloid epithelial or neuroendocrine neoplasms in a subset of cases. While some may superficially mimic biphasic synovial sarcomas based on subtle biphasic arrangements of plump rounded and spindled cells, their morphology (variable spindle and round cell features) and polyphenotypic immunoprofile (variable expression of epithelial, rhabdomyogenic and neurogenic markers such as S100, GFAP and others) are partially reminiscent of the recently reported category of *EWSR1::PATZ1* fusion sarcomas [8]. Their capacity for multilineage

immunophenotypic differentiation is in line with derangement of cellular differentiation pathways downstream the fusion transcript.

The observed morphological differences between both subgroups obviously raise the question whether all tumors presented in this study belong to the same entity or represent 2 fundamentally different neoplasms sharing same genetic event, the *EWSR1/FUS::POU2AF3* fusion. We believe several cases in our study offered a strong clue in support of a single entity with a wide morphological spectrum. Notably, the significant variation in cell shape and cellularity within the same tumors and between primary tumors and their recurrences suggests the presence of bland looking spindled morphology at one end and highly cellular undifferentiated round cell morphology at the other end of the spectrum with lot of transitional morphologies on the spectrum in-between. A similar morphological spectrum of morphologically low-grade appearing sarcomas with low cellularity on one end and frankly high-grade neoplasms with significantly different appearance on the other is a commonplace in several other soft tissue entities such as low-grade fibromyxoid sarcoma/sclerosing epithelioid fibrosarcoma, low-grade/high-grade myxoid liposarcoma or more recently within the spectrum of *EWSR1::PATZ1*-rearranged sarcomas [8-10].

The differential diagnosis of these tumors is defined by the predominant pattern seen in a given case and also influenced by the anatomical site and

immunohistochemical findings. The low-grade spindle cell tumors might be reminiscent of other spindle cell sarcomas with fibromyxoid stroma such as ossifying fibromyxoid tumor (OFMT) and low-grade fibromyxoid sarcoma (LGFMS). Features arguing against the diagnosis of OFMT were the wide infiltrative growth and lack of pseudocapsule and ossification (in the vast majority of cases).[11] The absence of abrupt transitions between collagenized and myxoid stroma and the lack of MUC4 expression (caveat: only 2 cases tested) argue against LGFMS.[12] Low-grade myxofibrosarcoma or - in case of a primary bone tumor - various forms of osteosarcoma may enter the differential as well (see later discussion). The high-grade round and spindle cell tumors may be difficult to distinguish from Ewing sarcoma, *CIC*-rearranged sarcoma, and other sarcomas with this morphology which can be achieved using histology, immunohistochemistry and, if necessary, by molecular methods[13]. While *EWSR1/FUS::POU2AF3* sarcomas can be added to a long list of mimickers of neuroendocrine neoplasms [14], the latter typically exhibit more diffuse expression of epithelial and neuroendocrine markers (typically coexpression of synaptophysin, chromogranin and/or INSM1) and in most cases, a primary lesion can be identified clinically. As already emphasized by Hiemenz et al[2], these tumors are in many aspects highly reminiscent of synovial sarcoma, particularly of those with predominantly spindle cell morphology and a confident distinction purely on morphological grounds is unreliable. However, with the use of novel highly specific and sensitive immunohistochemical

markers that are becoming available at many institutions, synovial sarcoma can most likely be excluded (caveat: only 1 case tested for SS18::SSX antibody) [15]. Nevertheless, while we believe that when present, some of the more recurrent histopathological features of *EWSR1/FUS::POU2AF3* tumors may raise suspicion for the diagnosis, high-throughput genetic assays such as RNA-sequencing represent the only way to reliably diagnose these tumors at this point. In addition, some cases are lacking the more characteristic histological traits and they cannot be distinguished from morphologically highly overlapping differential diagnostic entities that lack specific immunohistochemical markers such as low-grade myxofibrosarcoma, osteosarcoma or various myoepithelial or basaloid epithelial neoplasms without appropriate molecular studies.

Regarding the molecular background, among the 19 reported cases, 17 carried the *EWSR1::POU2AF3* fusion while two cases had *FUS* as the 5' fusion partner instead of *EWSR1*. While the number of published cases is low and the following observation might thus be merely coincidental, it is interesting to note that in 14/17 cases with *EWSR1::POU2AF3* fusion, the locations of genomic breakpoints seemed to follow an anatomical site-dependent pattern. Namely, nine out of 12 head and neck cases had genomic breakpoints located in exons 12-17 and only 3 cases in exons 9 or 10 of *EWSR1* gene. In contrast, all 5 cases located outside the head and neck area had breakpoints localized in exons 9 or

10. Exons 12-14 contain a central RNA recognition motif (RRM) which is involved in RNA and DNA binding (Fig. 6). Similar to Ewing sarcoma and many other *EWSR1*-rearranged tumors which usually have genomic breakpoints located in exons 6-8, the RRM is lost in non-head and neck cases [16-18]. In contrast, most of the reported head and neck cases kept the RRM domain. The binding of regulatory nucleic acids or ribonucleoproteins may potentially affect the function of the fusion protein. A difference in the pathogenesis of the translocation, including the specific microenvironment of the head and neck area might potentially be causative, while the exact significance and molecular basis remain unclear.

POU Class 2 Homeobox Associating Factor 3 (POU2AF3) gene [formerly named *Colorectal cancer associated 2* (*COLCA2)]* located on chromosome 11q23.1 has been associated with increased colorectal cancer risk in a genome-wide association study. The pattern of expression of the *POU2AF3* protein in neoplastic, stromal and immune cells in patients with higher-risk alleles for colorectal cancer suggested a tumor suppressor role.[20] However, the exact mechanism through which the POU2AF3 protein is deregulated remains unclear[1]. Moreover, *POU2AF3* codes for a transcriptional coactivator protein that through its OCA domain (Fig. 6) binds with the transcription factor POU2F3 which is critical for the development of tuft cells, a rare chemosensory lineage that coordinates immune and neural responses to foreign pathogens in

mucosal tissues. Recent studies have also revealed tuft-cell-like human tumors, particularly as a variant of small-cell lung cancer [19].

In conclusion, we reported additional 8 cases of *EWSR1::POU2AF3* sarcomas, further defining their clinicopathological features and for the first time emphasizing their potential for heterologous differentiation. Many cases exhibit relatively characteristic biphasic morphological features, whereas others may show epithelial, rhabdomyosarcomatous or osteosarcomatous differentiation or present as nondescript spindle and/or round cell sarcomas. Although further studies are needed to confirm whether all tumors with *EWSR1::POU2AF3* fusion represent a single entity, we believe that some of the partially overlapping clinicopathological features in our cases lend support for this notion. Since most of these tumors follow an aggressive clinical course and, in some cases, their low-grade morphology may be deceiving, the use of high-throughput molecular methods is recommended to achieve an early detection, enabling optimal treatment.

Acknowledgments: The authors are grateful to Dr. Wan-San Li from the Department of Pathology, Chi-Mei Medical Center, Tainan, Taiwan and Dr. Jen-Chieh Lee Department and Graduate Institute of Pathology, National Taiwan University Hospital, National Taiwan University College of Medicine, Taipei, Taiwan for performing molecular methods in case 3.

Compliance with Ethical Standards: The study was conducted following the rules set by the Faculty Hospital in Pilsen Ethics Committee. Informed consent was not required for the study.

Funding: This study was supported by study grant SVV 260652 from the Ministry of Education, Czech Republic (OK, EM, NK) and by the Cooperatio program, research area SURG. IVB is recipient of a post-doctoral mandate from the Klinische onderzoeks-en opleidingsraad (KOOR) of the University Hospitals Leuven.

Ethics and conflict of interest: The authors have no conflict of interest to disclose.

References

1. Agaimy A, Baneckova M, De Almeida J, et al. Recurrent EWSR1::COLCA2 Fusions Define a Novel Sarcoma With Spindle/Round Cell Morphology and Strong Predilection for the Sinonasal Tract. *Am J Surg Pathol.* 2022.
2. Hiemenz MC, Kaur J, Kuang Z, et al. POU2AF3-rearranged sarcomas: A novel tumor defined by fusions of EWSR1 or FUS to a gene formerly designated COLCA2. *Genes Chromosomes Cancer.* 2023.
3. Michal M, Rubin BP, Kazakov DV, et al. Inflammatory leiomyosarcoma shows frequent co-expression of smooth and skeletal muscle markers supporting a primitive myogenic phenotype: a report of 9 cases with a proposal for reclassification as low-grade inflammatory myogenic tumor. *Virchows Arch.* 2020;477:219-230.
4. Michal M, Berry RS, Rubin BP, et al. EWSR1-SMAD3-rearranged Fibroblastic Tumor: An Emerging Entity in an Increasingly More Complex Group of Fibroblastic/Myofibroblastic Neoplasms. *Am J Surg Pathol.* 2018;42:1325-1333.
5. Skalova A, Baneckova M, Laco J, et al. Sclerosing Polycystic Adenoma of Salivary Glands: A Novel Neoplasm Characterized by PI3K-AKT Pathway Alterations-New Insights Into a Challenging Entity. *Am J Surg Pathol.* 2022;46:268-280.
6. Agaimy A, Togel L, Haller F, et al. YAP1-NUTM1 Gene Fusion in Porocarcinoma of the External Auditory Canal. *Head Neck Pathol.* 2020;14:982-990.
7. Balan J, Jenkinson G, Nair A, et al. SeekFusion - A Clinically Validated Fusion Transcript Detection Pipeline for PCR-Based Next-Generation Sequencing of RNA. *Front Genet.* 2021;12:739054.
8. Michal M, Rubin BP, Agaimy A, et al. EWSR1-PATZ1-rearranged sarcoma: a report of nine cases of spindle and round cell neoplasms with predilection for thoracoabdominal soft tissues and frequent expression of neural and skeletal muscle markers. *Mod Pathol.* 2021;34:770-785.
9. Evans HL. Low-grade fibromyxoid sarcoma: a clinicopathologic study of 33 cases with long-term follow-up. *Am J Surg Pathol.* 2011;35:1450-1462.
10. Smith TA, Easley KA, Goldblum JR. Myxoid/round cell liposarcoma of the extremities. A clinicopathologic study of 29 cases with particular attention to extent of round cell liposarcoma. *Am J Surg Pathol.* 1996;20:171-180.
11. Miettinen M, Finnell V, Fetsch JF. Ossifying fibromyxoid tumor of soft parts--a clinicopathologic and immunohistochemical study of 104 cases with long-term follow-up and a critical review of the literature. *Am J Surg Pathol.* 2008;32:996-1005.
12. Doyle LA, Moller E, Dal Cin P, et al. MUC4 is a highly sensitive and specific marker for low-grade fibromyxoid sarcoma. *Am J Surg Pathol.* 2011;35:733-741.
13. Le Loarer F, Baud J, Azmani R, et al. Advances in the classification of round cell sarcomas. *Histopathology.* 2022;80:33-53.
14. Kasajima A, Konukiewitz B, Schlitter AM, et al. Mesenchymal/non-epithelial mimickers of neuroendocrine neoplasms with a focus on fusion gene-associated and SWI/SNF-deficient tumors. *Virchows Arch.* 2021;479:1209-1219.
15. Baranov E, McBride MJ, Bellizzi AM, et al. A Novel SS18-SSX Fusion-specific Antibody for the Diagnosis of Synovial Sarcoma. *Am J Surg Pathol.* 2020;44:922-933.
16. Wang X, Schwartz JC, Cech TR. Nucleic acid-binding specificity of human FUS protein. *Nucleic Acids Res.* 2015;43:7535-7543.
17. Sankar S, Lessnick SL. Promiscuous partnerships in Ewing's sarcoma. *Cancer Genet.* 2011;204:351-365.
18. Bridge JA, Fidler ME, Neff JR, et al. Adamantinoma-like Ewing's sarcoma: genomic confirmation, phenotypic drift. *Am J Surg Pathol.* 1999;23:159-165.

19. Wu XS, He XY, Ipsaro JJ, et al. OCA-T1 and OCA-T2 are coactivators of POU2F3 in the tuft cell lineage. *Nature.* 2022;607:169-175.
20. Peltekova VD, Lemire M, Qazi AM, et al. Identification of genes expressed by immune cells of the colon that are regulated by colorectal cancer-associated variants. *Int J Cancer.* 2014;134:2330-2341.

Figure legends

Figure 1. Case 1 (A-C). The tumor in case 1 consisted of spindle to stellate cells with mild to moderate atypia and fibromyxoid stroma. The primary tumor showed a striking arborizing vasculature and predominantly low cellularity (**A**), with only a small focus having more cellular, round cell features (**B**). The recurrent tumor consisted chiefly of more cellular spindled proliferation (**C**). **Case 2 (D-G)**. CT scan in case 2 showed a lytic tumor in the right frontal bone (**D**). This case was also hypocellular with scattered small to medium-sized nests having a more cellular, round cell appearance. Small, hyalinized vessels predominated (**E**). High-power view of one of the larger nests with more round cell appearance (**F**). High-power view of one of the small round cell aggregates (**G)**

Figure 2. Case 3. CT scan revealed an infiltrative lesion of soft tissue density, involving the right nasal cavity and frontal, ethmoid and maxillary sinus with multifocal calcifications (**A**). The tumor consisted of highly cellular sheets and fascicles of spindled cells and occasional round cells with little intervening stroma (**B, C**) Foci with round cells featuring more basophilic nuclei with finely stippled chromatin and typically one prominent pinpoint nucleolus (**D**). Some of the tumor cells showed osteogenic differentiation with production of osteoid matrix (**E**). In line with the observed osteogenic properties, the tumor cells showed a diffuse strong expression of SATB2 (**F**).

Figure 3. Case 4 (A, B). This case consisted purely of nests or loose dispersed sheets of round cells with basophilic nuclei with finely stippled neuroendocrine-like chromatin. It contained abundant small hyalinized vessels (**A**) and areas with myxoid stromal matrix which imparted a cordlike and pseudopapillary architecture (**B**). **Case 5 (C-F**). Case 5 showed a prominent biphasic arrangement consisting of predominantly spindle cell periphery (top), whereas towards the center (bottom), it contained round cells with neuroendocrine features with cordlike, pseudopapillary and pseudoglandular arrangement within a myxoid stroma (**C**). Transitional areas with round cells within the predominantly spindle cell background occasioning a resemblance to similar areas in case 2 (**D**). High-power view of round cells with neuroendocrine features forming pseudoglandular structures (**E**). Diffuse strong expression of CD56 (**F**).

Figure 4. Case 6 (A-F). Case 6 contained a sharply demarcated rhabdomyoblastic nodule (green line) (**A**). Most parts showed a biphasic arrangement and consisted of round cell nests with predominantly neuroendocrine nuclear features on a background of more ovoid to spindled cells having lighter chromatin (**B, C**). High-power view of the focus containing strap cells and rhabdomyoblasts with cross-striations (**D**). Markers of rhabdomyoblastic differentiation including myogenin were positive throughout the tumor (**E**) SATB2 expression was found almost exclusively in the round cell nests (**F**). **Case 7 (G, H).** The tumor also showed a biphasic arrangement with most parts of the tumor consisting of more loosely dispersed sheets of round cells with neuroendocrine features admixed with spindle cells (**G**). Numerous clear cells were present (**H**).

Figure 5. Case 8. Cellular stroma-poor areas (bottom) alternated with more hyalinized spindle cell regions containing scattered round cell nests (top) (**A**). Nests of round cells with neuroendocrine features on the hypocellular background featuring spindle to stellate shaped cells with little atypia were reminiscent of similar areas in cases 1 and 2 (**B**). Peripheral palisading of the round cells was present in some nests (**C**). A small focus with keratin 7-positive glands (upper inset) containing Alcian-blue-positive mucin (lower inset). **F-I:**

Multifocal expression of S100, GFAP, AE1/AE3, synapthophysin and INSM1 preferentially found within the round cell areas.

Figure 6. **Schematic depiction of the *EWSR1::POU2AF3* fusion** Dark blue, blue, green and yellow parts of the respective genes represent the regions that are retained in the fusion products, while the grey parts are lost. In non-head and neck cases, only the transactivation domain (TAD) (dark blue) of *EWSR1* is retained. In contrast, the head and neck cases contain both TAD and the RNA recognition motif (RRM) (blue) of *EWSR1*; in addition, some head and neck cases also retain the RanBP2 type Zinc finger (green). The OCA domain of POU2AF3 (yellow), which enables binding to POU domain-containing transcription factors, is almost completely retained in the fusion gene.

Figure 1

Click here to access/download;Figure;Figure 1.jpg

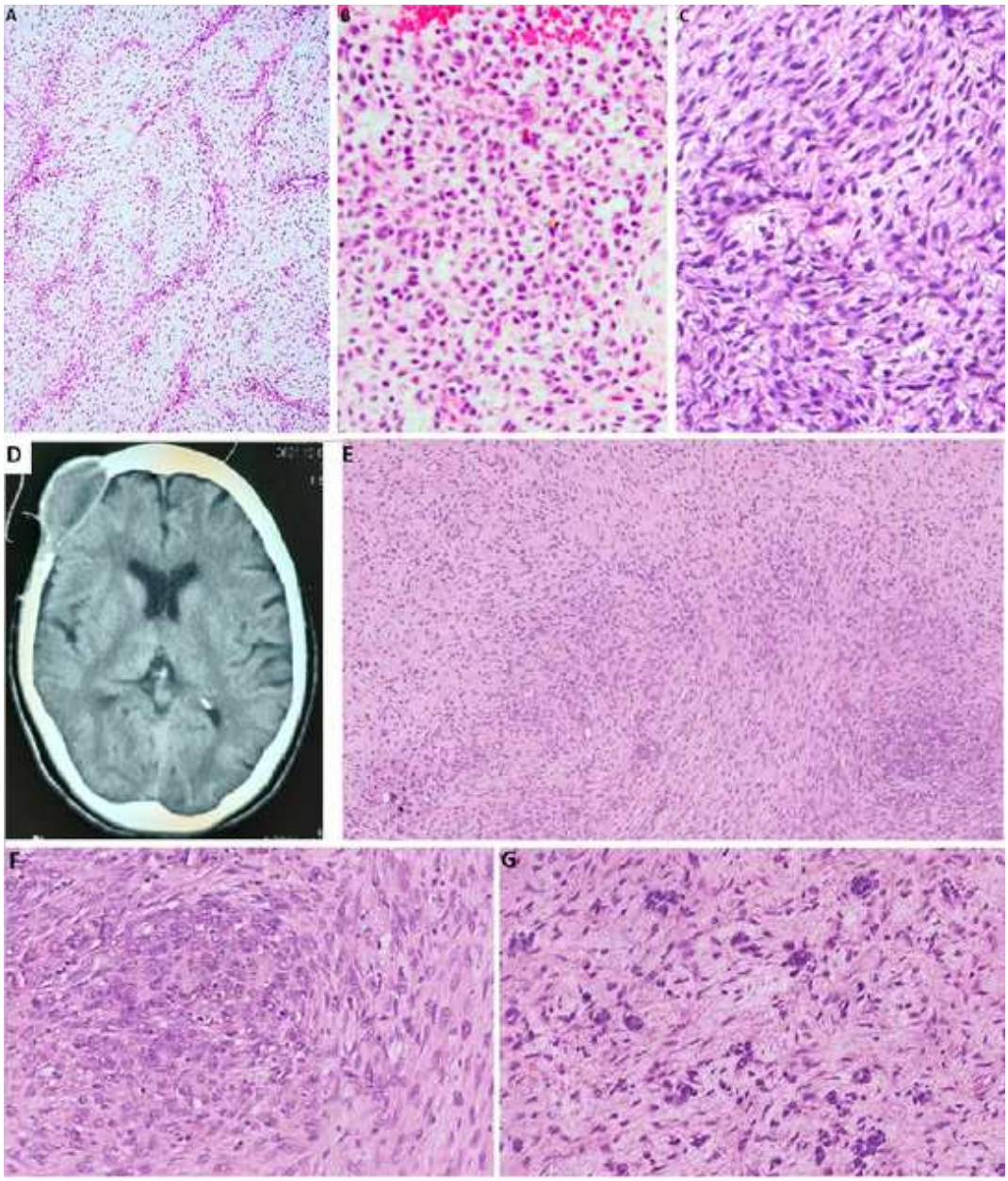

Figure 2

Click here to access/download;Figure;Figure 2.jpg

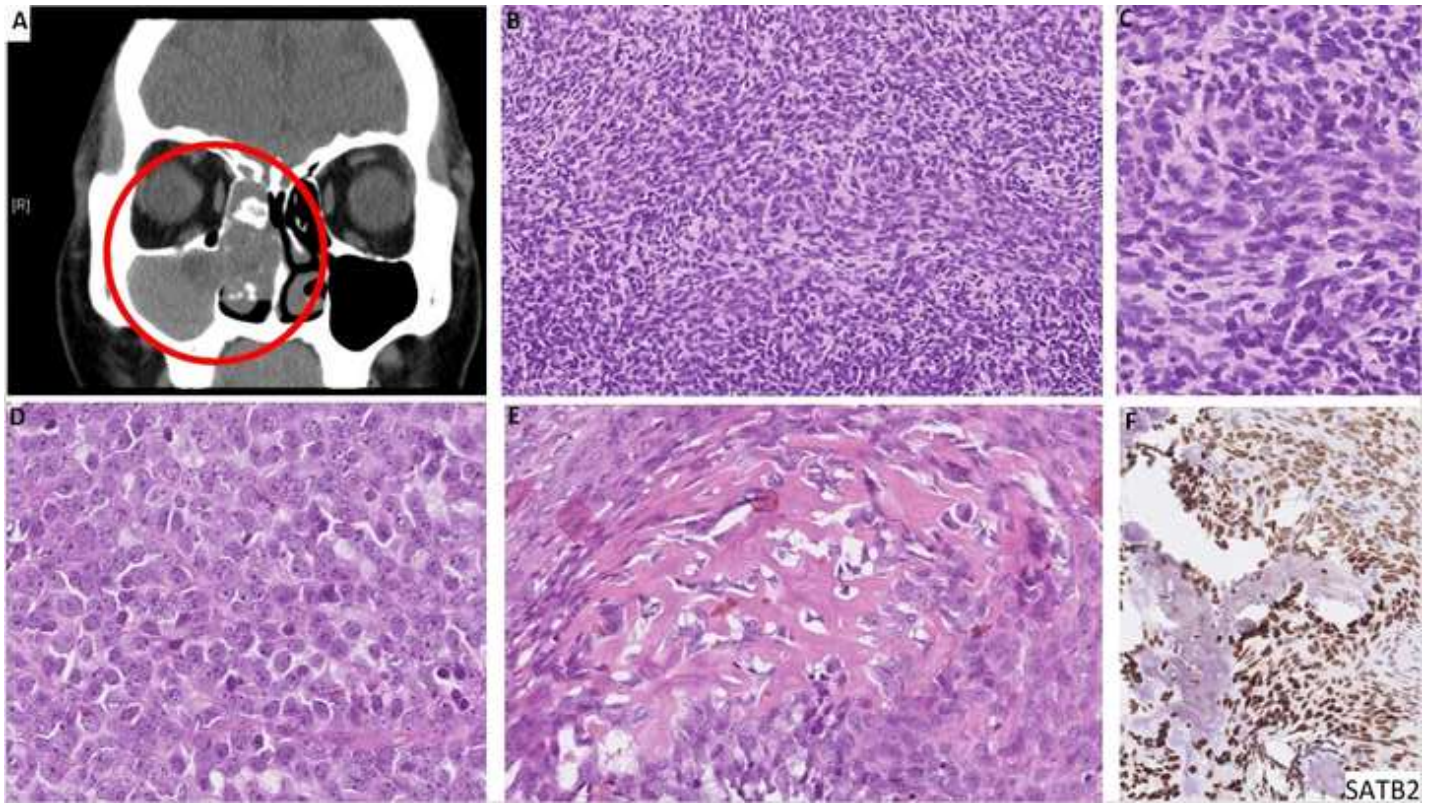

Figure 3

Click here to access/download;Figure;Figure 3.jpg

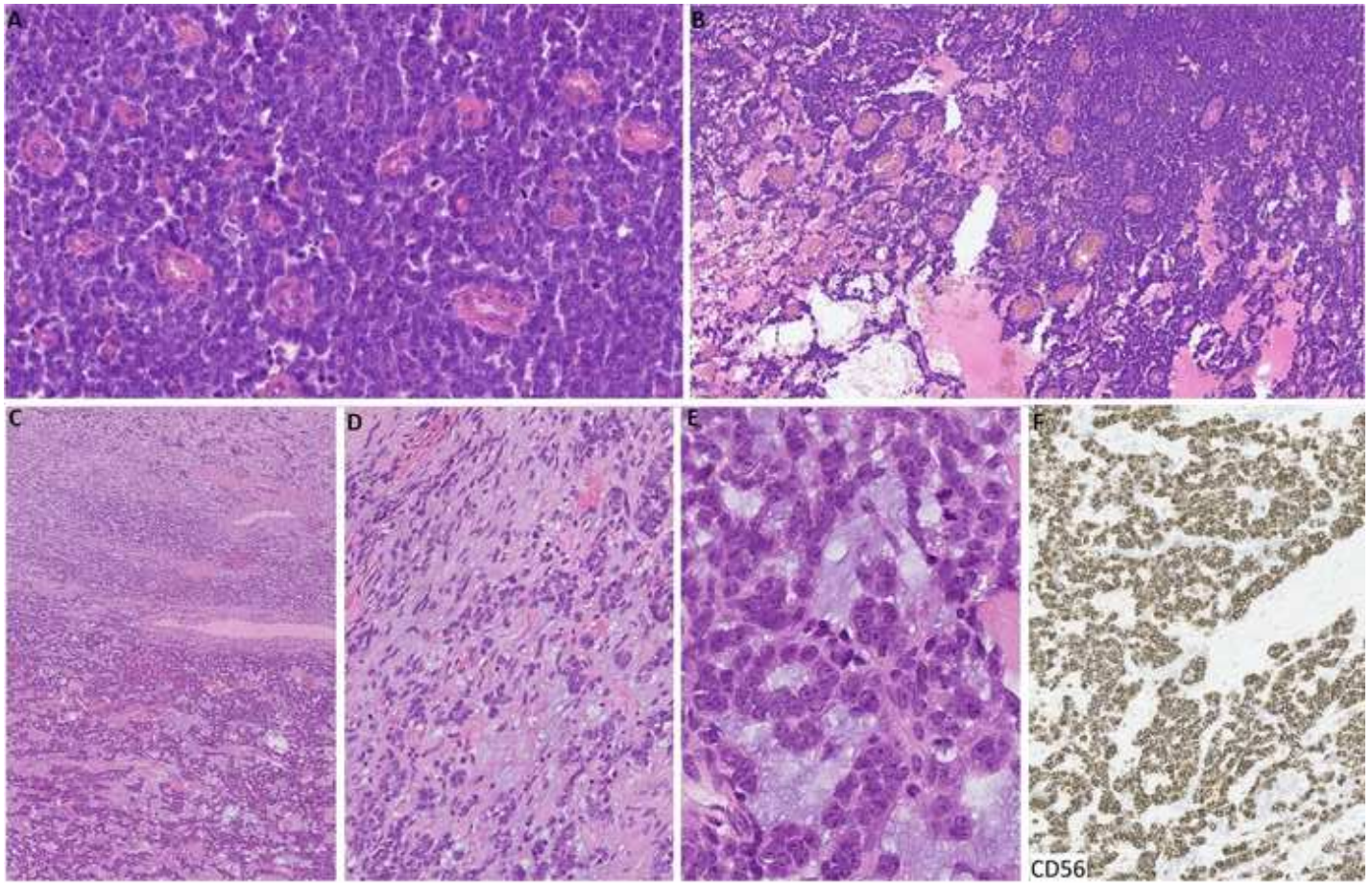

Figure 4

Click here to access/download;Figure;Figure 4.jpg

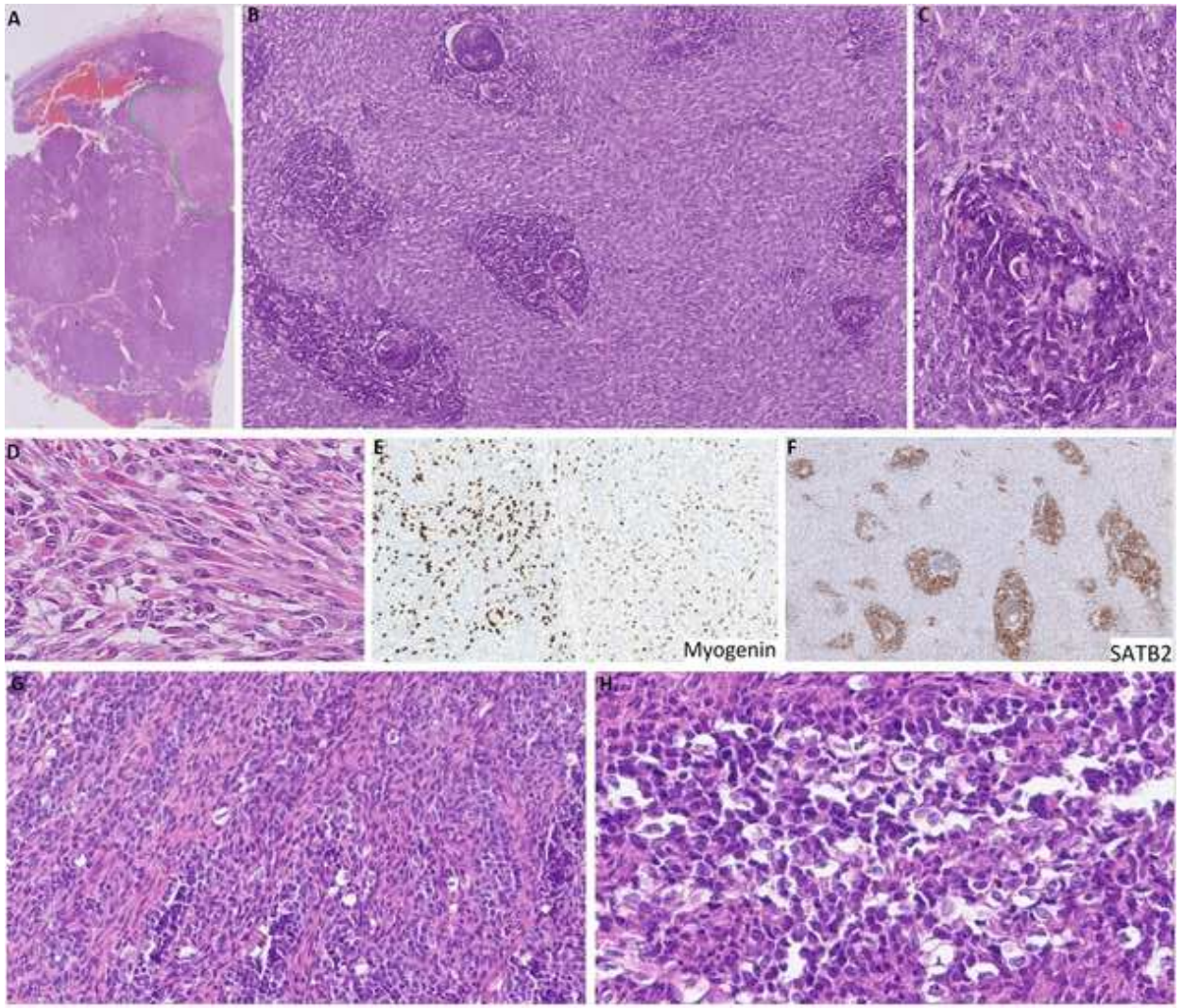

Figure 5

Click here to access/download;Figure;Figure 5.jpg

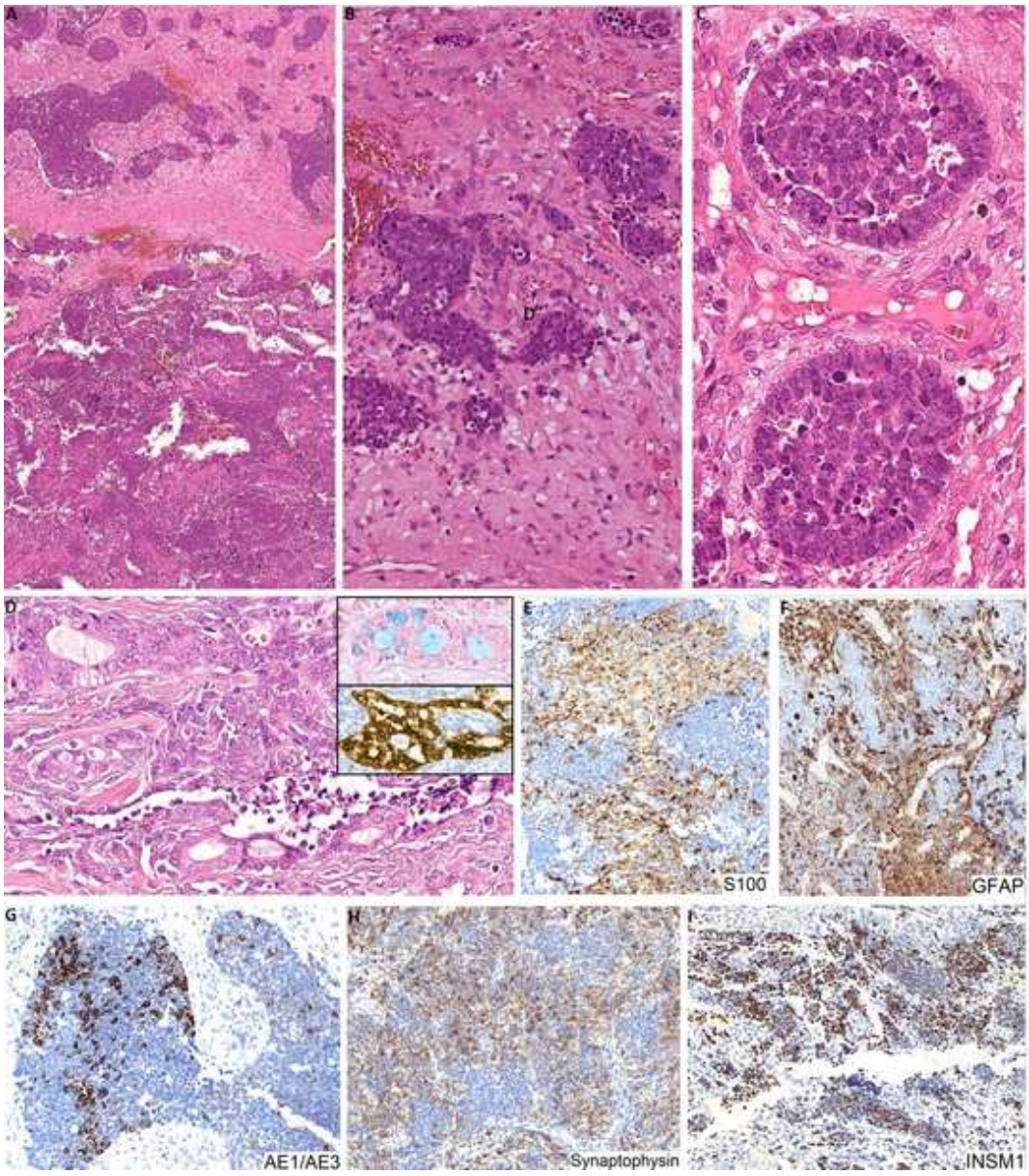

Figure 6

Click here to access/download;Figure;Figure 6.jpg

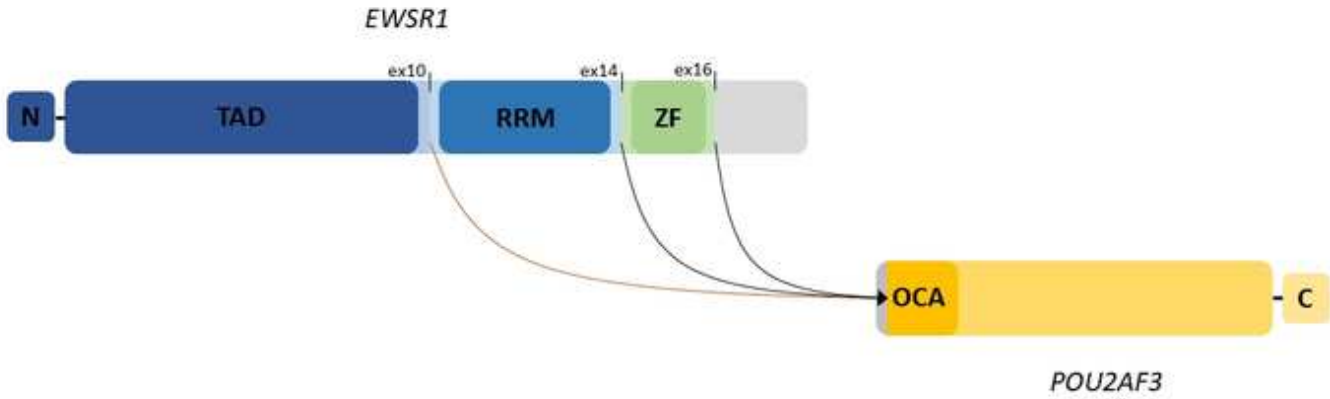

Table 1. Clinical features of *EWSR1::POU2AF3* tumors

Case #	Age/ sex	Tumor site	Size	Prior diagnosis	Treatment	Local recurrence/distant metastases (months after dx)	Status at last follow-up	Overall survival (months)
1	65/M	Sinonasal area (destructive lesion of ethmoidal and frontal sinuses)	2.9	Ossifying fibromyxoid tumor	Resection (R2) and adjuvant RT	recurrence and lytic lesion in the left ilium on PET-CT suspicious for mets (not biopsied) in 24 months	died of an unknown cause	24
2	60/F	Frontal bone (lytic bone lesion)	5.2x4.5x 2.5	Desmoplastic fibroma, Spindle cell sarcoma grade 2, Dedif. osteosarcoma	Resection (no residual disease on CT); CHT initiated after mets detected	Multiple lytic mets in bilateral frontal bones and at the base of the skull 7 months after surgery.	AWD	7
3	43/F	Sinonasal area (nasal cavity, frontal, ethmoid and maxillary sinuses)	NA	Osteosarcoma	Functional endoscopic sinus resection (R1), adjuvant proton RT,	No	AWD	4
4	46/M	Nasopharynx	NA	Ewing(-like) sarcoma; synovial sarcoma, myoepithelial tumor	Resection (R0), adjuvant RT and CHT	Multifocal bone mets (119)	AWD	122
5	72/M	L thigh	3.9	Intranodal palisaded myofibroblastoma	Resection (R0); adjuvant CHT and RT	No	NED	33.5
6	60/M	Lung (intraparenchymal)	4.2	Atypical Carcinoid	Resection (R0), mets resected	Local recurrence/multifocal pleural mets (22 and 38)	AWD	41.5
7	74/F	R proximal fibula (bone)	NA	Ewing(-like) sarcoma	Resection (R0) neoadjuvant and adjuvant RT and CHT	No	NED	53.5
8	37/M	Thoracic wall (soft tissue lesion with adjacent lytic rib involvement; no other tumor located elsewhere)	NA	Neuroendocrine carcinoma	Resection (R1) with RT (60Gy) and CHT (EP); mets treated with CHT (VAC)	mutifocal locoregional recurrence with pleural, pericardial, diaphragmatic and lymph node mets found in 24 months	AWD	30

NA: not available; RT: radiotherapy; CHT: chemotherapy; EP: Cysplatinum/Etoposide; VAC: Vincristine-D-Actinomycine-Cyclofosfamide NED: no evidence of disease; mets: metastases, AWD: alive with disease

Table 2 Click here to access/download;Table;Table 2 EWSR1-COL CA2.docx

Table 2. Histological, immunohistochemical and molecular features of *EWSR1::POU2AF3* tumors

Case #	Mits/10 HPF & Necrosis	AE1/AE3	EMA	S100	GFAP	NE markers (all available)	SAT-B2	Other positive IHC	Other negative IHC	*EWSR1* breakpoint	*POU2AF3* breakpoint
1	2/10 Absent	-	-	-	-	ND	-	SMA+; CD10+	Desmin; SOX10; MUC4, CDX2	Ex 14	Ex 2
2	2/10 Absent	+	ND	-	-	SYN–	++	ND	MUC4; ALK; NUT; Pan-Trk; STAT6; Desmin; SMA; Myo-D1; Myogenin; CD34; Beta-Catenin, CDX2	Ex 14-16	Ex 2
3	6/10 Present (10%)	-	-	-	+	SYN – CD56+	+++	ND	CD99; NKX2.2; SOX10; H3k27me3 retained; SS18::SSX; TLE1; Desmin; myogenin; STAT6	Ex 15	Ex 2
4	10/10 Present (10%)	++	+	+	++	SYN – CHROMO – CD56+	ND	CD99+++	Desmin; Myogenin; SMA	EX 14	Ex 2
5	9/10 Absent	-	-	++	++	SYN+ CHROMO- CD56+++	+	SMA+	OSCAR; Desmin; MyoD1; myogenin; SOX10; TLE1; BRAF; CD34; panTRK; CD99; CDX2	EX 9	Ex 2
6	4/10 Absent	++	-	+	+	SYN+ CHROMO+ CD56+++	++	Desmin/MyoD1/Myogenin ++; SMA+; membranous CD99+; MyoD1+; Myogenin+	BCOR; WT1; TLE1, CDX2	EX 9	Ex 2
7	8/10 Absent	++	-	ND	-	SYN– CHROMO–	ND	ND	Desmin; Myogenin; SMA; CD99	EX 9	Ex 2
8	24/10 Absent	+	+	++	++	SYN++ CHROMO++ INSM1+	-	CK5+; CK7+; SMA+	CD99; SOX10; TTF1; CDX2; CD34; p63; CK20; MC polyomavirus; calponin; WT1; ERG; CyclinD1 and ALK; Rb and INI1 retained; TP53 wt	EX 10	Ex 2
		5/8 63%	2/7 29%	4/7 57%	5/8 63%	CD56: 4/4 Any other: 3/7 (43%)					

mits/10 HPF: mitoses per 10 high-power fields; ND: not done; NE-like: neuroendocrine-like; SYN: synaptophysin; CHROMO: chromogranin; SMA: smooth muscle actin; EX: exon

Supplementary Table 1

Click here to access/download
Supplementary Material
Supplementary Table 1.xlsx

Supplementary File 1

REFERENCES

1. Eveson J.W., Auclair P., Gnepp D.R., El-Naggar A.K. Tumours of the salivary glands. In: Barnes L., Eveson J.W., Reichart P., Sidransky D., editors. Pathology and Genetics of Head and Neck Tumours. 3rd ed. Volume 9. IARC Press; Lyon, France: 2005. pp. 212–215. WHO/IARC classification of tumours.
2. WHO Classification of Tumours Editorial Board. Head and neck tumours [Internet; beta version ahead of print]. Lyon (France): International Agency for Research on Cancer; 2022 (WHO classification of tumours series, 5th ed.; vol. 9). Available from: https://tumourclassification.iarc.who.int/chapters/52.
3. Gao M., Hao Y., Huang M.X., Ma D.Q., Chen Y., Luo H.Y., Gao Y., Cao Z.Q., Peng X., Yu G.Y. Salivary gland tumours in a northern Chinese population: A 50-year retrospective study of 7190 cases. Int. J. Oral Maxillofac. Surg. 2017;46:343–349. doi: 10.1016/j.ijom.2016.09.021.
4. da Silva L.P., Serpa M.S., Viveiros S.K., Sena D.A.C., de Carvalho Pinho R.F., de Abreu Guimarães L.D., de Sousa Andrade E.S., Pereira J.R.D., Fonseca da Silveira M.M., Veras Sobral A.P., et al. Salivary gland tumors in a Brazilian population: A 20-year retrospective and multicentric study of 2292 cases. J. Craniomaxillofac. Surg. 2018;46:2227–2233. doi: 10.1016/j.jcms.2018.09.028.
5. Buchner A, Merrell PW, Carpenter WM. Relative frequency of solitary melanocytic lesions of the oral mucosa. J Oral Pathol Med. 2004 Oct;33(9):550-7. doi: 10.1111/j.1600-0714.2004.00238.x. PMID: 15357676.
6. Eveson JW, Cawson RA. Salivary gland tumours. A review of 2410 cases with particular reference to histological types, site, age and sex distribution. J Pathol. 1985 May;146(1):51-8. doi: 10.1002/path.1711460106. PMID: 4009321.
7. Bishop JA, Gagan J, Baumhoer D, et al. Sclerosing polycystic “adenosis” of salivary glands: a neoplasm characterized by *PI3K* pathway alterations more correctly named sclerosing polycystic adenoma. Head Neck Pathol. 2020;14:63–636.
8. Amatu A, Sartore-Bianchi A, Bencardino K, Pizzutilo EG, Tosi F, Siena S. Tropomyosin receptor kinase (TRK) biology and the role of NTRK gene fusions in cancer. Ann Oncol. 2019 Nov 1;30(Suppl_8):viii5-viii15.

9. Weinreb I, Seethala RR, Perez-Ordonez B, et al. Oncocytic mucoepidermoid carcinoma: clinicopathologic description in a series of 12 cases. Am J Surg Pathol. 2009;33:409–416.

10. Brannon RB, Willard CC. Oncocytic mucoepidermoid carcinoma of parotid gland origin. Oral Surg Oral Med Oral Pathol Oral Radiol Endod. 2003;96:727–733.

11. Corcione L, Giordano G, Gnetti L, et al. Oncocytic mucoepidermoid carcinoma of a submandibular gland: a case report and review of the literature. Int J Oral Maxillofac Surg. 2007;36:560–563.

12. Behboudi A, Enlund F, Winnes M, et al. Molecular classification of mucoepidermoid carcinomas-prognostic significance of the *MECT1-MAML2* fusion oncogene. Genes Chromosomes Cancer. 2006;45: 470–481.

13. Chiosea SI, Dacic S, Nikiforova MN, et al. Prospective testing of mucoepidermoid carcinoma for the *MAML2* translocation: clinical implications. Laryngoscope. 2012;122:1690–1694.

14. Seethala RR, Dacic S, Cieply K, et al. A reappraisal of the *MECT1/ MAML2* translocation in salivary mucoepidermoid carcinomas. Am J Surg Pathol. 2010;34:1106–1121.

15. Okabe M, Miyabe S, Nagatsuka H, et al. *MECT1-MAML2* fusion transcript defines a favorable subset of mucoepidermoid carcinoma. Clin Cancer Res. 2006;12:3902–3907.

16. Jee KJ, Persson M, Heikinheimo K, et al. Genomic profiles and *CRTC1-MAML2* fusion distinguish different subtypes of mucoepi-dermoid carcinoma. Mod Pathol. 2013;26:213–222.

17. Cipriani NA, Lusardi JJ, McElherne J, et al. Mucoepidermoid carcinoma. A comparison of histologic grading systems and relationship to MAML2 rearrangement and prognosis.

18. Skalova A, Vanecek T, Martinek P, et al. Molecular profiling of mammary analogue secretory carcinoma revealed a subset of tumors harboring a novel *ETV6-RET* translocation: report of 10 cases. Am J Surg Pathol. 2018;42:234–246.

19. Antonescu CR, Katabi N, Zhang L, et al. *EWSR1-ATF1* fusion is a novel and consistent finding in hyalinizing clear-cell carcinoma of salivary gland. Genes Chromosomes Cancer. 2011;50:559–570.

20. Matsuyama A, Hisaoka M, Hashimoto H. PLAG1 expression in mesenchymal tumors: an immunohistochemical study with special emphasis on the pathogenetical distinction

between soft tissue myoepithelioma and pleomorphic adenoma of the salivary gland. Pathol Int. 2012;62:1–7.

21. Patel NR, Sanghvi S, Khan MN, Husain Q, Baredes S, Eloy JA (2014) Demographic trends and disease-specific survival in salivary acinic cell carcinoma: an analysis of 1129 cases. Laryngoscope 124(1):172–178
22. Thompson LD, Aslam MN, Stall JN, Udager AM, Chiosea S, McHugh JB (2016) Clinicopathologic and immunophenotypic characterization of 25 cases of acinic cell carcinoma with high-grade transformation Head Neck Pathol 10(2):152–160
23. Skálová A, Sima R, Vanecek T et al (2009) Acinic cell carcinoma with high-grade transformation: a report of 9 cases with immunohistochemical study and analysis of TP53 and HER-2/neu genes. Am J Surg Pathol 33(8):1137–1145
24. Haller F, Bieg M, Will R et al (2019) Enhancer hijacking activates oncogenic transcription factor NR4A3 in acinic cell carcinomas of the salivary glands. Nat Commun 10(1):368
25. Haller F, Skálová A, Ihrler S et al (2019) Nuclear NR4A3 immunostaining is a specific and sensitive novel marker for acinic cell carcinoma of the salivary glands. Am J Surg Pathol 43(9):1264–1272
26. Haller F, Moskalev EA, Kuck S et al (2020) Nuclear NR4A2 (Nurr1) immunostaining is a novel marker for acinic cell carci-noma of the salivary glands lacking the classic NR4A3 (NOR-1) upregulation. Am J Surg Pathol 44(9):1290–1292
27. Wong KS, Mariño-Enriquez A, Hornick JL, Jo VY (2021) NR4A3 Immunohistochemistry reliably discriminates acinic cell carcinoma from mimics. Head Neck Pathol 15(2):425–432
28. Smith BC, Ellis GL, Slater LJ, et al. Sclerosing polycystic adenosis of major salivary glands: a clinicopathologic analysis of nine cases. Am J Surg Pathol. 1996;20:161–170
29. Skalova A, Michal M, Simpson RHW, et al. Sclerosing polycystic adenosis of parotid gland with dysplasia and ductal carcinoma in situ: report of three cases with immunohistochemical and ultrastructural examination. Virchows Arch. 2002;440:29–35
30. Petersson F. Sclerosing polycystic adenosis of salivary glands: a review with some emphasis on intraductal epithelial proliferations. Head Neck Pathol. 2013;7(suppl 1):S97–S106.

31. Petersson F, Tan PH, Hwang JSG. Sclerosing polycystic adenosis of parotid gland: report of a bifocal, paucicystic variant with ductal carcinoma in situ and pronounced stromal distortion mimicking stromal invasion. Head Neck Pathol. 2011;5:188–192.

32. Skalova A, Gnepp DR, Simpson RHW, et al. Clonal nature of sclerosing polycystic adenosis of salivary glands demonstrated by using the polymorphism of the human androgen receptor locus (HUMARA) as a marker. Am J Surg Pathol. 2006;30:939–944.

33. Hernandez-Prera J, Heidarian A, Wenig B. Sclerosing polycystic adenoma: conclusive clinical and molecular evidence of its neoplastic nature. Mod Pathol. 2021;34(suppl 2):773–774.

34. Bishop JA, Gagan J, Baumhoer D, et al. Sclerosing polycystic "adenosis" of salivary glands: a neoplasm characterized by PI3K pathway alterations more correctly named sclerosing polycystic adenoma. Head Neck Pathol. 2020;14:63–636

35. Skalova A, Bishop J, Ferlito A, et al. Newly described entities in salivary gland pathology. Am J Surg Pathol. 2017;41:e33–e47.

36. Fruman DA, Chiu H, Hopkins BD, Bagrodia S, Cantley LC, Abraham RT. The PI3K Pathway in Human Disease. Cell. 2017 Aug 10;170(4):605-635.

37. Yang J, Nie J, Ma X, et al. Targeting PI3K in cancer: mechanisms and advances in clinical trials. Mol Cancer. 2019;18:1–28.

38. Bishop JA, Gagan J, Krane JF, et al. Low-grade apocrine intraductal carcinoma: expanding the morphologic and molecular spectrum of an enigmatic salivary gland tumor. Head Neck Pathol. 2020;14:869–875.

39. Chiosea SI, Williams L, Griffith CC, et al. Molecular characterization of apocrine salivary duct carcinoma. Am J Surg Pathol. 2015;39: 744–752.

40. Dalin MG, Desrichard A, Katabi N, et al. Comprehensive molecular characterization of salivary duct carcinoma reveals actionable targets and similarity to apocrine breast cancer. Clin Cancer Res. 2016;22: 4623–4633.

41. Wang K, Russell JS, McDermott JD, et al. Profiling of 149 salivary duct carcinomas, carcinoma ex pleomorphic adenomas, and adenocarcinomas, not otherwise specified reveals actionable genomic alterations. Clin Cancer Res. 2016;22:6061–6068.

42. Santana T, Andrle P, Martinek P, et al. Biomarker immunoprofile and molecular characteristics in salivary duct carcinoma: clinicopathological and prognostic implications. Hum Pathol. 2019;93:37–47.

43. Griffith CC, Seethala RR, Luvison A, et al. *PIK3CA* mutations and PTEN loss in salivary duct carcinomas. Am J Surg Pathol. 2013;37: 1201–1207.

44. Lewis JT, Oliveira AM, Nascimento AG, Schembri-Wismayer D, Moore EA, Olsen KD et al (2012) Low-grade sinonasal sarcoma with neural and myogenic features: a clinicopathologic analysis of 28 cases. Am J Surg Pathol 36:517–525

45. Carter CS, East EG, McHugh JB (2018) Biphenotypic sinonasal sarcoma: a review and update. Arch Pathol Lab Med 142:1196–1201

46. Le Loarer F, Laffont S, Lesluyes T, Tirode F, Antonescu C, Baglin AC et al (2019) Clinicopathologic and molecular features of a series of 41 biphenotypic sinonasal sarcomas expanding their molecular spectrum. Am J Surg Pathol 43:747–754

47. Fritchie KJ, Jin L, Wang X, Graham RP, Torbenson MS, Lewis JE et al (2016) Fusion gene profile of biphenotypic sinonasal sarcoma: an analysis of 44 cases. Histopathology 69:930–936

48. Huang SC, Ghossein RA, Bishop JA, Zhang L, Chen TC, Huang HY et al (2016) Novel *PAX3-NCOA1* fusions in biphenotypic sinonasal sarcoma with focal rhabdomyoblastic differentiation. Am J Surg Pathol 40:51–59

49. Wang X, Bledsoe KL, Graham RP, Asmann YW, Viswanatha DS, Lewis JE et al (2014) Recurrent *PAX3-MAML3* fusion in biphenotypic sinonasal sarcoma. Nat Genet 46:666–668

50. Mechtersheimer G, Andrulis M, Delank KW, Volckmar AL, Zhang L, von Winterfeld M et al (2021) *RREB1-MKL2* fusion in a spindle cell sinonasal sarcoma: biphenotypic sinonasal sarcoma or chondromyxoid tumor in an unusual site? Genes Chromosom Cancer 60:565–570

51. Agaimy A, Din NU, Dermawan JK, Haller F, Melzer K, Denz A et al (2023) *RREB1::MRTFB* fusion-positive extra-glossal mesenchymal neoplasms: a series of five cases expanding their anatomic distribution and highlighting significant morphological and phenotypic diversity. Genes Chromosom Cancer 62:5–16

52. Buckingham M, Relaix F (2007) The role of *Pax* genes in the development of tissues and organs: Pax3 and Pax7 regulate muscle progenitor cell functions. Annu Rev Cell Dev Biol 23:645–673

53. Charville GW, Varma S, Forgo E, Dumont SN, Zambrano E, Trent JC et al (2016) PAX7 Expression in rhabdomyosarcoma, related soft tissue tumors, and small round blue cell neoplasms. Am J Surg Pathol 40:1305–1315

54. Folpe AL (2002) MyoD1 and myogenin expression in human neo-plasia: a review and update. Adv Anat Pathol 9:198–203

55. Agaimy A, Baneckova M, De Almeida J, et al. Recurrent *EWSR1::COLCA2* Fusions Define a Novel Sarcoma With Spindle/Round Cell Morphology and Stron Predilection for the Sinonasal Tract. Am J Surg Pathol. 2023 Mar 1;47(3):361-369.

56. Hiemenz MC, Kaur J, Kuang Z, et al. *POU2AF3*-rearranged sarcomas: A novel tumor defined by fusions of *EWSR1* or *FUS* to a gene formerly designated *COLCA2.* Genes Chromosomes Cancer. 2023. Aug; 62(8):460-470.

57. Peltekova VD, Lemire M, Qazi AM, et al. Identification of genes expressed by immune cells of the colon that are regulated by colorectal cancer-associated variants. Int J Cancer. 2014;134:2330–2341.

58. Michal M, Rubin BP, Agaimy A, Kosemehmetoglu K, Rudzinski ER, Linos K, John I, Gatalica Z, Davis JL, Liu YJ, McKenney JK, Billings SD, Švajdler M, Koshyk O, Kinkor Z, Michalová K, Kalmykova AV, Yusifli Z, Ptáková N, Hájková V, Grossman P, Šteiner P, Michal M. *EWSR1-PATZ1*-rearranged sarcoma: a report of nine cases of spindle and round cell neoplasms with predilection for thoracoabdominal soft tissues and frequent expression of neural and skeletal muscle markers. Mod Pathol. 2021 Apr;34(4):770-785. Erratum in: Mod Pathol. 2021 Nov;34(11):2092.

59. Grünewald TGP, Cidre-Aranaz F, Surdez D, et al. Ewing sarcoma. Nat Rev Dis Primers. 2018;4(1):5.

60. Tan AY, Manley JL. The TET family of proteins: functions and roles in disease. J Mol Cell Biol. 2009;1(2):82-92.

61. Abdou R, Baredes S. Population-based results in the management of sinonasal and ventral skull base malignancies. Otolaryngol Clin North Am. 2017; 50(2): 481-497.

62. Rekhi B, Sable M, Jambhekar NA. Histopathological, immunohistochemical and molecular spectrum of myoepithelial tumours of soft tissues. Virchows Arch. 2012;461:687–697.

63. Antonescu CR, Zhang L, Chang NE, et al. *EWSR1-POU5F1* fusion in soft tissue myoepithelial tumors. A molecular analysis of sixty-six cases, including soft tissue, bone, and visceral lesions, showing common involvement of the *EWSR1* gene. Genes Chromosomes Cancer. 2010;49: 1114–1124.

64. Flucke U, Palmedo G, Blankenhorn N, et al. *EWSR1* gene rearrangement occurs in a subset of cutaneous myoepithelial tumors: a study of 18 cases. Mod Pathol. 2011;24:1444–1450.

65. Suurmeijer AJH, Dickson BC, Swanson D, et al. A morphologic and molecular reappraisal of myoepithelial tumors of soft tissue, bone and viscera with *EWSR1* and *FUS* gene rearrangements. Genes Chromosomes Cancer. 2020;59:348–356.

66. Dalin MG, Katabi N, Persson M, et al. Multi-dimensional genomic analysis of myoepithelial carcinoma identifies prevalent oncogenic gene fusions. Nat Commun. 2017;8:1197.

67. Antonescu CR, Zhang L, Shao SY, et al. Frequent *PLAG1* gene rearrangements in skin and soft tissue myoepithelioma with ductal differentiation. Genes Chromosomes Cancer. 2013;52:675–682.

LIST OF OWN PUBLICATIONS

1. **Olena Koshyk**, Carina A. Dehner, Mari F.C.M. van den Hout, Isabelle Vanden Bempt, Raf Sciot , Hsuan-Ying Huang , Abbas Agaimy , Nasir Ud Din , Natálie Klubíčková, Elaheh Mosaieby, Alena Skálová, Květoslava Michalová, Patrick Schöffski, Andre M. Oliveira, Kevin C Halling, Sounak Gupta, John M. Gross, Johanna W.M. Nin, Michal Michal, Andrew L. Folpe, Kemal Kosemehmetoglu, Jorge Torres- Mora, Michael Michal. EWSR1::POU2AF3(COLCA2) Sarcoma: An aggressive, polyphenotypic sarcoma with a head and neck predilection. In press.

2. Skálová A; Agaimy A; Stanowska O; Baneckova M; Ptáková N; Ardighieri L; Nicolai P; Lombardi D; Durzynska M; Corcione L; Laco J; **Koshyk O**; Žalud R; Michal M; Vanecek T; Leivo I. Molecular Profiling of Salivary Oncocytic Mucoepidermoid Carcinomas Helps to Resolve Differential Diagnostic Dilemma With Low-grade Oncocytic Lesions. Am J Surg Pathol. 2020 Dec; 44(12):16121622, doi:10.1097/PAS.0000000000001590

3. Skálová A; Agaimy A; Vanecek T; Baněčková M; Laco J; Ptáková N; Šteiner P; Majewska H; Biernat W: Corcione L; Eis V: **Koshyk O**; Vondrák J: Michal M; Leivo I. Molecular Profiling of Clear Cell Myoepithelial Carcinoma of Salivary Glands With EWSR1 Rearrangement Identifies Frequent PLAG1 Gene Fusions but No EWSR1 Fusion Transcripts Am J Surg Pathol. 2021 Jan; 45(1):1-13 doi: 10.1097/PAS.0000000000001591

4. Skálová A; Baněčková M; Laco, J; Di Palma S; Agaimy A; Ptáková N; Costes-Martineau V; Petersson B; van den Hout M; de Rezende G; Klubíčková N; Koblížek M; **Koshyk O**; Vaneček T; Leivo I. Sclerosing Polycystic Adenoma of salivary Glands: A Novel Neoplasm Characterized by PIK-AKT Pathway Alterations-NEW Insights Into a Challenging Entity. Am J Surg Pathol. 46(2):268-280, 01 Feb 2022 Am J Surg Pathol. 2022 Feb; 46(2):268-280 doi: 10.1097/PAS.0000000000001807

5. Meyer A, Klubíčková N, Mosaieby E, Grossmann P, Kalmykova A, **Koshyk O**, Michal M. Biphenotypic sinonasal sarcoma with PAX3::MAML3 fusion transforming into high-grade rhabdomyosarcoma: report of an emerging rare phenomenon. Virchows Arch. 2023 Apr;482(4):777-782. doi: 10.1007/s00428-023-03501-0. Epub 2023 Jan 31. PMID: 36719455; PMCID: PMC10067655.

6. Klubíčková N, Grossmann P, Šteiner P, Baněčková M, Mosaieby E, **Koshyk O**, Michal M, Leivo I, Skálová A. A minority of cases of acinic cell carcinoma of the salivary glands

are driven by an NR4A2 rearrangement: the diagnostic utility of the assessment of NR4A2 and NR4A3 alterations in salivary gland tumors. Virchows Arch. 2023 Feb;482(2):339-345. doi: 10.1007/s00428-022-03464-8. Epub 2022 Dec 5. PMID: 36469101.

CONCLUSIONS

The Ph.D. thesis concludes postgraduate studies in pathology Olena Koshyk, MD. During the studies, the objectives were fulfilled over the study. With the coauthors, the author has documented the clinicopathological, morphological, immunohistochemical, and molecular characteristics of rare salivary gland and sinonasal tumors.

The result of the four-year study is one first-author work and 5 co-authored publications. The results of all papers presented in the doctoral thesis were published in various American and European journals with impact factors from 3,5 to 8,209.

ACKNOWLEDGMENTS

I would like to thank my supervisor Prof. MUDr. Alena Skálová for her help and assistance overall for 4 years of my postgraduate study and for her ongoing support, patience, and humanity in such a difficult time for me.

I would also like to thank Prof. MUDr. Michal Michal for his unceasing enthusiasm and faith in people, which makes them conquer new heights.

I'm also grateful to the CEO of CSD Medical Lab Oleksandr Dudin for the initiation of this work and his continued support.

I also very much appreciate the help of my colleagues at the Bioptical Laboratory, s.r.o. in Pilsen Martina Baněčková, Natálie Klubíčková, Liubov Kastnerova and especially Květoslava Michalová and Michael Michal.

The acknowledgments also go to Charles University in Prague, the Faculty of Medicine in Pilsen for the opportunity to attend a well-organized postgraduate study.

And of course, I'm also very grateful to my mom and husband for their faith in me and patience.